

POLITECNICO DI TORINO

Corso di Laurea Magistrale in Ingegneria Edile



Tesi di Laurea Magistrale

**MECHANICAL AND ECOLOGICAL
ASSESSMENTS OF ULTRA HIGH
PERFORMANCE - FIBER REINFORCED
CEMENTITIOUS COMPOSITES (UHP-FRCC)
JACKETING**

Relatore

prof. Alessandro P. Fantilli

Candidato

Lucia Paternesi Meloni

Aprile 2019

TABLE OF CONTENTS

LIST OF FIGURES	III
LIST OF TABLES	VIII
CHAPTER 1 INTRODUCTION	1
1.1 GENERAL BACKGROUND AND RESEARCH SCOPE	3
1.2 OUTLINE OF THE THESIS	5
CHAPTER 2 BACKGROUND AND LITERATURE REVIEW	7
2.1 CLASSIFICATION OF REINFORCED CEMENTITIOUS COMPOSITES	9
2.2 MIX DESIGN FOR UHP-FRCC	12
2.3 MECHANICAL PROPERTIES OF UHP-FRCC	23
2.4 ECOLOGICAL IMPACT OF UHP-FRCC	28
2.5 MATERIAL SUBSTITUTION STRATEGY: REDUCTION OF THE CO ₂ EMISSIONS	30
2.6 ECO-MECHANICAL ANALYSIS	34
2.7 APPLICATIONS OF UHP-FRCC: REPAIR AND REHABILITATION	36
CHAPTER 3 DESIGN AND EXPERIMENTAL INVESTIGATION	43
3.1 WORK EXPERIENCE AT LIFE CYCLE ENGINEERING LABORATORY	45
3.1.1 Brief description of the Laboratory	45
3.1.2 Work methodology	49
3.2 THE PURPOSE OF THE RESEARCH	52
3.3 PREVIOUS INVESTIGATIONS AT LIFE CYCLE ENGINEERING LABORATORY	53
3.4 TYPES OF CONCRETE CYLINDERS REINFORCED WITH UHP-FRCC JACKETS	54
3.4.1 Geometrical properties	55
3.4.2 Material properties	58
3.5 MIXING, CASTING AND CURING PROCEDURES	64
3.6 TESTING PROCEDURE AND EXPERIMENTAL DEVICES	73

CHAPTER 4 TEST RESULTS.....	79
4.1 MECHANICAL ANALYSIS	81
4.1.1 Compressive Stress.....	83
4.1.2 Mechanical parameters	97
4.1.3 Ductility	100
4.2 ECOLOGICAL ANALYSIS.....	103
4.3 ECO-MECHANICAL PERFORMANCE	106
4.4 DESIGN PROCEDURE	110
CHAPTER 5 CONCLUSIONS AND FUTURE RESEARCH.....	113
ANNEXES.....	119
ANNEX 1: GEOMETRICAL PROPERTIES.....	121
ANNEX 2: CODIFICATION OF SPECIMENS	123
ANNEX 3: SLUMP TEST.....	124
ANNEX 4: AIR CONTENT TEST.....	125
ANNEX 5: FLOW TABLE TEST	126
ANNEX 6: RESULTS MIXTURE FA0.....	127
ANNEX 7: RESULTS MIXTURE FA20	128
ANNEX 8: RESULTS MIXTURE FA50	130
ANNEX 9: RESULTS MIXTURE FA70	131
ANNEX 10: EVALUATION OF DUCTILITY	133
ANNEX 11: FAILURE MODES	135
REFERENCES.....	136

LIST OF FIGURES

Figure 2.1 - Classification of cementitious composites	9
Figure 2.2 - Classification of fiber reinforced cementitious composites	10
Figure 2.3 - Example of mix proportions by volume comparing UHP-FRCC with normal concrete	12
Figure 2.4 - Packing design	13
Figure 2.5 - Effect of porosity and of water/binder ratio on compressive strength	14
Figure 2.6 - Fly ash particles	16
Figure 2.7 - Physical effects of silica fume on the cement particles: filler effect and loosening effect	18
Figure 2.8 - Type of fibers	20
Figure 2.9 - Influence of d_{max} on fibre distribution	22
Figure 2.10 - Stress-Strain diagram of UHPC	23
Figure 2.11 - Stress-Strain diagram of UHP-FRCC Stress-Strain diagram of UHPC	24
Figure 2.12 - Typical tensile strain softening and hardening behaviour of HPF-RCC	24
Figure 2.13 - Schematic illustration of multi-scale fiber-reinforcement system	26
Figure 2.14 - Cement content in ordinary concrete and UHP-FRCC (Volume ratio)	29
Figure 2.15 - Cement and Fly Ash powders comparison; Finer and more spherical Fly Ash particles than Cement	30
Figure 2.16 - The impact of a cubic meter of UHP-FRCC, in terms of greenhouse gases emission, and carbon footprint	31
Figure 2.17 - The impact of a reinforced concrete beam made with different concretes (having different f_{cA})	31
Figure 2.18 - Mix proportion comparison (Volume ratio)	32
Figure 2.19 - Non-dimensional chart for assessing the eco-mechanical performances	34
Figure 2.20 - Eco-mechanical analysis at material scale	35
Figure 2.21 - Classes of application of fiber reinforced cement composites	36
Figure 2.22 - Typical application of HPFRCCs	37
Figure 2.23 - Applications of HPFRCCs for repair and strengthening of concrete	38

Figure 2.24 - Examples of selective use of HPFRCC in seismic resistant structures	38
Figure 2.25 - Casting phases of seismic retrofit intervention with UHP-FRCC	40
Figure 2.26 Apartment block G4, via Beffi, Coppito, before and after the intervention of seismic adaptation	40
Figure 2.27 - Concepts of applications of local "hardening" of structures with UHP-FRCC	41
Figure 2.28 Repair and protection of foundations and supports of the Valabres viaduct	41
Figure 3.1 - Members of Life Cycle Laboratory	46
Figure 3.2 - Life Cycle Laboratory: student's work stations	47
Figure 3.3 - Curing room with constant temperature of 20°C; Storage room	47
Figure 3.4 - Life Cycle Laboratory: experiment and casting area	48
Figure 3.5 - Life Cycle Laboratory: testing area	48
Figure 3.6 - Work methodology process	49
Figure 3.7 - Weekly meeting	50
Figure 3.8 - Example of mixes with a not appropriate workability	51
Figure 3.9 - Geometrical properties of samples	55
Figure 3.10 - Increasing thickness of the jackets	56
Figure 3.11 - Plastic molds used for core casting	57
Figure 3.12 - Paper molds used for jacket casting	57
Figure 3.13 - Abram cone to determine the saturated surface dry (SSD)	59
Figure 3.14 - Silica fume with bubbles; Sifted silica fume	60
Figure 3.15 - Micro-fibers; Macro-fibers	61
Figure 3.16 - Mixer used for casting UHP-FRCC	64
Figure 3.17 - Scheme of mixing process for concrete cores	64
Figure 3.18 - Mixing phases for concrete cores	65
Figure 3.19 - Slump test: equipment and measurement	66
Figure 3.20 - Device for measurement of air content	67
Figure 3.21 - Casting of concrete cores	68
Figure 3.22 - Concrete core after removing the mold	68
Figure 3.23 - Scheme of mixing process for UHP-FRCC (<i>FA0</i> , <i>FA20</i> , <i>FA50</i> , <i>FA70</i> mixtures)	69
Figure 3.24 - Mixing procedure for UHP-FRCC mixtures	70

Figure 3.25 - Flow table test of UHP-FRCC	71
Figure 3.26 - Preparation and casting of jacket	71
Figure 3.27 - Specimens after the steam curing	72
Figure 3.28 - Scheme of the process	72
Figure 3.29 - External strain gauge's geometry	73
Figure 3.30 - Vertical and horizontal external strain gauges applied on the jacket's surface	74
Figure 3.31 - Ineffectiveness of vertical strain gauges on the jacket's surface: elongation; bending effect	75
Figure 3.32 - Embedded strain gauge	75
Figure 3.33 - Embedded strain gauge's geometry	76
Figure 3.34 - Universal testing machine (UTM) used for the compressive test	76
Figure 3.35 - Compressive test: cracking process	77
Figure 4.1 - Example of average curve tracing	82
Figure 4.2 - Maximum compressive stress: UHP-FRCC FA0 jackets	83
Figure 4.3 - Stress-strain curves: FA0 jackets (Values normalized with f_{c_CORE})	84
Figure 4.4 - Maximum compressive stress: UHP-FRCC FA50 jackets	85
Figure 4.5 - Stress-strain curves: FA20 jackets	85
Figure 4.6 - Stress-strain curves: FA20 jackets (Values normalized with f_{c_CORE})	86
Figure 4.7 - Maximum compressive stress: UHP-FRCC FA20 jackets	86
Figure 4.8 - Stress-strain curves: FA50 jacket	87
Figure 4.9 - Stress-strain curves: FA50 jackets (Values normalized with f_{c_CORE})	87
Figure 4.10 - Maximum compressive stress: UHP-FRCC FA50 jackets	88
Figure 4.11 - Stress-strain curves: FA70 jackets	89
Figure 4.12 - Stress-strain curves: FA20 jackets (Values normalized with f_{c_CORE})	89
Figure 4.13 - Maximum compressive stress: UHP-FRCC FA70 jackets	90
Figure 4.14 - Maximum compressive stress: jackets with a thickness of 25 mm	91
Figure 4.15 - Comparison of jackets with thickness of 25 mm	91
Figure 4.16 - Maximum compressive stress: jackets with a thickness of 50 mm	92
Figure 4.17 - Comparison of jackets with thickness of 50 mm	92
Figure 4.18 - Relationship between the Thickness of Jacket and Compressive Stress	93
Figure 4.19 - Trend Lines (Relationship Thickness - Compressive Stress)	94

Figure 4.20 - Relationship between the Percentage of Fly Ash and the Slope	95
Figure 4.21 - Test results: Young modulus in compression; Compressive strength	96
Figure 4.22 - Poisson's ratio	99
Figure 4.23 - Strain gauges breakage	100
Figure 4.24 - Ductile behaviour of UHP-FRCC	101
Figure 4.25 - Energy absorption between σ_{\max} and $0,9 \sigma_{\max}$	102
Figure 4.26 - Main materials responsible for environmental impact	104
Figure 4.27 - Comparison of CO ₂ emissions of UHP-FRCC jackets	105
Figure 4.28 - Eco-Mechanical analysis: Compressive Stress	106
Figure 4.29 - Eco-Mechanical analysis: Ductility	108
Figure 4.30 - (a) Reference scheme; (b) Design process	110
Figure 4.31 - The ecological impact of UHP-FRCC jackets made with different mixtures (having different σ_{\max})	111
Figure 4.32 - The minimum ecological impact of a UHP-FRCC jackets (having a specific σ_{\max})	112
Figure 6.1 - Scheme of concrete cylinder reinforced with UHP-FRCC jacket	121
Figure 6.2- Crossing Sections	122
Figure 6.3 - Codification	123
Figure 6.4 - Codification of normal concrete cylinder, confined cylinder before and after casting	123
Figure 6.5 - Mold for Slump Test	124
Figure 6.6 - Schematic Diagram - Type-B Meter	125
Figure 6.7 - Flow Table and Accessory Apparatus	126
Figure 6.8 - Stress-strain curves: FA0 Jackets of 25 mm	127
Figure 6.9 - Stress-strain curves: FA0 Jackets of 50 mm	127
Figure 6.10 - Stress-strain curves: FA20 Jackets of 25 mm	128
Figure 6.11 - Stress-strain curves: FA20 Jackets of 37,5 mm	128
Figure 6.12 - Stress-strain curves: FA20 Jackets of 50 mm	129
Figure 6.13 - Stress-strain curves: FA20 Jackets of 75 mm	129
Figure 6.14 - Stress-strain curves: FA50 Jackets of 25 mm	130
Figure 6.15 - Stress-strain curves: FA50 Jackets of 50 mm	130
Figure 6.16 - Stress-strain curves: FA70 Jackets of 25 mm	131

Figure 6.17 - Stress-strain curves: FA70 Jackets of 37,5 mm	131
Figure 6.18 - Stress-strain curves: FA70 Jackets of 50 m	132
Figure 6.19 - Evaluation of ductility: FA0 mixture	133
Figure 6.20 - Evaluation of ductility: FA20 mixture	133
Figure 6.21 - Evaluation of ductility: FA50 mixture	134
Figure 6.22 - Evaluation of ductility: FA70 mixture	134
Figure 6.23 - Failure patterns: top view	135
Figure 6.24- Failure patterns: lateral view	135

LIST OF TABLES

Table 2.1 - Compressive strength classes of hydraulic binders	15
Table 3.1 - Jacket's dimensions and radius/thickness ratio	56
Table 3.2 - Materials	58
Table 3.3 - Mix proportion of concrete cores	59
Table 3.4 - Mechanical properties of fibers	61
Table 3.5 - Mix proportion (weight %) referred to the binder	62
Table 3.6 – Mix proportion of UHP-FRCC jackets	62
Table 4.1 - List of tested samples	81
Table 4.2 - Compression test results of normal concrete cores	84
Table 4.3 - Summary table of test results	90
Table 4.4 - Parameters of trends lines	94
Table 4.5 - Mechanical Parameters	98
Table 4.6 - Ductility evaluation: normalized areas	102
Table 4.7 – CO ₂ emissions: UHP-FRCC jackets	104
Table 6.1 - Slump Test: results	124
Table 6.2 - Air Content Test: results	125
Table 6.3 - Flow Table Test: results	126
Table 6.4 - Mixture FA0: jackets of 25 mm	127
Table 6.5 - Mixture FA0: jackets of 50 mm	127
Table 6.6 - Mixture FA20: jackets of 25 mm	128
Table 6.7 - Mixture FA20: jackets of 37,5 mm	128
Table 6.8 - Mixture FA20: jackets of 50 mm	129
Table 6.9 - Mixture FA20: jackets of 25 mm	129
Table 6.10 - Mixture FA50: jackets of 25 mm	130
Table 6.11 - Mixture FA50: jackets of 50 mm	130
Table 6.12 - Mixture FA70: jackets of 25 mm	131
Table 6.13 - Mixture FA70: jackets of 37,5 mm	131
Table 6.14 - Mixture FA70: jackets of 50 mm	132

CHAPTER 1

INTRODUCTION

1.1 General background and research scope

The fast-growing demand for a more sustainable and longer life structures has been creating new challenges in the field of building and civil engineering, particularly regarding materials.

In this regard, concrete has played a very important role in the development of structures and infrastructures: due to its relatively low cost, acceptable performances and a flexible production process, it is considered one of the main building materials used all over the world.

However, in the last decades, the need for new solutions with higher performance than the conventional concrete has emerged, and more comprehensive approaches have been developed to improve the behaviour of construction materials. In particular, the lack of durability and ductility has represented two key issues for new challenging research and studies.

For these reasons, Ultra High-Performance Fiber-Reinforced Cementitious Composites (henceforth, UHP-FRCC) has been developed to meet the recent requests in the construction sector.

An additional aim of the cement industry is to decrease the negative impact on environment: the industrial production of UHP-FRCC represents a reasonable strategy to achieve this goal due to the use of copious amounts of industrial by-product, higher structural performance, lower maintenance and long life.

Strictly concerning the nature of UHP-FRCC, it is a highly dense, fiber-reinforced cementitious composite material that has a compressive strength of more of 150 MPa, combined with acceptable tensile and flexural strengths.

These high mechanical properties are achieved by the use of different kinds of fine aggregates, a high content of cementitious materials, a very low water/cement ratio and the incorporation of high-strength ductile steel fibers, that considerably enhances the ductility of this material.

Moreover, UHP-FRCC is featured by superior structural and durability performance in aggressive environmental conditions, and particularly it is a solution for the repair, strengthening and seismic retrofitting of structural members of old structures.

According to this premise, the present experimental thesis follows this direction: normal concrete cylinders have been reinforced with UHP-FRCC jackets to simulate the confinement effect of columns made of ordinary concrete.

Different layouts for jackets and different UHP-FRCC mixtures have been designed and studied in order to achieve the best mechanical and ecological solutions.

In fact, it is necessary to specify that this high-performance material has a parallel high environmental impact: a large quantity of CO₂ is released during the cement production, particularly in the calcination of limestone, transportation, manufacturing and construction procedures.

To overcome this issue, in this experimental investigation industrial by-product, as fly ash, are used in order to decrease the environmental impact (i.e., pollution) and to suggest eco-friendlier solutions.

The specimens have been compared using an eco-mechanical chart that allows to simultaneously displaying both ecological and mechanical properties, with the purpose to select that ones with a combination of high mechanical and ecological features.

1.2 Outline of the thesis

The present experimental thesis consists of six chapters. First, the experiments have been carried out; then, results are presented; finally, findings are accurately discussed.

Chapter 1. Introduction

This chapter consists of a brief overview of the contents of this thesis, as well as research scope, objectives and investigation strategy.

Chapter 2. Background and literature review:

This chapter presents a full background and literature review related to UHP-FRCC compositions and properties. After a first general description and classification, a detailed characterisation of the materials for the mix design is presented. The main characteristics of the UHP-FRCC are shown, both from the mechanical and the ecological standpoints; an eco-mechanical analysis is proposed for assessment. To conclude, several applications of UHP-FRCC are presented and discussed.

Chapter 3. Design and experimental investigation

This chapter presents the work experience and methodology at Life Cycle Engineering Laboratory, that gave me the opportunity to develop this research. Moreover, previous investigations are proposed to have a wider reference framework.

Follow a detailed explanation of the experimental program: concrete cylinder reinforced with UHP-FRCC jackets are described, from both geometrical and material properties, and all the experimental procedures are reported (mixing, casting, and testing).

Chapter 4. Test results

In this chapter, the results stemming from tests are presented and discussed. Two separate analyses of the mechanical and ecological performances are carried out, and then they are combined in order to simultaneously evaluate all the aspects of the jacketing. A proposal for a new design model for the jackets is also advanced.

Chapter 5. Conclusions and future researches

This chapter contains a summary of the main findings of the experimental research and subjects remained for future studies. Some final remarks are also reported.

CHAPTER 2

BACKGROUND AND LITERATURE REVIEW

2.1 Classification of Reinforced Cementitious Composites

Concrete is one of the most widely utilised materials in building and infrastructure fields. However, it should be immediately noted that concrete presents some weaknesses, such as a brittle behaviour, low tensile strength, strain capacity, fracture toughness and energy absorption capacity.

For these reasons, in the last five decades new fiber-reinforced cementitious composites (henceforth, FRCCs), featured by distributed fibers in the matrix, have been developed to overcome the aforementioned problems related to its utilisation.

It is necessary to point out that the fiber reinforcement has different role compared to the steel bars. In fact, steel bars are principally used to increase the tensile load-bearing capacity and shear capacity of concrete [2]; on the other hand, steel fibers improve post cracking behaviour by regulating the crack opening and propagating, and they enhance the ductility of the concrete or, to be more appropriately, its energy absorption capacity [3]. Certainly, FRCCs might improve the impact and abrasion resistances, and increase the fatigue properties [4]. Nowadays several types of innovative FRCC are available.

From this perspective, new advanced cementitious materials have been developed: it is the case of Ultra-high performance fiber-reinforced cementitious composites (UHP-FRCCs).

UHP-FRCCs belong to the group of high performance fiber-reinforced cementitious composites (HPFRCCs): in turn, they take part of the family of Fiber Reinforced Concrete (FRC), as shown in Figure 2.1.

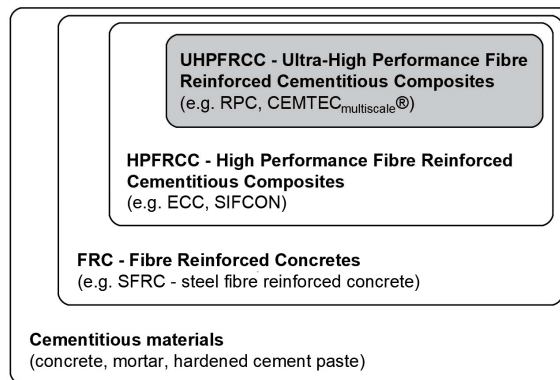


Figure 2.1 - Classification of cementitious composites [5]

UHP-FRCCs can be a precious answer to enhance the resistance of buildings and infrastructures due to their ultra-high strength, high ductility, durability and energy absorption capacity compared with normal concrete or traditional FRCC.

This versatile material is also suitable for seismic design application and it can ensure a long service life of structures on the basis of its crack tolerance.

Regrettably, the literature doesn't offer many reports of works and researches on UHP-FRCC, while lot of information are available concerning fiber-reinforced cementitious composites materials.

Overall, the term "high-performance" and the adjective "advanced" are conferred to materials used in engineering field that show much better performances than the conventional ones.

The terminology of "ultra-high performance" can be retrieved in another classification by JSCE (Figure 2.2), that establishes a link between strength and ductility of the categories of cementitious composites (Figure 2.2).

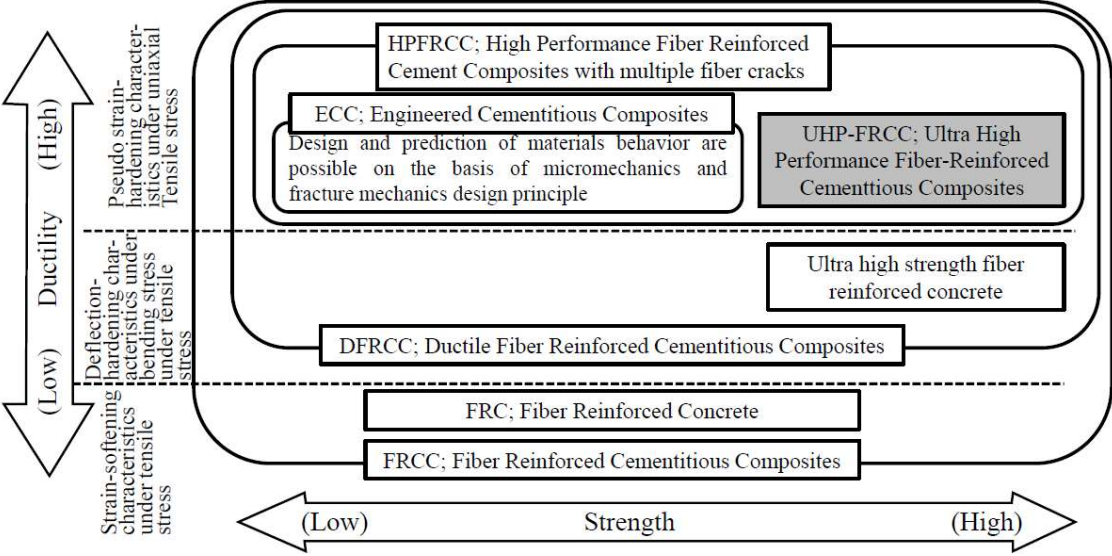


Figure 2.2 - Classification of fiber reinforced cementitious composites (JSCE 2008)

As it can be seen in the figure, UHP-FRCCs show primarily very high strength, elevate high ductility, and outstanding durability, particularly when compared to high strength concrete or traditional cementitious composites.

UHP-FRCCs have been examined including the advantage of both UHPC and FRCC. The combination with steel fibers in the mix design is the responsible of the improvement of the toughness and ductility of UHPC and consequently moderates the brittle behaviour the traditional cementitious composites exhibit under tensile loading.

The seminal investigation about UHP-FRCC has been carried out in 1987 by Bache in Denmark through the development of compact reinforced composite technology. This particular technology, whose applications are remarkably still active, implies a large amount of metal fiber added to a cement matrix to manufactured prefabricated structural members for buildings, strengthened by conventional methods designed without considering the mechanical contribution of fibers.

Other initial researches on UHP-FRCC have been performed in France during the 1990s: these led to the develop of Reactive Power Concrete (RPC), which played an important role in the distribution of the new material all over the world to use UHP-FRCC as structural applications such as bridges and buildings, and in decorative and architectural elements as well. Therefore, CEMTEC multiscale was developed by the Laboratoire Central des Points et Chaussées (LCPC) in France as a commercial product (Boulay et al. 2004) [6].

Several UHP-FRCC structures have been constructed in different countries such as Australia, France, Canada, Germany, Korea, USA, New Zealand and Japan too. The first application of UHP-FRCC goes back to 1997, with a footbridge constructed at Sherbrook (Canada), while the first footbridge without any traditional reinforcements was built in Seoul (Korea) in 2002.

Furthermore, several UHP-FRCC structures were constructed in Japan, as Miraibashi in Sakata as footbridge (2002) and some structures of airport runway in Haneda international airport (2007).

In addition, due to the lack of literature about this new material, JSCE (2004) published a recommendation of design and construction of ultra-high strength fiber reinforced concrete structures.

2.2 Mix design for UHP-FRCC

UHP-FRCC is composite material that presents, compared to ordinary concretes and to those with high resistance, properties decidedly higher in terms of resistance, durability and long-term stability, largely derived from characteristics of its main components - the cement matrix and the fibers - e from their interaction.

The mix design aims to identify the correct quantitative relationships among the components, suitable for obtaining desired physical-mechanical performance and defined rheological system. The design activity of the mixture therefore consists in continuous optimisation over time of the mixture itself, according to the physiological variations of the properties of components and operating conditions.

UHP-FRCC is made up of cement, aggregates, water, additives, and fibres. The distinctions between this “special” material and traditional concretes mix design are above all the low water/binder ratio, the size of the aggregate and the use of different fibers (Figure 2.3).

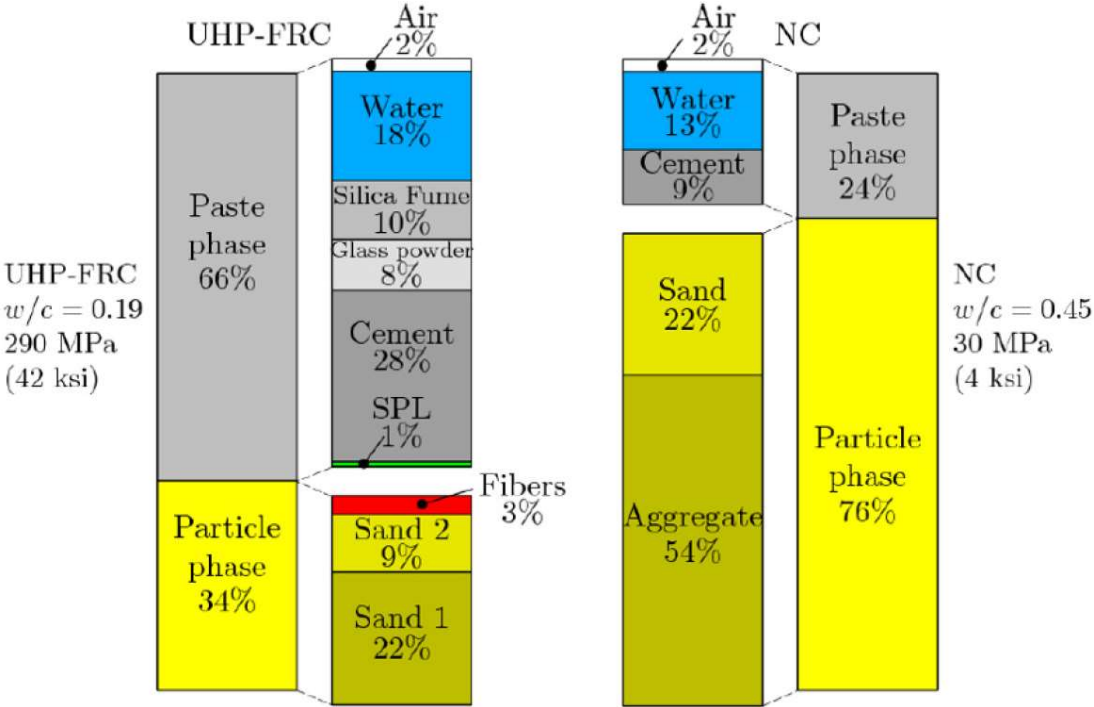


Figure 2.3 - Example of mix proportions by volume comparing UHP-FRCC with normal concrete [7]

To obtain a suitable workability a relatively amount of superplasticizer is added to the mix.

One of the main characteristics of the UHP-FRCC is the packing density of all granular constituents, that is considerably dense due to the presence of with ultra-thin addition, as silica fume particles [8]. With this shrewdness, the durability and the mechanical properties are significantly improved, compared to a conventional concrete.

With the term “packing density” it is indicated the volume percentage of solids for each volume unit. This will increase with the presence of smaller sized particles able to fill the voids between the larger sized particles in the matrix (Figure 2.4).

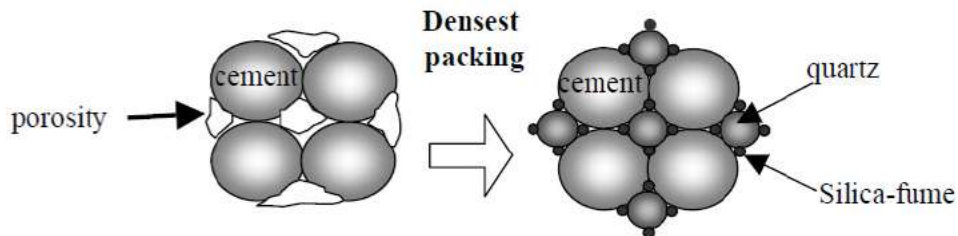


Figure 2.4 - Packing design

The reason we want to obtain a dense particle packing in concrete, is connected to the interfacial transition zone, identified as that part of the micro-structure in which there is adhesion between cement paste or matrix and the external surface of the aggregates.

This part represents the weakest area from which the micro-cracks propagate when the concrete is stressed. To increase the capacity of aggregate adhesion - paste or cement matrix, fillers and mineral additions must be used, along with the use of maximum diameters, ranging in general from 12 to 20 mm.

The reduced maximum diameters of the aggregates allow not only an easier workability, but also the achievement of an excellent homogeneity of the concrete, avoiding any "blocking" phenomena in the most critical points in the sections of the structural element. The porous structure also allows higher water transport through the transition zone, and deteriorating processes such as alkali-silica reaction, sulphate attack and ingress of chlorides [9].

Therefore, the mechanical properties are affected by the heterogeneity of the material due to the presence of large crystals of CH and the high presence of pores and interstitial voids around them, as well as, at a larger scale, the weakness and consistency of the transition zone, in their turn connected to the size of the aggregates, to the density of granular compactness and to the water/binder ratio.

Another crucial parameter to ensure high properties of the mix is the water to binder (w/b) ratio: for binder we mean the reactive materials in the matrix, as cement and ultra-thin addition.

Values of w/b ratio below 0,20 guarantees a reasonable equilibrium between the flowability of the mix and the strength of the hardened concrete [10].

In the Figure 2.5 it is shown how the porosity and the water/binder ratio can influence the compressive strength of the mix.

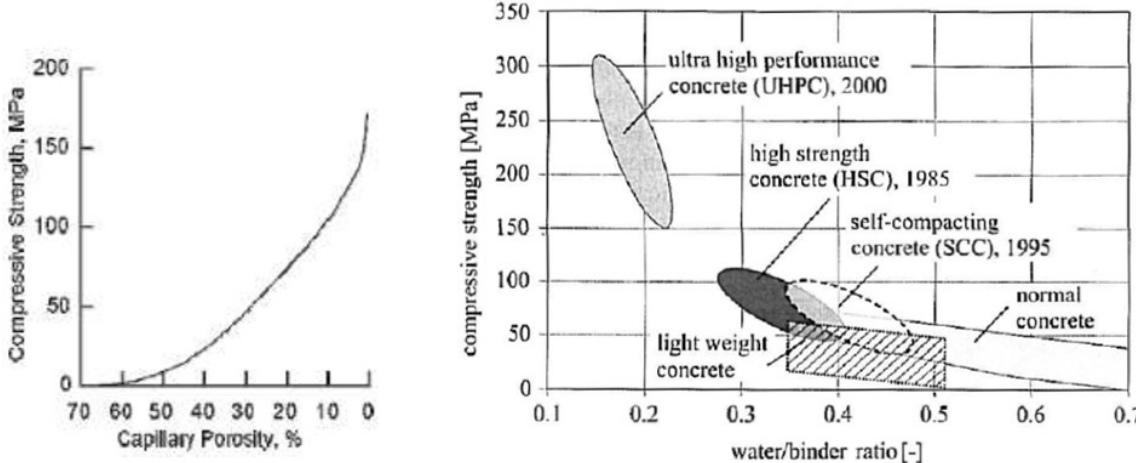


Figure 2.5 - Effect of porosity [11] and of water/binder ratio [12] on compressive strength

Following, a description of the main constituents, identifying their main technical characteristics of interest for the production of UHP-FRCC and showing its strengths and weaknesses to fully meet the performance requirements.

Cement

The study of the design of high strength calculations provides a careful assessment of the mechanical performance of cements suitable for obtaining the required compressive strength characteristics. High strength concretes require the use of high mechanical strength cements. The European legislation established three classes of resistance and compression of hydraulic binders, as reported in Table 2.1, taken from the UNI EN 197-1 (2011), update of the UNI EN 197-1 (2006).

Table 2.1 - Compressive strength classes of hydraulic binders

Concrete Strength Class		Compressive Strength (MPa)			
		2 days	7 days	28 days	
32,5	L*	-	$\geq 12,0$	$\geq 32,5$	$\leq 52,5$
	N**	-	$\geq 16,0$		
	R***	$\geq 10,0$	-		
42,5	L*	-	$\geq 16,0$	$\geq 42,5$	$\leq 62,5$
	N**	$\geq 10,0$	-		
	R***	$\geq 20,0$	-		
52,5	L*	$\geq 10,0$	-	$\geq 52,5$	-
	N**	$\geq 20,0$	-		
	R***	$\geq 30,0$	-		

*Normal-hardening Cement; **Rapid-hardening Cement; *** Low- hardening Cement

All cements conforming to UNI EN 197-1 (2011) can be used. As for ordinary concrete, the correct choice of the type of cement is normally dictated by requests related to specific applications: for example, for large amount of mixture, the reduction of the hydration calories may be required, and a solution could be Low Heat Cement.

The most suitable types of cement are certainly those having a compressive strength class in plastic mortar of 52.5 MPa. However, the choice of the correct class of cement to be used in recipes must be considered as a function of particular restriction or casting

conditions, such as, for example, a certain development of resistance over time, the structural element section, etc.

Overall, the amount of cement contained in the UHCFRCC is almost twice that of conventional concrete and his content in the mix lies bet between 600 to 1200 kg/m³: sometimes the quantity could be reduced to pursue high environmental performances.

About the fineness of the cement, it may have values ranging from 3000 to 4500 cm²/kg. Because of the very low water/binder ratio, not all the cement particles can take part in the reaction phenomenon: in fact, the remaining cement will work as inert contributing to the particle packing.

Fly ash

Fly ash is obtained as a by-product of the combustion of pulverised coal in the thermoelectric plants. It occurs in the form of almost spherical particles (5-90 µm) often hollow. The round shape of these particles improves the workability of the UHP-FRCC, increases the cohesion of the dough and reduces its sensitivity to changes in the water content (Figure 2.6Figure 2.6 - Fly ash particles).



Figure 2.6 - Fly ash particles

They haven't autonomous binding abilities, but if mixed with mortar they act as a binder. They have positive effects on the hardened concrete, allowing a further increase in mechanical strength even after 28 days, reducing creep phenomena and increasing

durability. Concrete mixes containing fly ash have lower water permeability, due to the low porosity, and a greater resistance to chemical attack.

The fact that fly ash is pozzolan is not of secondary importance; it is indeed an excellent adjuvant in the fight against the phenomenon of the alkali-aggregate reaction. The fly ash also contributes to the durability of the elements exposed to the attack of chlorides; they allow a constant increase of the mechanical resistance particularly evident already between 7 and 28 days, exceeding the limits reached by concretes of equal characteristics, but packed only with Portland Cement.

The fly ash contributes to the slowdown of the grip in the early hours: this feature is valuable for huge casting and/or in the summer season. This slight delay phenomenon allows better hydration of the cement by reducing cracking or surface dusting phenomena. Fly ash can be used to replace part of the cement, in order to achieve better environmental performance: this topic will be discussed in chapter XX.

Overall, the FA's advantages are numerous:

- the reduction of the own weight of the structures (as they are used as cement substitutes);
- less and cheaper processing and easier transport;
- the improvement of the fire performance of the material;
- the improvement of environmental performance (due to the possibility of recycling of the material, the conservation of aggregate rocks and sand, the protection of the coasts and environments where it intervenes with the mines, the reduction of polluting emissions).

Silica fume

Silica fume is a by-product of the electric furnace production industry of metallic silicon and ferrosilicon alloys. It appears as amorphous silica in the form of microspheres, smaller than $0,1 \mu\text{m}$, which in the mixtures can be allocated in the interstices between the cement granules ($1-50 \mu\text{m}$) (Figure 2.7).

Aggregates

The aggregates occupy a significant portion, in volumetric terms, in the micro and macro structure of the mixture, and their quality, both physical and mechanical, also affects the final physical-mechanical properties of the concrete mix.

In particular, in the choice between the different potential materials, the form and nature of the various aggregates, including their maximum diameter, and the performance aspect must be kept in mind.

The grain size distribution may arrange a high packing density: the biggest portions of the aggregate have usually been removed, privileging a particle size that is below 1 mm [14]: small size aggregates are essential to prevent high fracture energy that occurs in the interface between aggregate and cement paste.

Moreover, is important to choose aggregate with high mechanical strength to avoid that they become weak section of the concrete. For example, it is recommended the use of calcined bauxite or granite, due to their mechanical properties.

Within UHP-FRCC wollastonite is commonly employed as one of the aggregates: it is a calcium meta-silicate (CaSiO_3) mineral with particles close to cement particles by size.

Wollastonite is easily available, acicular, inert of high elastic modulus. Its fibers are used as well to reinforce UHP-FRCC: they are very fine and able to enhance flexural strength and to change pre-peak and post-peak load behaviour of hydrated cement and cement-silica fume system [15].

About of the choice of the sand, often silica sand is used in UHP-FRCC. It is more expensive than the natural sand, with an average particles size of 0.2 mm. Nevertheless, adding normal sand to the mix, good mechanical performance and ductile behaviour are still preserved.

Super-plasticizer

Superplasticizers, also called high range water reducers, are chemical admixtures used to achieve a good workability of freshly concrete mixes. In fact, the packing density is

significantly high due to the fine size of the aggregates in the blend. For this reason, superplasticizers are required and suitable to increase the flow characteristics in densely packed systems.

A considerable amount, up to 5 mass-% of the cement, is necessary for the production of self-consolidating concrete and high performance concrete composites [12].

Furthermore, the water reducers have a solid content of around 30%: it has to be taken into account that the remaining liquid portion is counted as a part of the total liquid of the mixture.

The development of UHP-FRCC has been possible also due to the progress of SP additives. Especially the polycarboxylate ether-based superplasticizers allow the reduction of the water to cement ratio without negatively affecting the workability of the blend [16].

Fibers

The addition of fibers is one of the reasons of the high mechanical performances of UHP-FRCC, both in terms of ductility, tension and compressive strength. In fact, concrete is a brittle material and shows an unsatisfactory post-crack behaviour with a rapid failure of the specimen.

There are many types of fibers (Figure 2.8), but steel fibers are preferred over other type of fibers (polypropylene, nylon, carbon, etc.) due to advantageous properties, as high strength, high modulus of elasticity and high ductility.

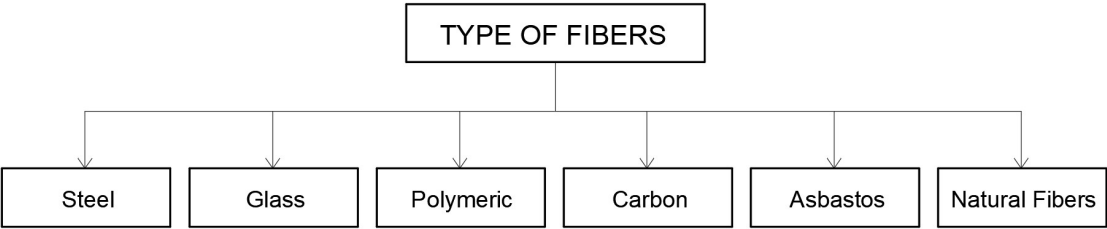


Figure 2.8 - Type of fibers

Steel fibers combined with low water/cement ratio mixtures can overcome the gap between the cracks. The role of fibers in the cracking process will be explained in detail in the next section.

Moreover, the concrete represents a protective environment against the corrosion by the alkaline agents. Nearer to the surface where the concrete may be carbonated, steel fibres may corrode in the presence of moisture. However, the corrosion doesn't lead to substantial damage for the structures.

The portion of fibers used to reinforce a concrete composite is calculated as a percentage of the total volume of the blend and it is called *Volume fraction* (V_f). Another parameter that describe the fibers is the *Aspect ratio* (l/d), obtained by dividing the fiber length (l) by its diameter (d).

For the description and the comparison of the properties between different UHP-FRCC, the *Fiber Factor*:

$$\text{Fibre Factor} = V_f \cdot l/d \text{ [17]}$$

In ordinary fibre reinforced concretes, the range of the length of the steel fibers is between 12 mm and 65 mm, and common diameters vary from 0.45 to 1 mm. Furthermore, the values of volume fraction are between 0.23% to 2%.

Concerning the UHP-FRCC, the length of the fibers may be smaller than 12 mm, and their volume can reach the 11% of the total volume.

In UHP-FRCC, the fibers are generally smaller than 12 mm, and the total content can be as high as 11 % by volume.

Nevertheless, it has been demonstrated that the best results in term of fresh and hardened concrete characteristics are obtained with a content of steel fibers of approximately 2,5 vol% with an aspect ratio between 40 to 60 [17].

If a large volume of fiber is added, the workability of the mixture will decrease and the cost of the UHP-FRCC will increase significantly. Consequently, it is necessary to minimise or optimise the content of fibers in order to achieve a required toughness and ductility. The content of this section was cited by Fantilli *et al.*(2009), who proposed an analytical model to predict the average crack spacing in high performance fiber reinforced cementitious composites (HPFRCC) based on a cohesive interface analysis.

Moreover, to guarantee a low porosity, the fibers length should be compare to the maximum diameter of the aggregates. In case of maximum grain size approximately of 0.5 mm, the fibers length should at least be 10 times higher than the maximum aggregate diameter.

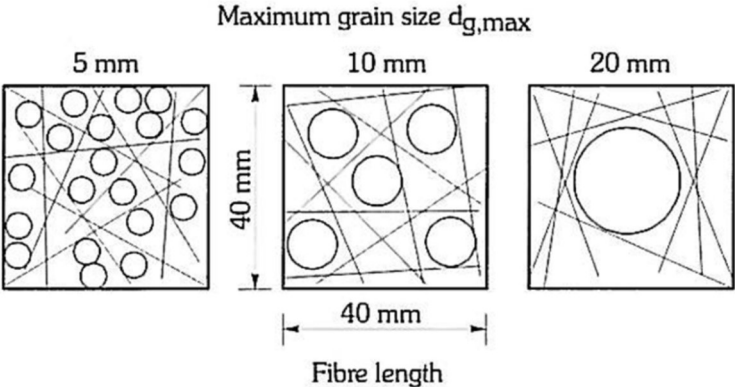


Figure 2.9 - Influence of d_{max} on fibre distribution [19]

In UHP-FRCC, the fibers added to the mixture are generally a combination of short and long fibers: when it is necessary a high workability, the amount of smaller fibers will be larger. However, different type of fiber are used according to the concrete type and his application, with the aim of optimising the shape, the size, and the percentage of volume.

2.3 Mechanical properties of UHP-FRCC

UHP-FRCC is defined as a new material, with exceptional properties, as very high strength capacity in compression, high ductility, high toughness and low permeability, compared to conventional concrete.

Typical values of compressive strength of UHP-FRCC are in the range between 150 and 220 MPa, but higher strengths can be reached, until around 400 MPa [20].

These performing mechanical properties are directly linked to the dense and interconnected microstructure with high homogeneity and to the low water/binder ratio: the porosity is considerably reduced, and a high durability is guaranteed [21].

On the contrary, due to the packing density, this material may be also very fragile. In the Figure 2.10, it is shown a typical stress-strain curve of UHPC without fibers: the concrete exhibits an elastic behaviour.

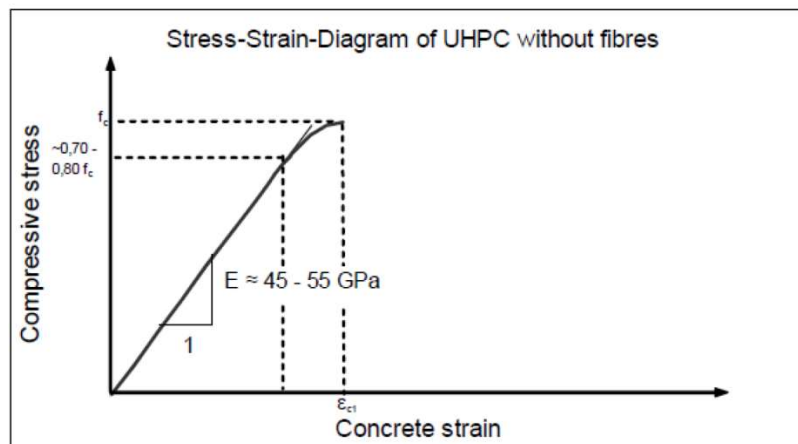


Figure 2.10 - Stress-Strain diagram of UHPC [22]

Therefore, UHPC without fibre reinforcement exhibit a very dramatic and brittle failure under compressive load. To overcome this brittle behaviour, fibers are added due to their restraining and confining effects [23], to obtain a ductile failure (Figure 2.11). The slope of the descending branch principally depends on the characteristics of the fiber, as their content, geometry (length and diameter), stiffness and orientation.

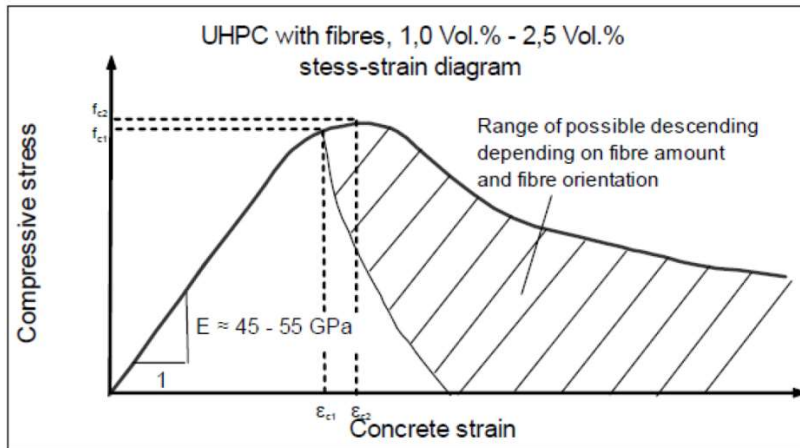


Figure 2.11 - Stress-Strain diagram of UHP-FRCC Stress-Strain diagram of UHPC [22]

Naaman and Reinhardt demonstrated the potential of HPF-RCC [24] [25], as shown in Figure 2.12.

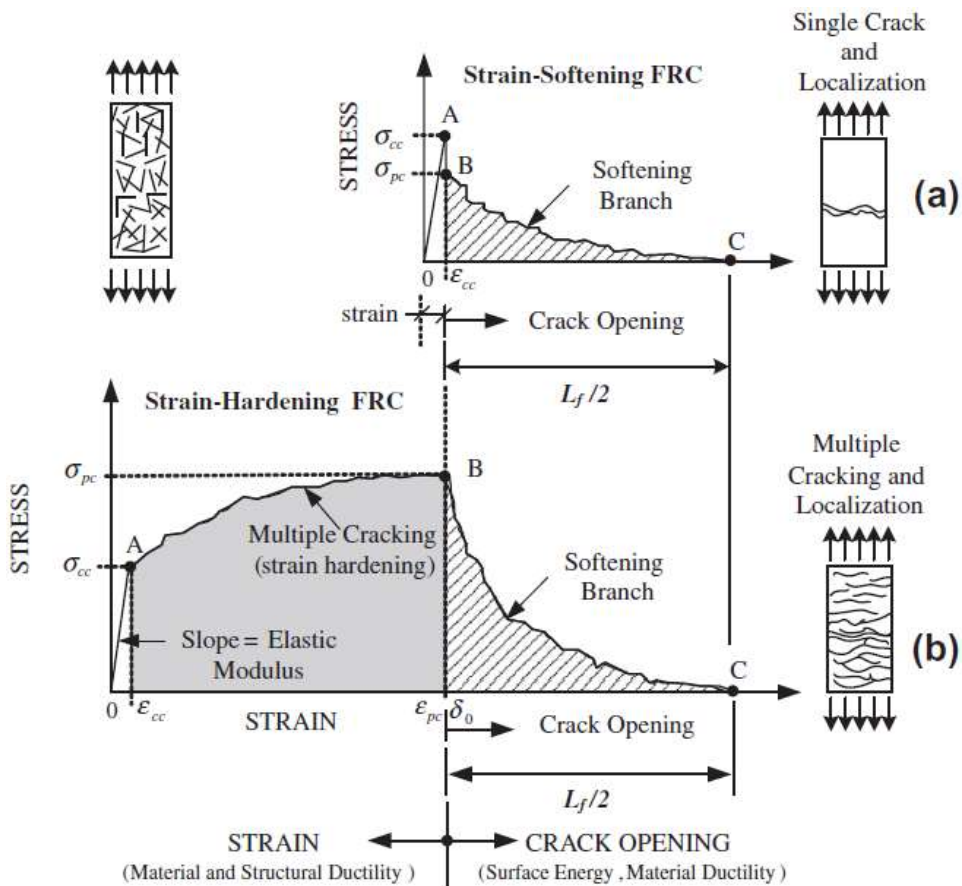


Figure 2.12 - Typical tensile strain softening (a) and hardening behaviour of HPF-RCC (b) [25]

After the manifestation of the first crack, HPF-RCC exhibits pseudo strain-hardening response and multiple cracking behaviour.

Consequently, it provides an extraordinary energy absorption before the fracture, and experiences distributed cracking with very small crack size prior to crack localisation.

UHP-FRCC, therefore, can be a practical answer to improve the resistance of buildings and other infrastructures thanks to their ductility and energy absorption capacity, coupled with the ultra-high strength.

For a better and clearer understanding of the cracking process of UHP-FRCC, Rossi proposed the following definitions [20]:

- “A *microcrack* is a crack whose length can be considered to be very small in relation to the size of a specimen or a structure”;
- “A *macrocrack* is a crack whose length cannot be considered to be very small in relation to the size of a specimen or a structure”;
- “An *active crack* is a crack whose edges undergo normal or tangential displacements”;
- “A *critical and active crack* is a crack which leads to a concentration of stresses and a localisation of strains within a volume of concrete”.

Logically, it follows from these definitions that an *active macrocrack* is an *active microcrack* that has become critical.

The transition from the material behaviour to the structure behaviour can be described as a sequence of two phases. At first, the microcracks are distributed randomly and without a prevailing orientation: the macroscopic mechanical behaviour remains essentially the same and it is intrinsic to the material. Subsequently, macrocracks occur and they are initially distributed in various orientations, in the same manner of the microcracks. On the contrary, in this case, the macroscopic mechanical behaviour will depend on the position of the macrocracks in the specimen and, in this case, it is considered structural.

In a general sense, short fibers are principally required to act on microcracks, while long fibers are mostly involved in macrocracks. In Figure 2.13 it is exemplified the role played by the micro and the macro fibers during cracking process.

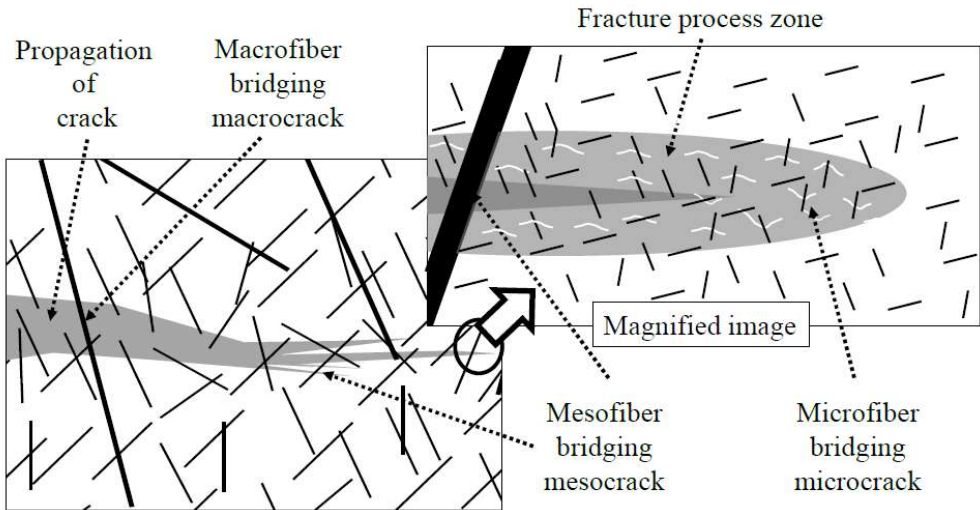


Figure 2.13 - Schematic illustration of multi-scale fiber-reinforcement system [26]

Under compression load, microcracks are initially generated randomly, with a preferential orientation that is parallel to the applied stress. This orientation is ruled by the presence of two phases in cementitious composite (cement paste and aggregates), that have different stiffness: under longitudinal compression, tensile stress, develops perpendicular to the direction of the compressive stress, assuming that these cracks are created by tension. In the second step, microcracks join together and contribute to the formation of macrocracks, that progress parallel to the direction of compressive stress. Then, diagonal cracks appear and, growing in size, they create a diagonal descending plane at the scale of the specimen.

Moreover, the high proportion of short fibers improves both tensile strength and ductility at the material scale, whereas the addition of long fibers permits to increase the ductility at structure scale. Instead, the compressive strength results less influenced by the amount

of short fibers; on the contrary, the bearing capacity and the ductility at structural scale continue being enhanced by long fibers.

Regarding the durability, researches show that UHP-FRCC has very good durability properties. A significant study of Graybeal confirms that the durability characteristics of UHP-FRCC are considerably better than those of traditional concrete [27].

Toledo Filho [28] also reaches the same conclusion in their study. With a probabilistic analysis, they found that the cover thickness made of UHP-FRCC could be a factor of 10 less than for normal concrete, continuing maintaining the same protection of the reinforcement bars.

For these reasons, UHP-FRCC may be a suitable material for surface protection and it may be used in impermeable situations, particularly under extreme conditions, as roads, or marine structure.

All these high mechanical properties of UHP-FRCC, however, deal with a parallel high ecological impact, that will be analysed in the next section.

2.4 Ecological impact of UHP-FRCC

Concrete is the most frequently used building material in the world and its annual production is of approximately 10 billion m³ [29] [30].

In the European Union, the building and construction sector is responsible for about the 40% of total energy consumption; moreover, in the European countries the building industry causes around 70% of the total material flow [31].

Furthermore, the concrete industry accounts for around 8% of total anthropogenic CO₂ emissions on a global scale, whose approximately 90-95% is attributable to the production of Portland cement [32] [33]. This derives, at first, from the de-acidification of limestone, that represents the main raw material in cement production and, secondly, from the energy compounds required to reach the calcination temperature of 1450 °C.

The remainder CO₂ is linked to the transportation of raw materials and finished products and to manufacturing and construction procedures [34].

These data show the dramatic priority that should be given to the sustainability in the building sector. Consequently, besides the efforts in the development of new construction materials, the question of sustainability has gained more and more consideration in the last years and has become one of the main focuses in the field of construction materials industry.

A considerable potential reduction of the environmental and ecologic impact of concrete may lie in a partial substitution of cement with other substances that may act as binders. This has a very important significance particularly for what concerns concrete materials with a high cement content, as the UHP-FRCC used for this research.

In this experimental investigation the high amount of cement used for UHP-FRCC is the main cause of the considerable high environmental impact. In fact, as it can be seen in Figure 2.14, the volume of cement present in a UHP-FRCC mixture is about three or even four times higher than that contained in an ordinary concrete blend.

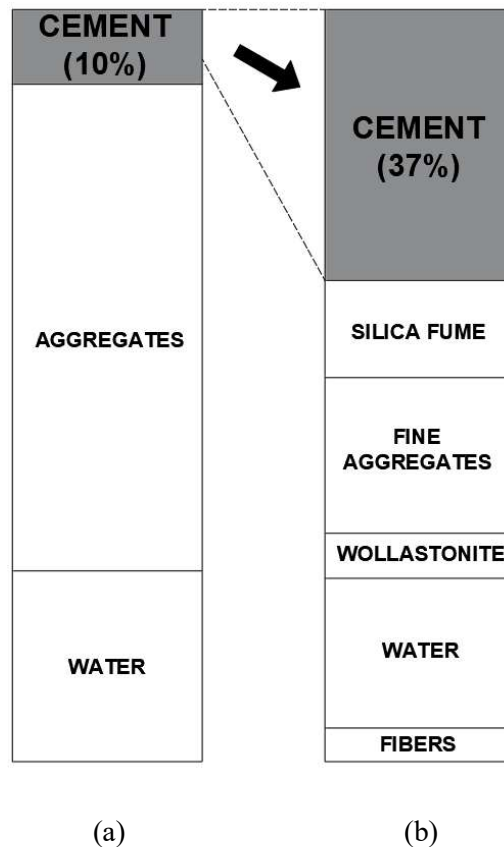


Figure 2.14 - Cement content in (a) ordinary concrete and (b) UHP-FRCC (Volume ratio)

To evaluate the ecological performances, the parameter considered is the amount of CO_2 released during the activities linked with the production of 1 m^3 of UHP-FRCC. Accordingly, in the following section a substitution strategy to reduce the CO_2 emission is going to be presented.

2.5 Material substitution strategy: reduction of the CO₂ emissions

As outlined in the previous section, the cement manufacture has a dramatic impact on environment.

For this reason, in this experimental research the “material substitution strategy” is analysed and developed. The “material substitution strategy” is shown in Habert and Roussel’s work [35] and, as the name suggests, it is a strategy based on a partially replacement of cement with other substances, with the aim to low the environmental impact.

During the experimental investigation, different amounts of cement were substituted with fly ash, a waste by-product derived from coal burning (Figure 2.15)



Figure 2.15 - (a) Cement and Fly Ash powders comparison; (b) Finer and more spherical Fly Ash particles than Cement

The choice of fly ash is due to the fact that its CO₂ emissions are far lower than those of cement and, additionally, fly ash mixed with mortar acts as a binder [36].

Although the main advantage of fly ash lies in the reduction of the environmental impact resulting from the reduction of cement, it presents also other qualities as the improvement of workability of concrete, the enhancement of strength, water tightness and durability of concrete at advanced ages. A previous study [37] shows the progressive decrease of the ecological impact, in terms of CO₂, NO_x, SO_x and PM emissions of mixes containing different percentage of fly ash (Figure 2.16)

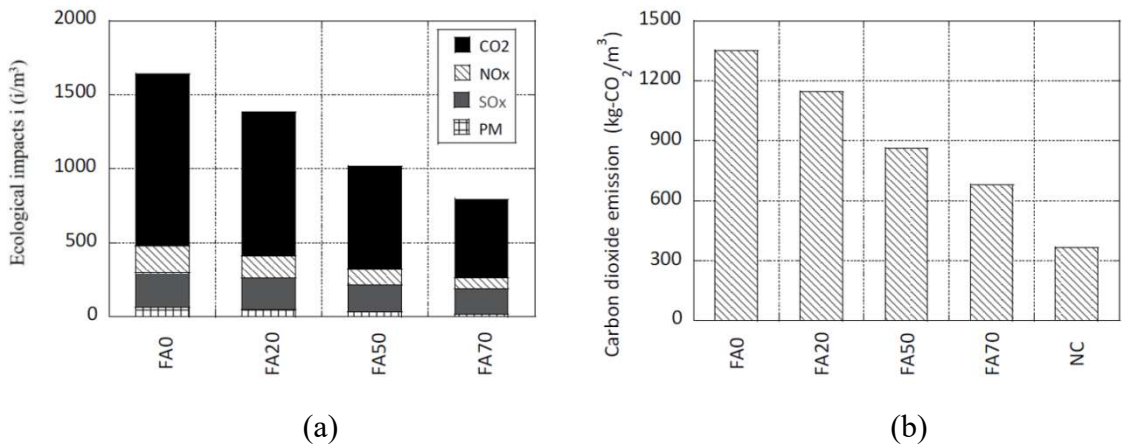


Figure 2.16 - The impact of a cubic meter of UHP-FRCC, in terms of greenhouse gases emission (a), and carbon footprint (b) [37]

Moreover, Fantilli *et al.* (2009) investigated the impact of a reinforced concrete beam with different mixtures having different amount of fly ash in substitution of cement. The following graph (Figure 2.17) illustrates how values of f_{cA} can be reached with different percentages of substitution of the cement, despite with different amount of CO₂ released in the environment.

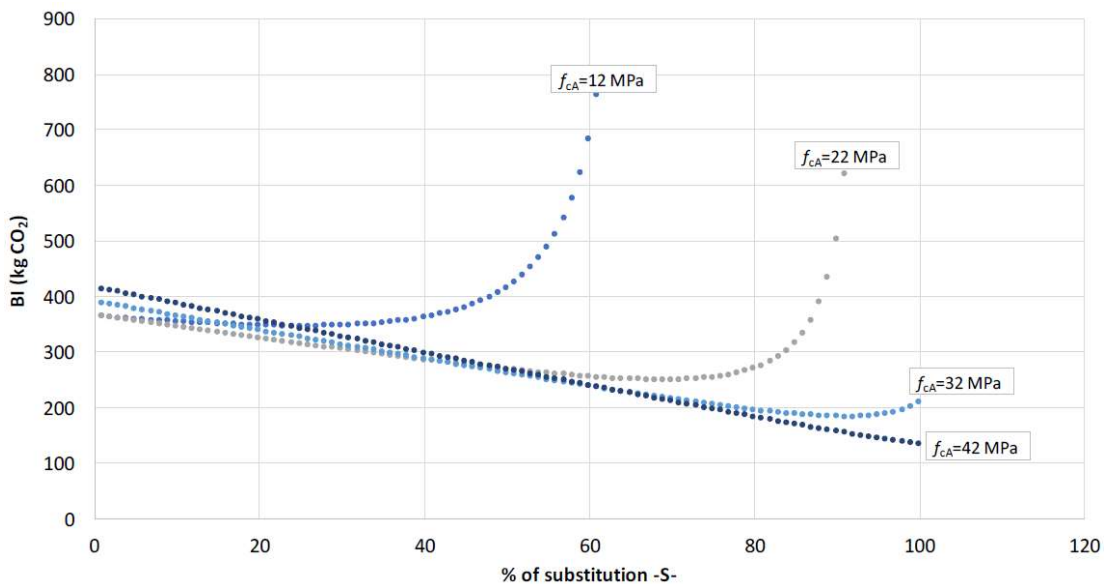


Figure 2.17 - The impact of a reinforced concrete beam made with different concretes (having different f_{cA}) [38]

As mentioned above, because of fly ash particles are finer and more spherical than Portland cements ones, the microstructure of UHP-FRCC is denser and featured by low porosity, thereby exhibiting excellent durability [39].

Consequently, substituting part of the cement content with fly ash may be an decisive choise to achieve very good properties of UHP-FRCC.

Whereas the amount of fly ash in a cementitious composites is above the 50%, concrete is usually defined as High Volume Fly Ash (HVFA) [40]. Moreover, HVFA concrete shows high resistance to freezing and thawing cycling, low water permeability, great response to chloride ion penetration, and high resistance to both carbonation and sulphate attack [41].

In Figure 2.18, a first anticipation of the “material substitution strategy” is shown: four UHP-FRCC mixes with different percentages in volume of cement replaced by fly ash are considered.

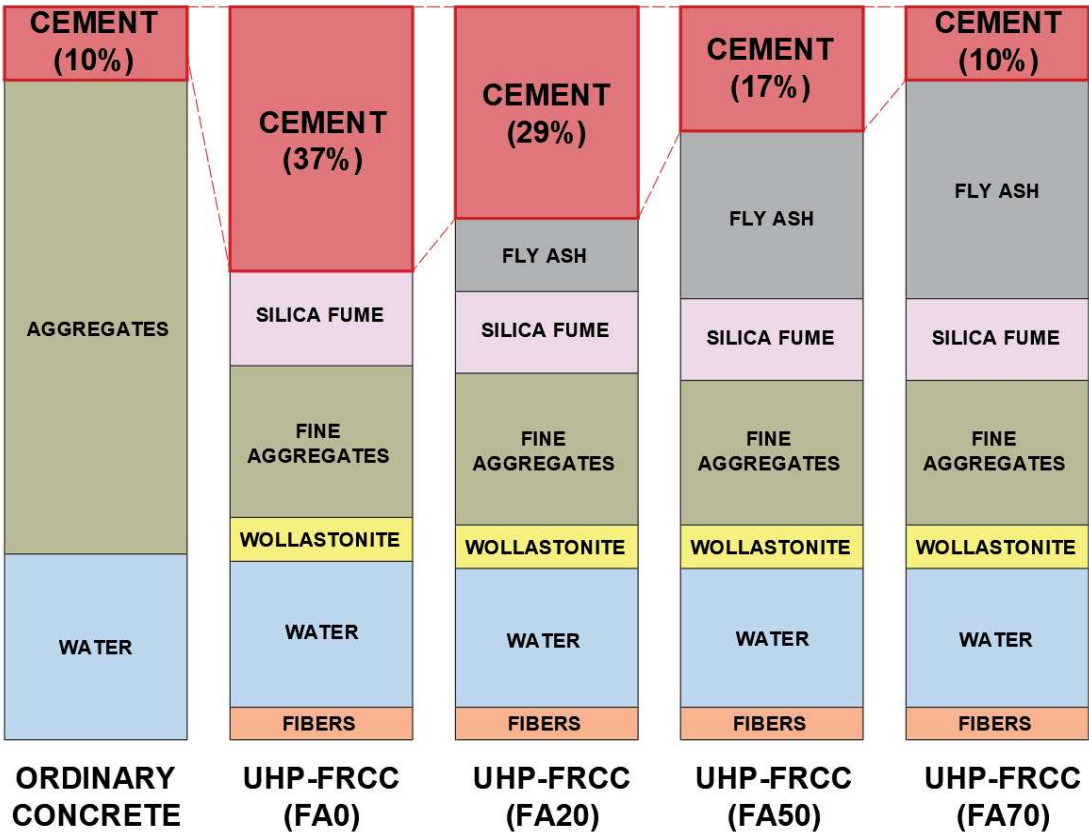


Figure 2.18 - Mix proportion comparison (Volume ratio)

As it can be seen from the figure, for FA70 mixture (with 70% of cement substituted by fly ash), the total amount of cement is the same of that of an ordinary concrete mix proportion.

Indeed, the substitution of cement with HVFA doesn't always lead to advantageous results: in fact, even if a high percentage of fly ash has benefits on the ecological impact, it contributes to the reduction of the strength of Ultra High-Performance-Fiber Reinforced Cementitious Composites, especially at early age [42].

In fact, sometime the benefits on the environment don't compensate the decrease of the compressive strength, which is not always higher than 150 MPa.

In that capacity, the replacement of cement with fly ash should be investigated and managed with the aim of balancing both mechanical and ecological performances. For this reason, the *eco-mechanical analysis*, described in the next section, may be useful to find the proper amount of cement substitution.

2.6 Eco-mechanical analysis

An *eco-mechanical analysis* was proposed by Fantilli e Chiaia [43]: it was performed with the purpose of finding the best ecological solution without compromising the mechanical performance of ultra high-performance fiber-reinforced cementitious composites.

This analysis is conducted with a chart (Figure 2.19). On the horizontal axis the mechanical response is reported: it is described by the Mechanical Index (MI) divided by MI_{inf} , the lowest bound value of the mechanical characteristics. On the vertical axis, indeed, the ecological performances are reported, defined by the Ecological Index (EI) divided by EI_{sup} , being the uppermost bound value of ecological impact represented by EI_{sup} .

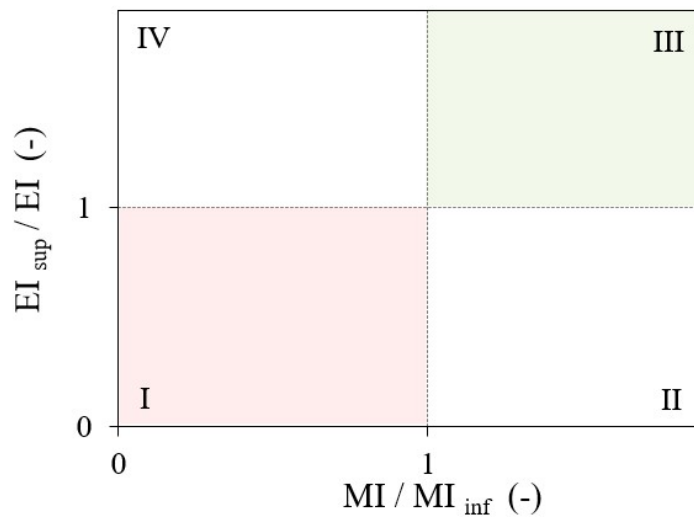


Figure 2.19 - Non-dimensional chart for assessing the eco-mechanical performances

Therefore, four different zones (quadrants) can be distinguished within the diagram:

- Zone I: Low mechanical performances – Low ecological performances
- Zone II: High mechanical performances – Low ecological performances
- Zone III: High mechanical performances – High ecological performances
- Zone IV: Low mechanical performances – High ecological performances

Certainly, the purpose of this research is to investigate different solutions falling in the green region of Figure 2.19.

Regarding the ecological performances, the mass of CO₂ released by the production of 1 m³ of UHP-FRCC was considered as an environmental indicator.

Moreover, different mechanical parameters were analysed to represent the mechanical performances, i.e. the maximum compressive stress and the ductility.

In Figure 2.20 an eco-mechanical analysis at material scale is presented [44]: in this case the normal concrete is compared with different UHP-FRCC mixtures. The mechanical index (MI) is assumed to be the compressive strength of concrete; for this reason, all the points fall in the Zone II, due to the high mechanical performances but weak ecological features.

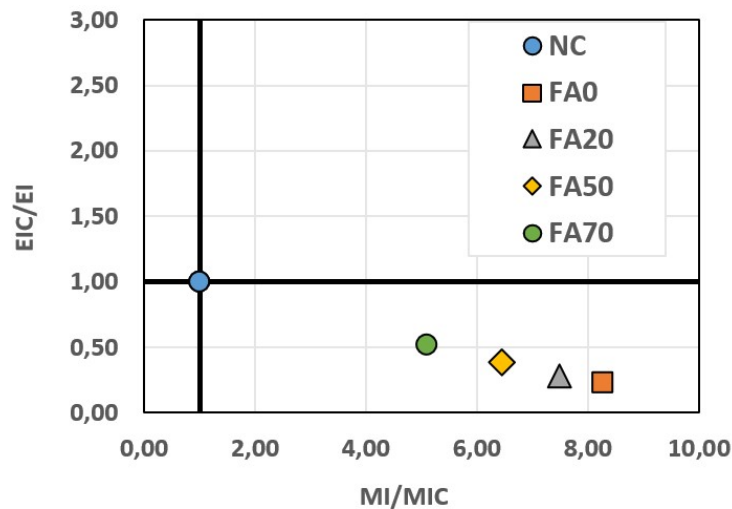


Figure 2.20 - Eco-mechanical analysis at material scale [44]

For this experimental research, two different eco-mechanical analyses have been carried out, and described in Chapter XXX.

2.7 Applications of UHP-FRCC: repair and rehabilitation

Several applications of fiber reinforced concrete composites have been advanced, from stand-alone constructions, as cement panels, sheets, pipes, slabs and prefabricated elements, to hybrid solutions, in combination with other structural material (e.g., normal concrete, steel, and so forth). Moreover, UHP-FRCC is increasingly used for process of reconstruction and rehabilitation of the existing buildings (Figure 2.21) [45].

Another relatively recent application is the seismic retrofitting, aimed at improving the system behaviour of old structures and at letting the structural components reaching the desired performances. Other significant examples can be found in jacketing to strength columns, beams and walls, lining for tunnel and other special structures, such as particular bridges, super high-rise buildings and offshore platforms.

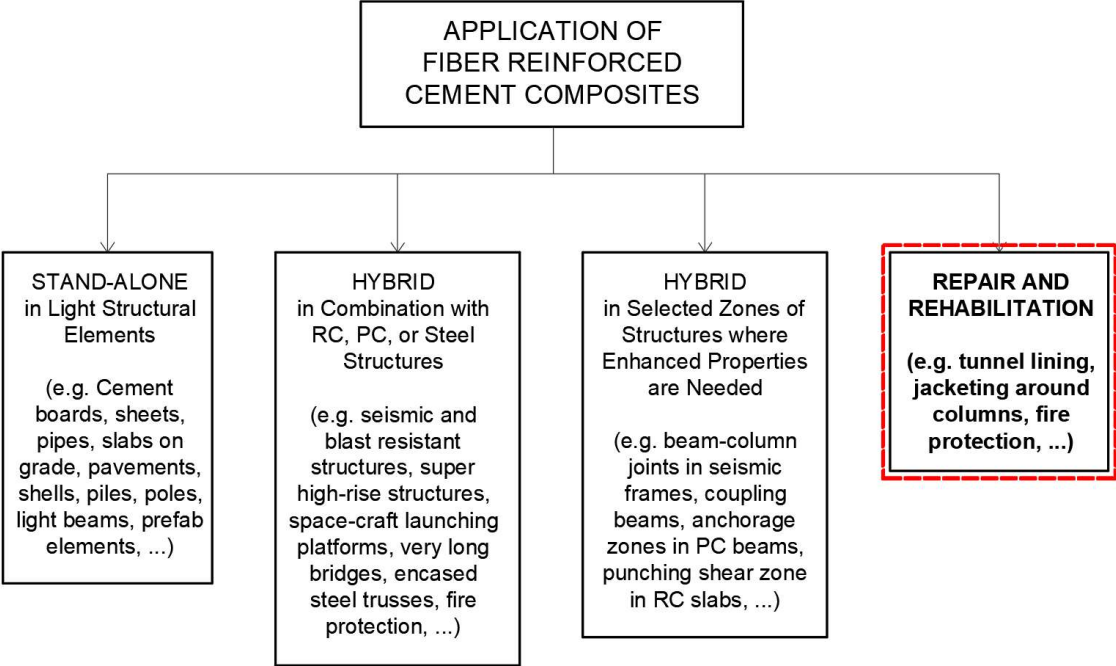


Figure 2.21 - Classes of application of fiber reinforced cement composites

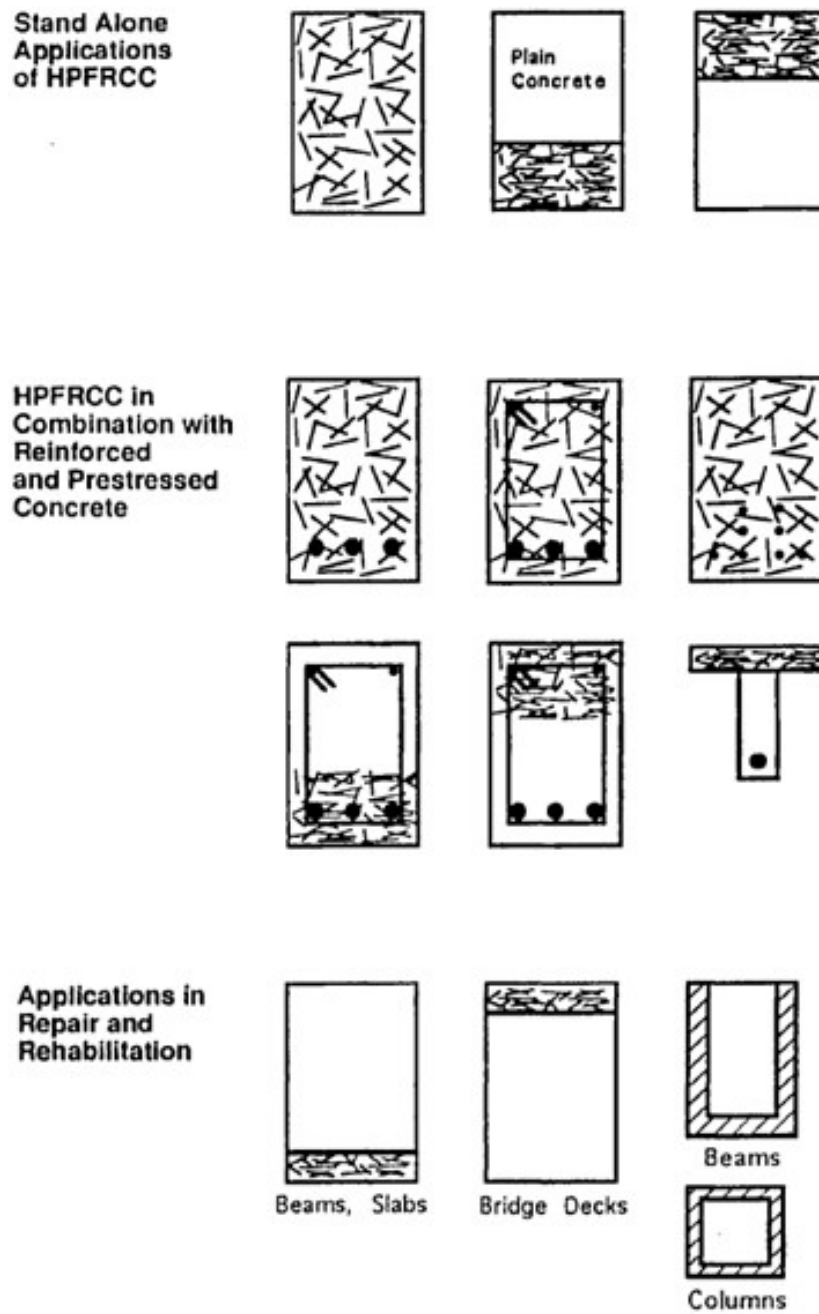


Figure 2.22 - Typical application of HPFRCCs [46]

One of the most well-known and relevant applications of FRCCs is precisely the retrofitting of existing structures, and especially the jacketing of concrete columns and beams.

The chief aim is to employ UHP-FRCC to ‘harden’ those parts of the structure that are exposed to high environmental and mechanical loading, leaving the other zones subjected to a relatively moderate exposure in their original shape (Figure 2.23 a and Figure 2.24).

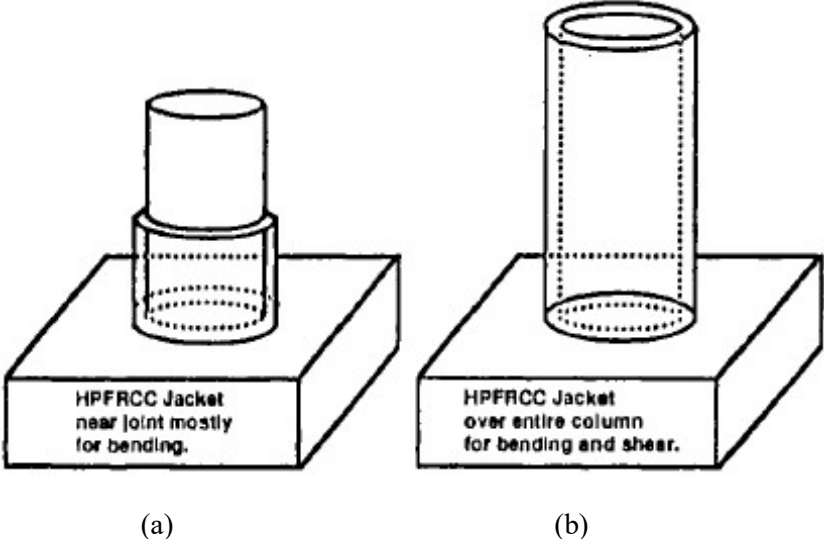


Figure 2.23 - Applications of HPFRCCs for repair and strengthening of concrete [47]

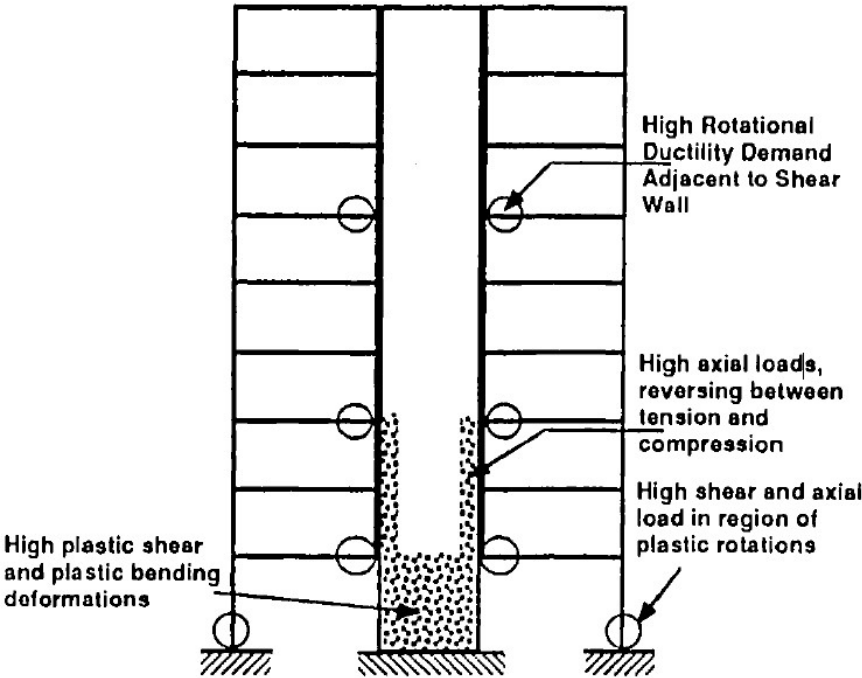


Figure 2.24 - Examples of selective use of HPFRCC in seismic resistant structures

This idea might be utilised not only for old constructions, but also for the new ones; this inevitably leads to composite structural elements combining conventional reinforced concrete and UHP-FRCC.

The combination of the protective and load carrying properties with the mechanical performance of reinforcement elements offers an efficient way to increase the stiffness of the structures.

In earthquake predisposed areas the priority, immediate and urgent necessity is the strengthening of unreinforced masonry. The recent earthquakes in the central areas of Italy, especially in L'Aquila (2009) and Amatrice (2016), have highlighted the inadequacy of most of the existing historical structural system. The falling down of masonry buildings without seismic adjustments is one of the most relevant causes of serious damages and mortalities after strong earthquakes worldwide, especially in historic zones and in low and middle income countries.

In the city of L'Aquila, following the strong earthquake that hit the city, some damaged structures were reinforced with relative new technologies, which imply the use of UHP-FRCC.

An example is the seismic retrofit intervention of a reinforced concrete building in Coppito (AQ) (Figure 2.25 and Figure 2.26).

The design choice of the jacketing in UHP-FRCC for seismic improvement was aimed at the widespread activation of the entire construction of ductile mechanisms with the consequent plasticisation of the sections without causing any collapse of the structure. The jacketing was carried out using micro fiber-reinforced concrete (*Tecnochem*, 2012), allowing a homogeneous reinforcement to be achieved, and ensuring an appropriate confinement effect as well as an increase in the bending and shear strength of the structural elements, while improving the durability of the structure thanks to the performance of the micro concrete matrix itself. The seismic intervention included the jacketing of beams, columns and nodes [48].



Figure 2.25 - Casting phases of seismic retrofit intervention with UHP-FRCC



Figure 2.26 Apartment block G4, via Beffi, Coppito, before and after the intervention of seismic adaptation

UHP-FRCC is also applied for cover particular zones of reinforced concrete structures, as bridge piers and retaining walls, due to their extreme exposure to aggressive substances, such as salts and other de-icing agents.

These components generally show inadequate durability if they are made with traditional reinforced concrete. Moreover, UHP-FRCC is able to guarantee both needed durability and mechanical performance of such structural elements.

For these reasons, since 2004 UHP-FRCC is employed in Switzerland on existing reinforced concrete bridge deck slabs as thin watertight layers, replacing the currently used waterproof films.

The first application in this field of UHP-FRCC was for rehabilitation and enlargement of a short length road bridge subjected to heavy traffic (Figure 2.27).

The examination of construction costs showed that this rehabilitation operation obtained with UHP-FRCC was less expensive than traditional methods, that nevertheless provide lower performances in terms of durability and life-cycle costs.

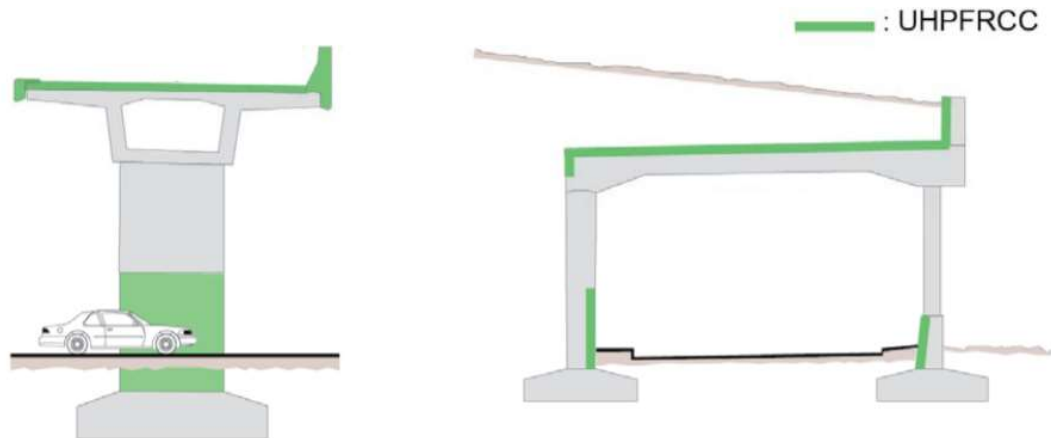


Figure 2.27 - Concepts of applications of local "hardening" of structures with UHP-FRCC [49]

Another effective example of jacketing made by UHP-FRCC is the Valabres bridge in France. Due to degraded parts at the bottom of the pillars, a structural reinforcement was likely to be necessary. In this case, a subtle UHP-FRCC protecting shell was cast in place around the existing structure, after removing the degraded portions of the columns.



Figure 2.28 Repair and protection of foundations and supports of the Valabres viaduct

In short, the UHP-FRCC is remarkably suitable for strengthening structures sited in seismic zones, for constructions with foundation problems and for elements subjected to aggressive environmental conditions.

Because of the embryonic literatures in this field compared to the relevance of the topic, the main purpose of this research thesis is focused on the investigation of the behaviour of normal concrete structures, reinforced with UHP-FRCC jackets, that may be used in several retrofitting, maintenance and repair applications.

CHAPTER 3

DESIGN AND EXPERIMENTAL INVESTIGATION

3.1 Work experience at Life Cycle Engineering Laboratory

3.1.1 Brief description of the Laboratory

The present experimental investigation has been carried out at Life Cycle Engineering Laboratory (henceforth, LCEL), a high-tech structure in which research projects relating building materials and structural solutions are designed and developed.

Therefore, this laboratory, managed by highly qualified and specialised personnel, significantly contributes to research and education of the Department of Architecture and Building Science of the Graduate School of Engineering at Tohoku University.

The Laboratory is equipped with several testing apparatus and measuring instruments for mechanical and physical tests. The activities range from experimentation on structures and structural elements, to the chemical-physical and mechanical experimentation of building materials. In addition to tests on concretes, bricks, mortars, steel, rocks, the laboratory is equipped to perform experimental tests on innovative materials, including steel or polymeric fibers.

Sectors that play an important role in these areas are the characterisation and the study of fiber-reinforced cement-based composite materials and structural elements, in particular for structural reinforcement and the anti-seismic adaptation of building and civil structures.

The studies cover the mechanical features of the individual components (fibers and matrices), the composites, and the reinforced structural elements (concrete and steel) as well as the analysis of their durability and the non-destructive testing in situ.

One of the main tasks of the LCEL is to develop experimental researches and investigations in an environmentally responsible manner, giving priority to solutions with reduced ecological impact.

In this Laboratory, students from different countries of the world work synergistically on research projects, under the careful supervision of professors, academic scholars and technical staff (Figure 3.1).

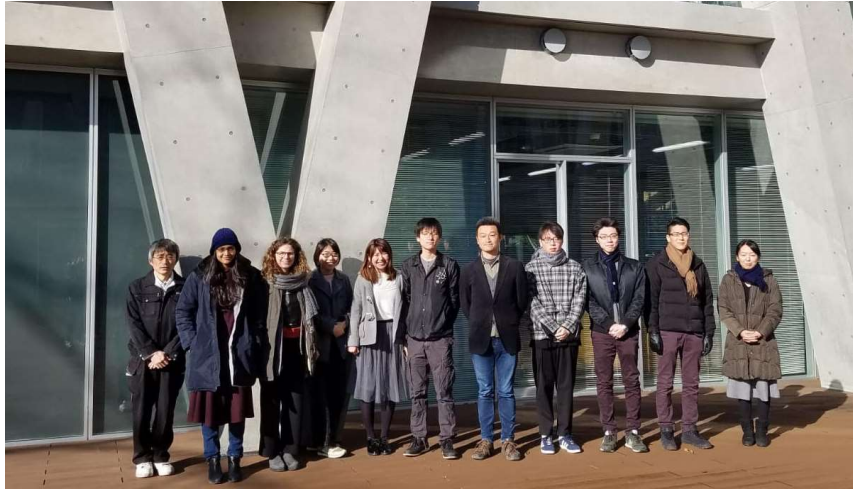


Figure 3.1 - Members of Life Cycle Laboratory

The Laboratory is composed of different areas:

- *Student's work stations* (Figure 3.2): each student has a desk used for the preparation and the organisation of the experiments. Moreover, bench instruments and other equipment for test are available.
- *Curing chamber* (Figure 3.3a): it is a room with a constant temperature of 20°C and a humidity of 95% used to keep and conserve the specimens until the day of testing. In this way the process of hardening is constant and not subject to temperature changes.
- *Storage room* (Figure 3.3b): proper precautions for the storage of cement and other binders such as duration and place of storage, arrangement, atmospheric moisture content, etc. are necessary. These materials are collected in a specific room with a controlled atmospheric moisture content and temperature to preserve their integrity.
- *Experiment and casting area* (Figure 3.4): the casting of cementitious composites and other experiment are carried out in an equipped area of the laboratory.

- *Testing area* (Figure 3.5): different Universal Testing Machines (UTM) are used to test the tensile strength and compressive strength of materials. These are versatile instruments that can perform many standard tensile and compression tests on materials, components, and structures.



Figure 3.2 - Life Cycle Laboratory: student's work stations



(a)



(b)

Figure 3.3 - (a) Curing room with constant temperature of 20°C; (b) Storage room



Figure 3.4 - Life Cycle Laboratory: experiment and casting area



Figure 3.5 - Life Cycle Laboratory: testing area

3.1.2 Work methodology

In order to meet the requirements in the most efficient and effective way, a working methodology identifying the key phases of the process has been implemented to achieve the research objectives.

The main scheme of the experimental work is illustrated in the Figure 3.6.

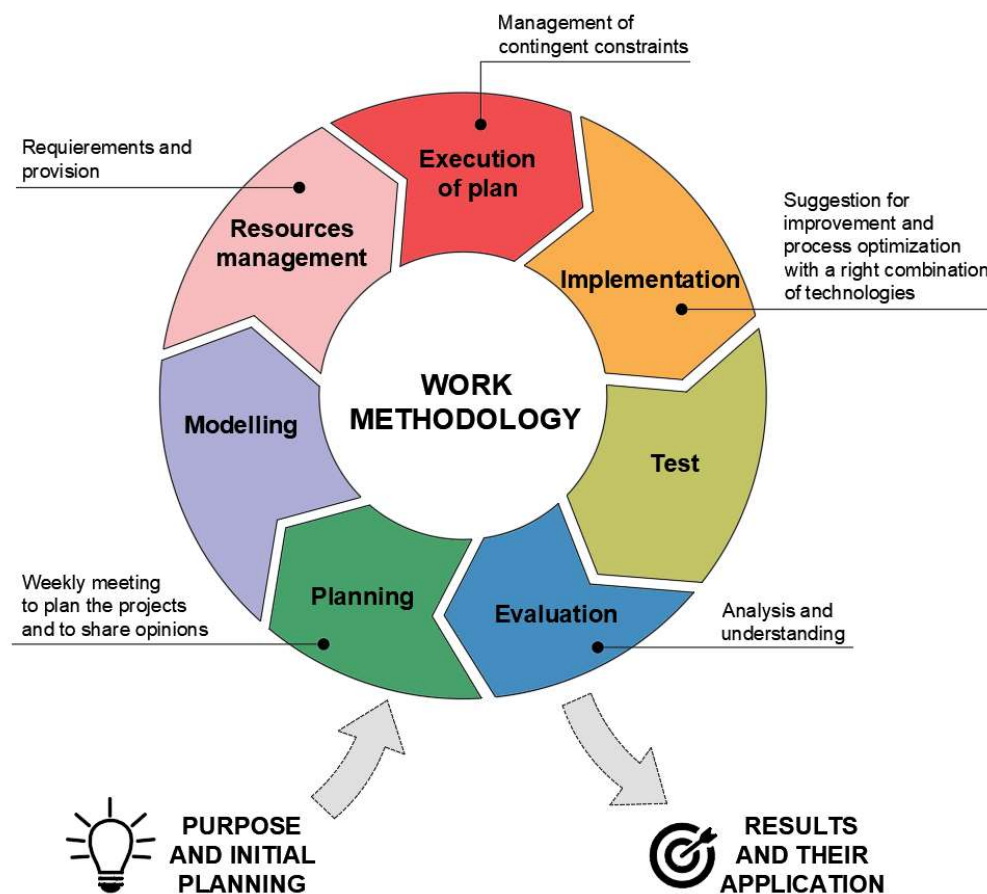


Figure 3.6 - Work methodology process

First, previous studies related to the current research were comprehensively studied and analysed to identify the key points of the research and to find the aspects to be reviewed and developed, with deep investigation paid to the concrete jacketing technique.

After this preliminary phase, the process consists in the following macro-moments:

- *Planning*: it is the process of deciding in detail how to do something before you actually start to do it. After the initial purpose and summary objectives for this research, a constant planning is carried forward: the schedule of experiment is shared and discussed with all the members of the Laboratory during the weekly meeting (Figure 3.7) in order to avoid practical problems, as overlap in the use of instrumentations, and above all to exchange views and ideas to improve and optimise the experimental plan.



Figure 3.7 - Weekly meeting

- *Modelling*: it is the phase in which, starting from a theoretical point of view, a punctual tangible model is described and designed. In the case of this research, it is the choice of the geometry of the samples and the materials composition.
- *Resources management*: due to the wide range of materials used in this experimental research, it is a daily duty to check their availability and, when necessary, the supply request.
- *Execution of plan*: it is the practical step, when the theoretical speculations and the conceptual modelling are put into practice. In this case, the execution of plan refers to the activities of cementitious composites casting, with all the supporting phases (preparation of materials and equipment). It is one of the most crucial moments, because sometimes contingent constraints have to be faced. Obviously.

some experiments couldn't work as we expected, for example wrong amount of water reducers may entail mix that are too much fluid or, on the contrary, not workable (Figure 3.8). For this reason, several trials were carried out to verify and to eventually slightly adjust the percentage of each material in the mix, in order to reduce the changes of failure during the main experiments.



Figure 3.8 - Example of mixes with a not appropriate workability

- *Implementation:* each experiment is subjected to a continuous process of optimisation with a right combination of technologies, adapting to the new requirements occurred during the execution phase.
- *Test:* after the preparation of the sensors and the equipment for the test, uniaxial compression loading tests were carried out to study the ultimate load and the evolution of the deformation.
- *Evaluation:* testing results of the specimens were collected, refined, analysed and compared. Conclusion and recommendations were issued based on the experimental program results and data analysis.

This cyclic process leads to results that are used for practical applications, and also as a starting point for new investigations.

3.2 The purpose of the research

As already explained in the literature overview of UHP-FRCC (see Chapter 2), cementitious composites with low water/binder ratio combined with a proper quantity of fibers (steel, polymeric, glass, etc) show by far higher mechanical performances than traditional concrete. Notably, UHP-FRCCs used in rehabilitation and retrofitting solutions decrease the brittleness of the structures and increase their energy absorption capacity. Moreover, the high compressive strength, obtained through dense particle packing, leads to other advantages, as high durability, improved resistance against freeze-thaw cycles and various chemicals.

The main goal of this experimental research is precisely to simulate a retrofitting application of concrete structural columns: cylinder specimens, whose dimensions are smaller than real columns, made of normal concrete are reinforced with UHP-FRCC jackets in order to investigate and analyse their behaviour under compressive load.

The ultimate load carrying capacity will be considered as the main mechanical parameter, as well the energy absorption capacity, strongly linked to the ductility of the sections and of the hole structure.

Specifically, this research is focused on three main aspects:

1. Investigating the confinement effect of UHP-FRCC jacketing, in order to find a relationship between the size of the jackets and the mechanical properties, in terms of maximum compressive stress and ductility.
2. Evaluating the performances of samples with the same shape but changed material composition: as anticipated in Chapter 2.5, cement may be replaced in different percentage by fly ash, with a view to achieve a lower environmental impact.
3. Correlating the mechanical responses of UHP-FRCC jacketing with the ecological performances, in order to figure out what are the best eco-mechanical solutions among several options.

All these key points are analysed in the remainder of the thesis.

3.3 Previous investigations at Life Cycle Engineering Laboratory

This experimental research has been preceded by other investigations on ultra high-performance fiber-reinforced cementitious composites conducted at Life Cycle Engineering Laboratory.

Suzuki Keita¹ investigated the behaviour of UHP-FRCC beams containing high volume of fly ash under tensile stress, assessing the mechanical properties and the CO₂ emissions. More related to the goal of this thesis, two studies on UHP-FRCC jacketing were carried out from previous students of Tohoku University: both researches investigated the behaviour of concrete samples (cylinders and beams) confined with this high-performance material, subjected to compressive or tensile stress.²

Taking as a starting point these researches, and particularly their suggestions to extend the experimental project, a wider investigation on confined concrete cylinder has been performed, which in many aspects implemented some techniques used in previous studies. In particular, more layouts for specimens have been designed and then tested in order to achieve a complete range of results for a robust experimental model.

As suggested, new tests have been performed by changing the thickness of the jackets, by investigating the increase in stiffness not predicted previous studies, and different UHP-FRCC layers, in terms of binder composition, have been implemented [44].

To have the possibility to compare directly this research with the previous ones, the same layout and mix proportion for concrete cores was used; moreover, concerning the UHP-FRCC mixtures, the same mixing, casting, curing and testing procedures have been conducted.

¹ Suzuki Keita, “Mechanical and ecological properties of ultra high performance – fiber reinforced cementitious composites containing high volume fly ash”, Master thesis, Life Cycle Engineering Laboratory, Life Cycle Engineering Laboratory, Tohoku University, 2016

² Monica Longo, “The behaviour of concrete confined by Ultra High Performance – Fiber Reinforced Cementitious Composite”, Life Cycle Engineering Laboratory, Tohoku University, 2017

Valerio Lisi, “Ecological and mechanical properties of ultra high performance – fiber reinforced cementitious composites containing fly ash”, Life Cycle Engineering Laboratory, Tohoku University, 2018

3.4 Types of concrete cylinders reinforced with UHP-FRCC jackets

As anticipated, the present research study aims at investigating the behaviour of concrete cylindrical samples reinforced with UHP-FRCC jackets and subjected to uniaxial compression, with a view to recreate a retrofitting system.

Different types of jackets were designed and casted, combining variations in size and in materials composition.

Relating the size of the UHP-FRCC jackets, four thickness were chosen, compatibly with the availability of the molds (a detailed description of the geometry can be found in the following section).

As mentioned in Chapter 3.2, one of the main purposes of the present experiment is to find a correlation between the size of the jackets and the mechanical properties, especially in terms of maximum compressive stress. Accordingly, this may be investigated with more specimens made of the same material but of different sizes.

The literature doesn't show evidences in this area of the research, but a positive linear relationship, meaning an increasing compressive stress of the sample with the increasing of the thickness of the jacket, can be supposed to hold. In this way, in case a direct proportionality exists, the amount of UHP-FRCC could be computed to achieve the desired mechanical performances.

More concerning the composition of the UHP-FRCC mixes, following the "material substitution strategy" four mixtures were prepared, modifying only the percentage of cement and fly ash, being unchanged the portions of other materials (that will be described in detail in Chapter 3.4.2):

- FA0: 0% of cement replaced by fly ash
- FA20: 20% of cement replaced by fly ash
- FA50: 50% of cement replaced by fly ash
- FA70: 70% of cement replaced by fly ash

From this point on, the notations FA0, FA20, FA50, FA70 will be used to indicate the UHP-FRCC mixtures with a specific substitution of cement.

In order to estimate the influence of the fly ash on the mechanical properties and to establish various eco-mechanical solutions, the mechanical performances of samples with the same shape but a different mix design will be evaluated.

3.4.1 Geometrical properties

The concrete cylinders have a radius (r_0) of 50 mm and a height (H) of 200 mm length. The UHP-FRCC jackets were designed with a length (H_1) of 178 mm, lower than that of concrete core ($H_1 < H$). In this way, the jacket contributes only to the confinement effect on the cores, without taking part of the compression process.

The varying characteristic is the thickness of the jacket (t_i). As anticipated, four dimensions were considered: 25 mm, 37.5 mm, 50 mm and 75 mm, respectively.

Geometrical characteristics of the specimens realised are schematized in Figure 3.9 and shown in detail in Annex 1.

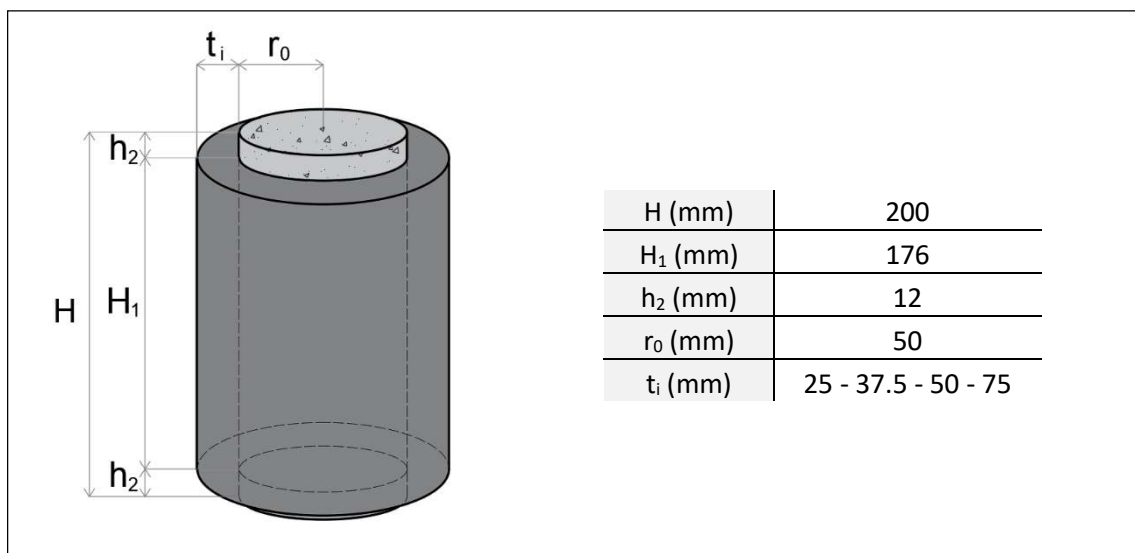


Figure 3.9 - Geometrical properties of samples

It has been opted for a constant interval of increasing thickness of 12.5 mm to be as precise as possible in finding a relationship between these different samples (Table 3.1 and Figure 3.10).

Furthermore, the thickness of 75 mm was added to the series although it doesn't represent a realistic layout for confinement: in fact, in real situation of retrofitting of columns, the layer used to reinforce existent structures doesn't exceed the radius of the concrete building blocks.

Indeed, it may be helpful to extent the experimental cases to a more general and theoretical law.

Table 3.1 - Jacket's dimensions and radius/thickness ratio

t_i	Thickness (mm)	UHP-FRCC Volume (m ³)	r_0/t_i	
t_0	25	0,0017	$r_0/t_0 (-)$	0,5
t_1	37,5	0,0029	$r_0/t_1 (-)$	0,75
t_2	50	0,0042	$r_0/t_2 (-)$	1
t_3	75	0,0073	$r_0/t_3 (-)$	1,5

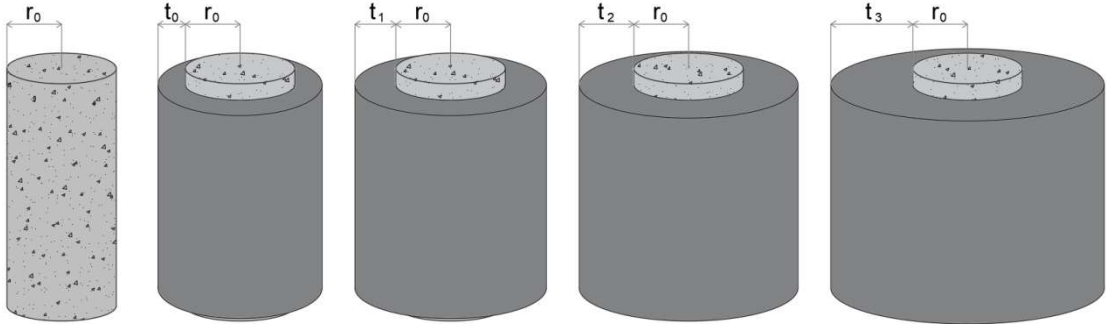


Figure 3.10 - Increasing thickness of the jackets³

To cast the concrete cores, plastic molds containing embedded stain gauges were used (Figure 3.11).

³ The concrete core without jacket is considered as having a virtual jacket with a thickness of zero millimeters.



Figure 3.11 - Plastic molds used for core casting

Paper cylinders, with 178 mm height and different radius, respectively 150 mm, 175 mm, 200 mm and 250 mm, were used to cast the UHP-FRCC jackets around the cores. The base of the jacket's molds was made of wooden rings with 12 mm in height and inner radius equal to the cores' radius R (Figure 3.12).



Figure 3.12 - Paper molds used for jacket casting

Both the plastic and paper molds were wasted after being removed; for technical reasons, the wooden rings uniquely could be reused multiples times.

3.4.2 Material properties

All the materials used for the concrete cores or for the jackets are shown, with their symbol, in Table 3.2.

Table 3.2 - Materials

Materials	Symbol	Density (g/cm ³)
High Early Strength Portland Cement	HESP C	3,14
Sand	S	2,60
Coarse	C	2,69
(Tap) Water	W	1,00
Superplasticizer (S78)	SP ₁	1,05
Low Heat Cement	LH C	3,24
Fly Ash	FA	2,20
Silica Fume	SF	2,20
Silica Sand	Ss	2,60
Wollastonite	Wo	2,90
Superplasticizer (SSP104)	SP ₂	1,05
Defoaming Agent	DA	1,01
Micro-fibers	OL	7,85
Macro-fibers	HDR	7,85

The concrete cores were made of High Early Strength Portland Cement, fine aggregates (sand with diameters between 0 and 5 mm), coarse aggregates (5-25 mm), water and superplasticizer. The use of a superplasticizer suitable for normal concrete was implemented to improve the workability of the mixture.

The knowledge of the basic properties of aggregates is needed to develop successful concrete mix designs: in particular, prior to mixing, the amount of water needs to be adjusted.

In these experimental investigations, both coarse and sand aggregate were used in saturated surface dry condition (SSD).

The saturated surface dry condition occurs when all the internal pores are filled with water (saturated), but the surface is dry. This state is generally used as the reference for mix design and is obtained by immersing the aggregates in water until all the internal porosity was saturated, then drying the surface of the particles.

In case of the coarse aggregates, this condition is achieved with little effort because of the big surface of these particles, but it is not the same for the sand.

In fact, it is almost impossible to get the surface of all of the particles dry without drawing out the water from the internal pores. Thus, the saturated surface dry condition for fine aggregate can be measured performing the slump test with a little Abram cone: a conical mold is filled with sand or aggregate, and then packed. Removing the mold, the sand slumps slightly, and the SSD condition is achieved (Figure 3.13).

If the aggregate preserves the shape of the mold, it is in damp or wet condition. This last condition occurs after the aggregate has been immersed in water but not only all internal pores are saturated, but also the surface is wet.



Figure 3.13 - Abram cone to determine the saturated surface dry (SSD)

The mix proportion of concrete cores is summarised in Table 3.3.

Table 3.3 - Mix proportion of concrete cores

HESP C (kg/m ³)	S (kg/m ³)	C (kg/m ³)	W (kg/m ³)	SP (kg/m ³)
300,3	836	900,3	171,7	1,7

For the jackets, four types of UHP-FRCC were prepared (FA0, FA20, FA50, FA70). The materials used are the same for each mix, only the proportions have different values. The binder is made of High Early Strength Portland Cement to give rapid hardening and setting properties, silica fume and fly ash. The silica fume was preliminarily sifted with a 0.6 mm sifting to minimise the presence of aggregated particles in the form of bubbles (Figure 3.14).

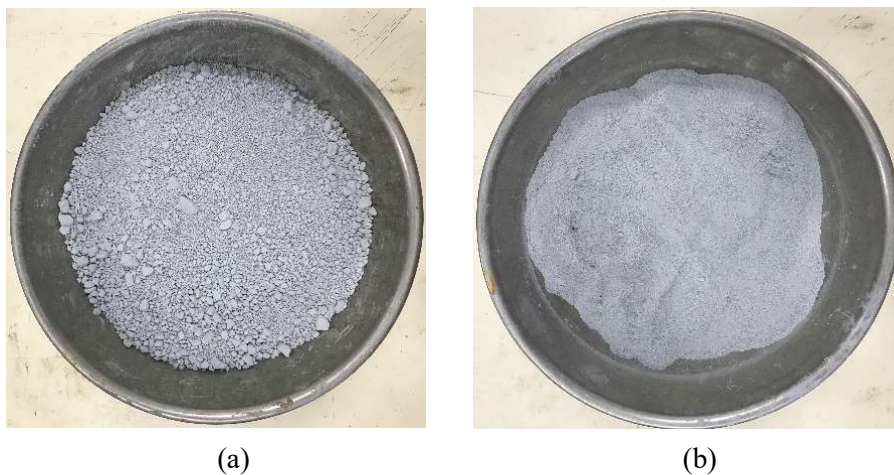


Figure 3.14 - (a) Silica fume with bubbles; (b) Sifted silica fume

Moreover, silica sand and wollastonite fibers were added as dry aggregates. A specific superplasticizer for UHP-FRCC (SSP104) and a de-foaming agent were diluted in water to create flowing without increasing the quantity of water.

To reinforce the mixes, steel fibers (micro and macro) were added: the volume fractions of micro-fibers and macro-fibers are respectively 1% and 1.5%. This ratio has been chosen because it better ensures the properties of ductility and durability.

Fibre length is a parameter that have be definite during the project phase. It is commonly accepted by literature that the length of the fiber should be at least 3 times the maximum aggregate size to guarantee a suitable behaviour of fibres inside cementitious composites. After having defined, also a suitable slenderness has to be chosen. Even if this is not a properly structural project parameter, the strong influence that it has on the matrix and fiber bond has to be taken into account, as, moreover, the effects on the ductility of UHP-FRCC.

Since the slenderness is defined as fibre length to diameter ratio, establishing the slenderness or the fiber diameter is the same thing once its length has been defined.

In this experimental research, the micro-fibers that have been chosen are straight steel fibers with lengths of 6 mm, and the macro-fibers are steel-hooked fibers with a length of 30 mm, as seen in Figure 3.14. The combination of this two typologies of steel fiber allows you to cope with the different cracks inside the matrix.

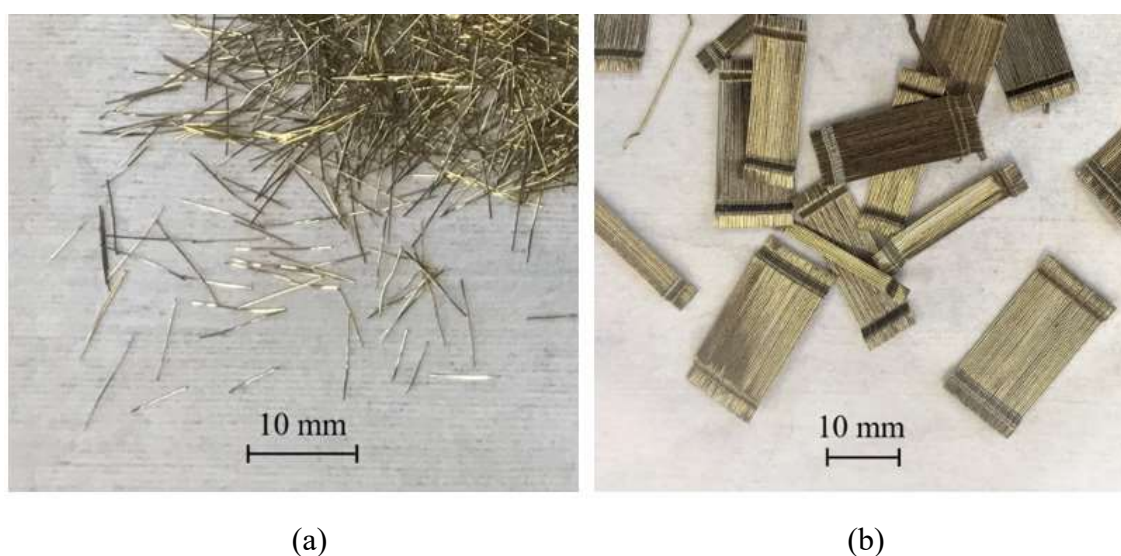


Figure 3.15 - (a) Micro-fibers; (b) Macro-fibers

The geometrical and mechanical properties of the fibers are shown in Table 3.4.

Table 3.4 - Mechanical properties of fibers

Notation	Shape	Density (g/cm ³)	Length (mm)	Diameter (mm)	Aspect ratio (L/D)	Tensile strength (MPa)	Young's modulus (GPa)
OL	Straight	7,85	6	0,16	37,5	2000	206
HDR	Hooked	7,85	30	0,38	78,9	3000	206

As anticipated, four different types of mixes of UHP-FRCC were prepared for jackets: FA0, FA20, FA50, FA70.

The differences between these mixes are the percentages of the binder's components: low heat cement, fly ash and silica fume are used with different amount. The volume of superplasticizer may variate a little, from 2.20 to 2.60 percent of the binder, to achieve an appropriate workability. Anyway, the total content of water, that is one of the main parameters, were kept constant.

Table 3.5 shows the mix proportion of UHP-FRCC mixtures referred to the binder, in terms of weight percentage. As it can be seen, in the mixture FA0 there is no substitution of cement with fly ash, instead in the case of FA20, FA50 and FA70 respectively 20%, 50% and 70% of the cement is replaced with fly ash. Then, the percentage by weight of cement contained in the binder then drops from 82% (maximum content for FA0) to 24,6% (minimum content for FA70).

Table 3.5 - Mix proportion (weight %) referred to the binder

Mixture	Binder (B)			Ss /B	Wo/B	W/B	SP/B	DA/B
	LH C/B	FA/B	SF/B					
FA0	82	-	18	35	13	13,8	2,2	0,02
FA20	65,6	16,4	18	35	13	13,52	2,6	0,02
FA50	41	41	18	35	13	13,52	2,6	0,02
FA70	24,6	57,4	18	35	13	13,52	2,6	0,02

Mix proportion of UHP-FRCC jackets in kg/m³ are shown in Table 3.6.

Table 3.6 – Mix proportion of UHP-FRCC jackets

Mixture	LH C (kg/m ³)	FA (kg/m ³)	SF (kg/m ³)	Ss (kg/m ³)	Wo (kg/m ³)	W (kg/m ³)	SP (kg/m ³)	DA (kg/m ³)
FA0	1217,52	-	267,26	519,67	193,02	214,70	32,67	0,30
FA20	939,24	234,81	257,72	501,12	186,13	204,74	37,23	0,29
FA50	558,33	558,33	245,12	476,63	177,03	194,74	35,41	0,27
FA70	324,43	757,00	237,39	461,59	171,45	188,59	34,29	0,26

These mixes have an extremely low water-binder ratio (w/c), typical for Ultra-High Performance Fiber Reinforced Cementitious Composites.

As indicated by literature, a typical range values of w/b ratio for UHP-FRCC, that is between 0.13 and 0.20.

In this experimental research, for every mix, it has been chosen a value of w/b ratio of 0.16, that guarantees a good balance between the flowability properties and the strength of the hardened concrete.

In fact, a cementitious composite that does not flow well will increase the risk of defects in the concrete as air pockets and porous surface which might lead to a decrease in bearing capacity and durability of the structure element. For this reason, due to the low water to binder ratio, UHP-FRCC contains a high amount of chemical admixtures to reduce the water demand of the concrete mix but, at the same time, to sustain its good workability.

The total content of water is given by the liquid phases of all the material: in this case, it computed as the sum of the tap water, the defoaming agent and the liquid phase of the superplasticizer (70% of the weight).

3.5 Mixing, casting and curing procedures

Embedded strain gauges were installed inside in the middle of the molds before casting the concrete cores. Other additional samples of normal concrete were casted without any devices to asset the mechanical properties with no reinforcement.

An Omuni Mixer with a capacity of 30 liter was used both for concrete cores and UHP-FRCC jackets. Differently to the traditional mixers, it has a different mechanism suitable for casting Fiber-Reinforced Concrete thanks to the possibility to change the speed and to give random swing to the materials (Figure 3.16).

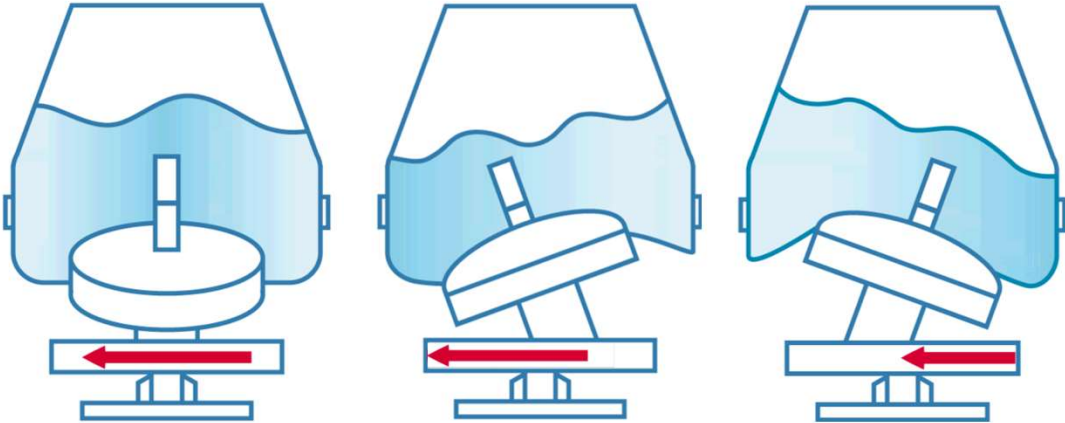


Figure 3.16 - Mixer used for casting UHP-FRCC

The mixing procedure for the concrete cores is shown in Figure 3.17: (1) HESP cement and sand were mixed for 1 minute; (2) water, pre-mixed with superplasticizer, was then added, and this mortar was mixed for 3 minutes. (3) Finally, coarse was added in the mixture and then mixed for additional 3 minutes.

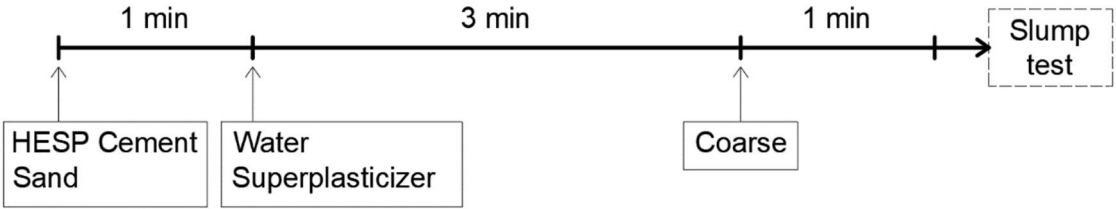


Figure 3.17 - Scheme of mixing process for concrete cores

The mixing phases for the concrete cores are shown in Figure 3.18.



Figure 3.18 - Mixing phases for concrete cores

Once the mixture was complete but before casting, the temperature of the concrete was measured, the slump test and the air content test were performed.

Slump test

This test was performed according to the “*Standard Test Method for Slump of Hydraulic Cement Concrete*” (ASTM C 143/C 143M – 03) and his scope was to guarantee the concrete’s workability and consistency before being casted. In fact, the strength of concrete mainly depends on the degree of its compaction. Consistency of concrete is another way of expressing workability, but it is more restricted to the water content. Consequently, concrete of the same consistency could be different in workability. The slump test is used to measure the consistency of concrete: it does not properly evaluate the workability of concrete, but it is very useful in noticing variations in the uniformity of a mix of given nominal proportions. Mixes characterised by stiff consistency have zero slump. An increase in slump may denote, for instance, that the humidity content of aggregate has unpredictably increased. An additional cause could rely on a change in the grading of aggregate. High and low values of slump are immediate warning and make the mixer operator to remedy the situation.

The test is carried out using a metal mould in the shape of a truncated cone, known as a slump cone or Abrams cone, that is open at both ends and equipped with handles. The mould has a diameter of base of 200 mm (± 2 mm), a diameter of top of 100 mm (± 2 mm)

and it has a height of 300 mm (± 2 mm). Before starting the test, the internal surface of the mould should be clean and humid but free from extra moisture.

The mould is put on a plane, horizontal, rigid and non-absorbent surface and should be firmly held against the surface below. It is filled with fresh concrete in three layers, each approximately one-third of the volume. For each layer, the mixture is tamped with 25 strokes of the tamping rod measuring 600 mm in length and 16 mm in diameter, ensuring to penetrate just the layer and avoiding compacting the underlying tier.

After the top layer has been compressed, with a rolling motion of the tamping rod the exceeding concrete should be taken away. Before completing the test, the surface should be cleaned from eventual concrete residues. Then, the mould is carefully removed in vertical direction, avoiding lateral or torsion movements.

Immediately the slump is measured by calculating the difference between the height of the mould and of the highest point of the surface of the specimen.

The results of the Slump Test obtained for normal concrete mixtures of each series are set out in the Annex 3.



Figure 3.19 - Slump test: equipment and measurement

Air content test

Air content is relevant in determining the quality of a mix: the air pockets permit hardened concrete to better adapt the pressures caused by freeze-thaw cycles, avoiding cracking, especially in a cold space. The amount of air may affect the strength of the mixture and

it is also responsible for the external surface of the concrete. Consequently, the air content should respect the features of the experiment.

The air content of a sample was measured with a pressure meter, according to the “*Standard Test Method for Air Content of Freshly Mixed Concrete by the Pressure Method*” (ASTM C231 – 03). Specifically, the Pressure Method “B” was used.

The measuring bowl, made of hard metal not easily attacked by cement paste, is filled in three layers of approximately equal volume. Each layer is compressed with a metallic tamping rod for 25 strokes and the sides of the bowl are hit with a mallet for 15 times to remove any vacuums left by the tamping road. When the bowl is full, the exceeding concrete should be struck off using the strike-off bar until the surface is perfectly aligned with the top of the container (Figure 3.20).

After an accurate cleaning of the instrument, the cover assembly is placed on the bowl, the bleeder valve is closed, and the dial should be pumped until the calibrated initial pressure value is reached. To stabilise the gauge, it is necessary to opening the blender valve a little bit. With the lever at the top of the cover, the pressure was released, and the air content is read on the gauge. This value represents the apparent air content A_1 : by subtracting the aggregate correction factor “G”, determinate according to the ASTM C231 – 03 as well, the actual amount of air in the sample A_s could be found with this relationship:

$$A_s = A_1 - G$$



Figure 3.20 - Device for measurement of air content

The results of the Air content Test obtained for normal concrete mixtures of each series are set out in the Annex 4.

After completing these preliminary tests, concrete cores were cast, trying to reach a better compaction as possible (Figure 3.21).



Figure 3.21 - Casting of concrete cores

Once the the procedure of casting was completed, the specimens were left for 48 hours in the molds and after their removal (Figure 3.22). The concrete cores were placed in the curing room, where the temperature was 20°C and relative humidity 95%.



Figure 3.22 - Concrete core after removing the mold

After 11 days from the cast of the concrete cores, the specimens were reinforced with the jackets.

The mixing procedure that includes the type of mix, the order of introduction of the materials into the mixer, and the energy of mixing (duration and power), has been the same for all the mixtures (FA0, FA20, FA50, FA70 mixtures).

The mixing procedure for the jackets is articulated in 5 steps (Figure 3.23):

1. low heat cement, fly ash, silica fume, wollastonite and silica sand were mixed for 5 minutes;
2. water, pre-mixed with the superplasticizer, and the defoaming agent, were then added, and this mortar was mixed for 9 minutes;
3. 1/3 of the steel fibers (micro and macro) was dispersed into the mortar mixture and then mixed for 1 minute;
4. an additional 1/3 of fibers was added, and mixing was resumed for 1 minute more;
5. the last portion of fibers was added and mixed for the last 1 minute.

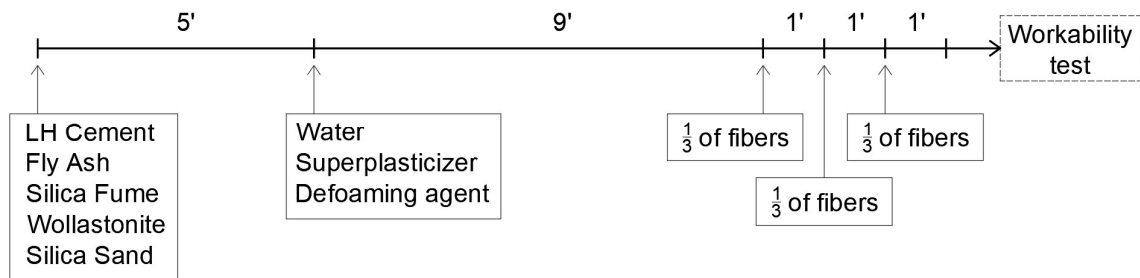


Figure 3.23 - Scheme of mixing process for UHP-FRCC (FA0, FA20, FA50, FA70 mixtures)

The “evolution” of the UHP-FRCC mixture is shown in Figure 3.24: contrary to the normal concrete, ultra-high fiber-reinforced cementitious composites need a long time of mixing before reaching a proper consistency and workability.

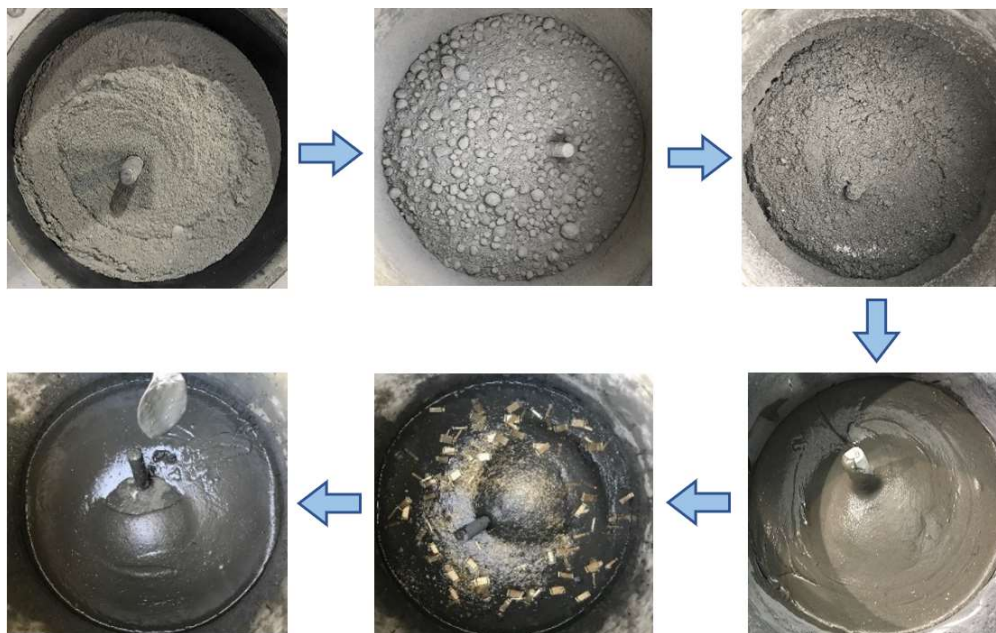


Figure 3.24 - Mixing procedure for UHP-FRCC mixtures

After completing the mixture and before casting, the temperature of the concrete was measured, and both the Flow Table Test and the Air Content Test were performed to measure the fresh properties of the UHP-FRCC.

Flow table test

The workability of the mixture was measured by the flow of the mortar, according to the “*Standard Test Method for Flow of Hydraulic Cement Mortar*” (ASTM C1437 – 07). The standard flow test uses a conical frustum shape with a diameter of 300 mm.

After carefully cleaning the flow table top, the mould is placed at its centre and filled with 3 layers of mortar. Each layer of about 25 mm in thickness is tamped 20 times with a tamper tamping rod.

The excessive mortar is cut off by drawing the straight edge of a trowel with a sawing motion across the top of the mould. Then, the mould is lifted away from the mortar and immediately the table is dropped through a height of 12.5 mm, 25 times in 15 seconds.

The initial and final diameters of the mortar sample are used to calculate flow (Figure 3.25). Flow is defined as the increase in diameter divided by the original diameter multiplied by 100, according to the following equation:

$$Flow = [(D_{avg} - D_o) / D_o] \cdot 100^*$$

* D_{avg} = Average base diameter; D_o = Original base diameter



Figure 3.25 - Flow table test of UHP-FRCC

The results of the Flow Table Test obtained for UHP-FRCC mixtures of each series are set out in the Annex 5.

After performing this test, UHP-FRCC jackets were casted, preserving the top of the concrete core and trying to make as flat as possible the surface of the jacket, using also a vibrator to reduce the presence of bubbles (Figure 3.26).



Figure 3.26 - Preparation and casting of jacket

Two days after casting the jackets, the paper formworks were removed, and the specimens were subjected to steam curing for the following 48 hours. The completed concrete core reinforced with UHP-FRCC jacket is shown in Figure 3.27.



Figure 3.27 - Specimens after the steam curing

Lastly, they were stored in the humidified room until the testing day, that were carried out after 28 days from cores casting. The whole process is depicted in Figure 3.28.

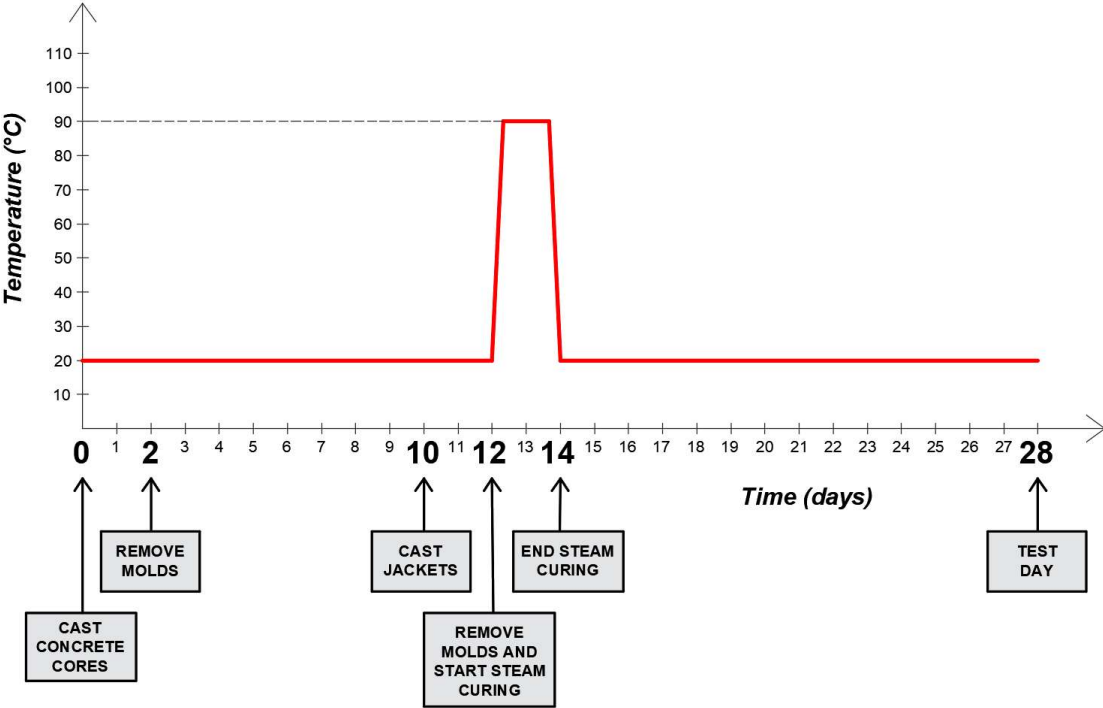


Figure 3.28 - Scheme of the process

3.6 Testing procedure and experimental devices

The concrete cores reinforced with UHP-FRCC jackets were tested under uniaxial compression and the deformation is the controlled parameter.

To record the strain during the experiment external strain gauges and embedded strain gauges were used.

Strain gauges are electrical sensors designed to convert mechanical motion into an electronic signal: electrical resistance varies proportionally to the amount of strain in the device.

In this framework, the most widely used gauge is the bonded metallic strain gauge: it consists of a very fine wire or metallic foil arranged in a grid pattern. The grid is bonded to carrier, a thin backing which is attached directly to the test specimen. Therefore, the strain experienced by the test specimen is transferred directly to the strain gauge, which responds with a linear change in electrical resistance.

The sensors used in these experiments were wire strain gauges utilising a transparent plastic backing impregnated with polyester resin. The gauge length is of 60 mm and, since the backing is transparent, the bonding position can easily be checked in the installation works (Figure 3.29).

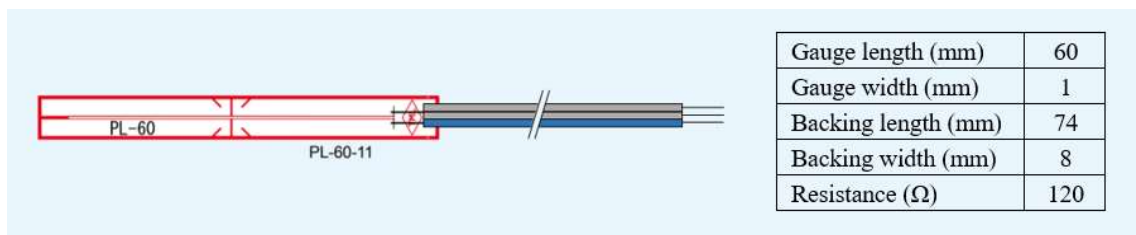


Figure 3.29 - External strain gauge's geometry

Four strain gauges were applied on the jacket's surface, two in the vertical direction and two in the horizontal direction (Figure 3.30). The vertical gauges measured the strain along the longitudinal axis, while the horizontal ones recorded the transversal dilatation.

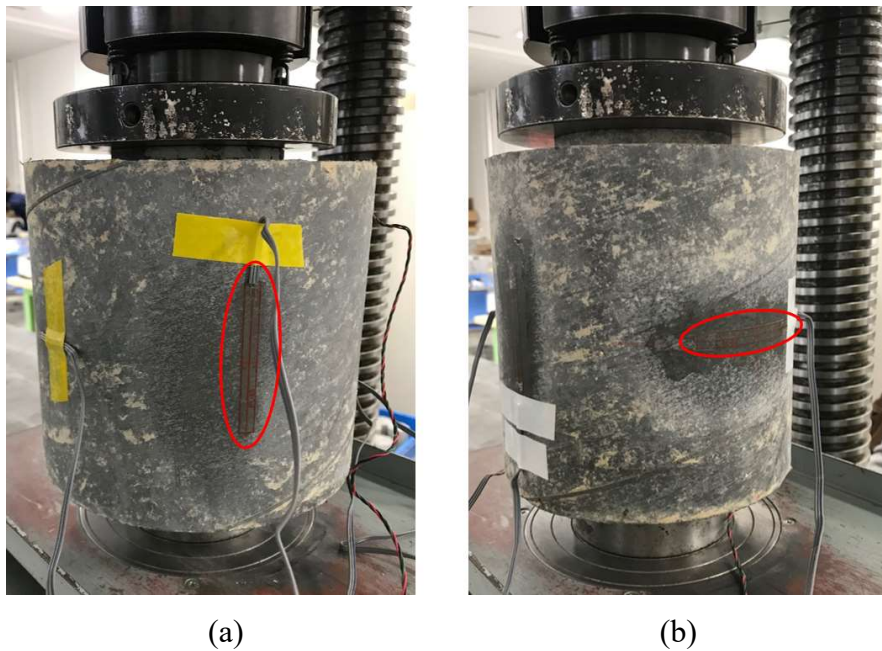


Figure 3.30 - Vertical (a) and horizontal (b) external strain gauges applied on the jacket's surface

As described by previous experiences [44], the vertical strain gauges attached on the jacket's surface don't provide reliable results for detecting the vertical strain.

In fact, due to the bending effect on the jacket, negative values for deformation (i.e., elongation) are recorded by these strain gauges applied on the jacket surface (Figure 3.30a).

When a load is applied only on the core part, the farthest portion of the jacket's surface starts to dilate without following the vertical axis, but assuming a trapezoidal shape (Figure 3.30b).

On the contrary, the concrete cores exposed to the uniaxial compression load should show positive deformation (i.e., compression), due to the crushing phenomenon.

According to these observations, the external vertical strain gauges can be considered as not suitable to describe the real compressive process because they don't reproduce the vertical deformations that have to be investigated, that is the stress-strain relationship of the cylinders confined within UHP-FRCC jackets.

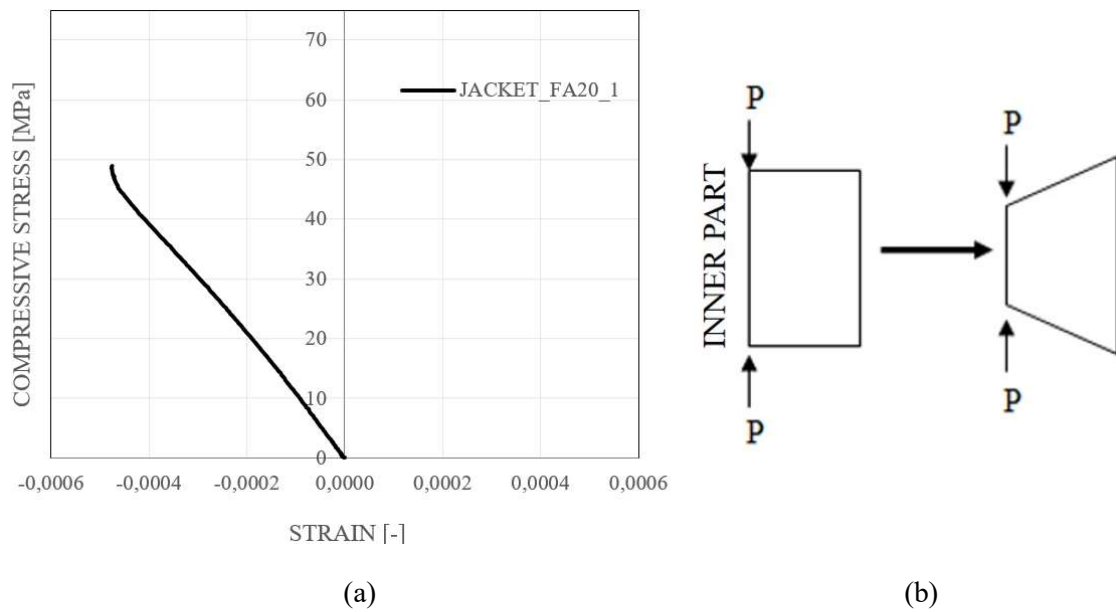


Figure 3.31 - Ineffectiveness of vertical strain gauges on the jacket's surface: elongation (a); bending effect (b) [50]⁴

Due to the unsuitability of vertical strain gauges to record the vertical strain of concrete core during the compressive test, embedded strain gauges have been considered an appropriate alternative for the scope, and were then introduced (Figure 3.32).

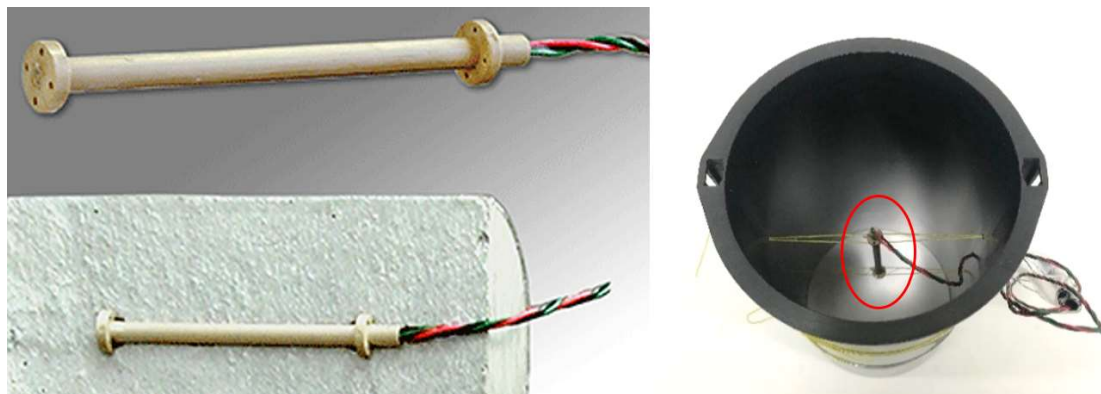


Figure 3.32 - Embedded strain gauge

⁴ It is depicted the strain measured by vertical strain gauges on a cylinder confined with a FA20 jacket [50].

The embedded strain gauges chosen in these experiments consist of a 3-wires system incorporated at the centre of the concrete cores, that permit to obtain a more accurate value for the vertical displacement of the specimens.

These gauges are expressly designed for the measurement of internal strain of concrete or mortar under loading test. These are they are positioned exactly in the middle of the plastic molds and then the concrete is casted.

Moreover, these gauges employ super engineering plastics as the backing for sealing the sensing element, which provide for excellent waterproofing.

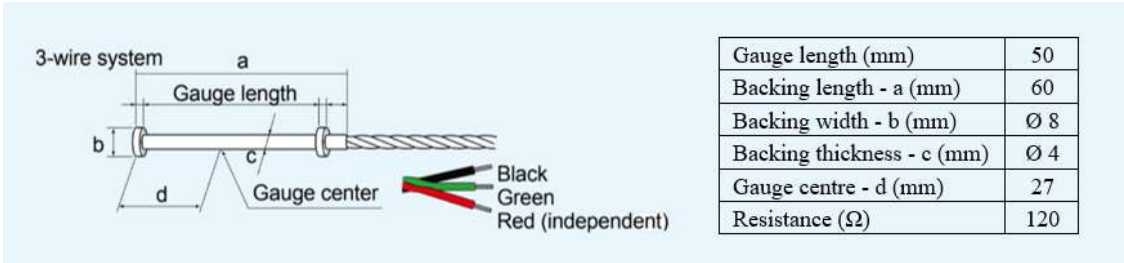


Figure 3.33 - Embedded strain gauge’s geometry

To conduct compression test a universal testing machine (UTM) with a maximum capacity of 1000 kN was used. The specimen was placed in the machine between the two grips, and the cables of the strain gauges were connected to the UTM in order to record the displacements (Figure 3.34).



Figure 3.34 - Universal testing machine (UTM) used for the compressive test

Throughout the tests, the control system and its associated software recorded the load and extension or compression of the specimen.

The uniaxial compression test was conducted under manual mode and the test was stopped when the jacket surface was completely damaged (Figure 3.35).

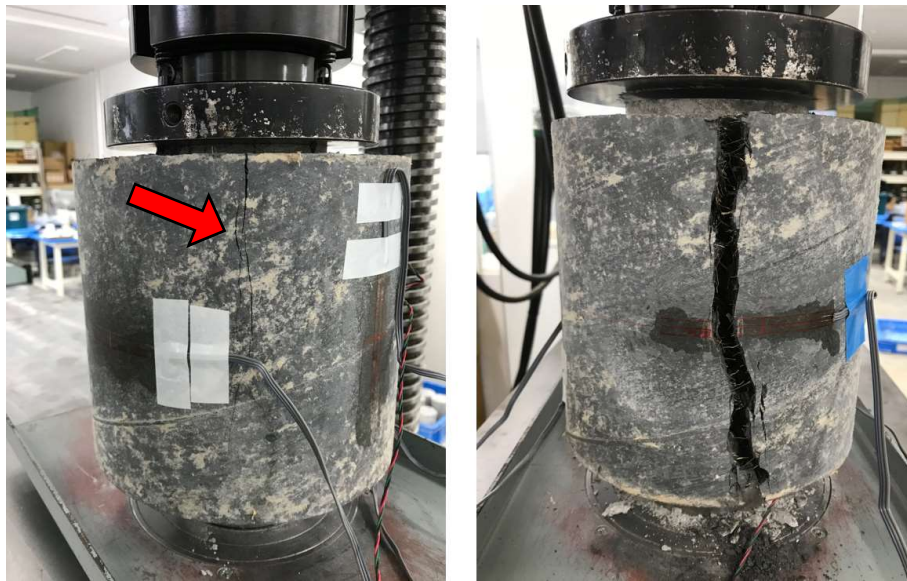


Figure 3.35 - Compressive test: cracking process

After having carefully described all the procedures, the results of all performed tests will be presented and discussed in the following chapters.

CHAPTER 4

TEST RESULTS

4.1 Mechanical analysis

Uniaxial compression tests were carried out to establish the mechanical properties of concrete cylinders reinforced with UHP-FRCC jackets.

The mechanical performances were assessed by analysing the ultimate load carrying capacity, the mechanical parameters and the energy absorption capacity, directly related to the ductility of the samples.

Four series of tests were performed (Table 4.1). The first one consists of 9 normal concrete samples reinforced with UHP-FRCC jackets with 20% of cement replaced by fly ash (FA20), having a thickness of 37.5 mm, 50 mm and 75 mm, respectively. The second series involves 6 normal concrete samples confined by UHP-FRCC FA70 jackets and the third series lies in 6 normal concrete cylinders reinforced with UHP-FRCC FA50 jackets. For both, the thicknesses of jackets were of 37.5 mm and 50 mm. The last series provided jackets with no substitution of cement with fly ash (FA0): 6 sample are tested, and the size of the jackets were of 25 mm and 50 mm.

For each combination of size and mixture of jackets, 3 samples were designed, and the average values were considered for the analysis. Furthermore, for each series, one concrete core with no reinforcement were tested to estimate the mechanical properties without UHP-FRCC jackets. A previous investigation provided also results related jackets of 25 mm made of UHP-FRCC of 20% and 70% of cement replaced by fly ash (FA20 and FA70).⁵

Table 4.1 - List of tested samples

Series	Mixture	Thickness of jacket (mm)			
		25	37,5	50	75
1°	FA0	○	X	○	X
2°	FA20	○	○	○	○
3°	FA50	○	X	○	X
4°	FA70	○	○	○	X

⁵ Valerio Lisi, "Ecological and mechanical properties of ultra high performance – fiber reinforced cementitious composites containing fly ash", Life Cycle Engineering Laboratory, Tohoku University, 2018

All the specimens have been coded and the codification is shown in Annex 2. As explained in Chapter 3.6, the experiments were performed under deformation control: recording simultaneously applied loads and respective displacements, stress-strain curves were obtained. It has been analysed the range of strains between 0 and 0,015: strains greater than 0.015 weren't considered meaningful for the investigations due to the fact that they are close to breaking point. Consistently, assessments and evaluations presented in the next sections refer to average strain-stress curves: they were obtained from the average points of three curves (representative of three samples with same size and mixture), considering an interval of strain of 0.0005, as shown in Figure 2.1.

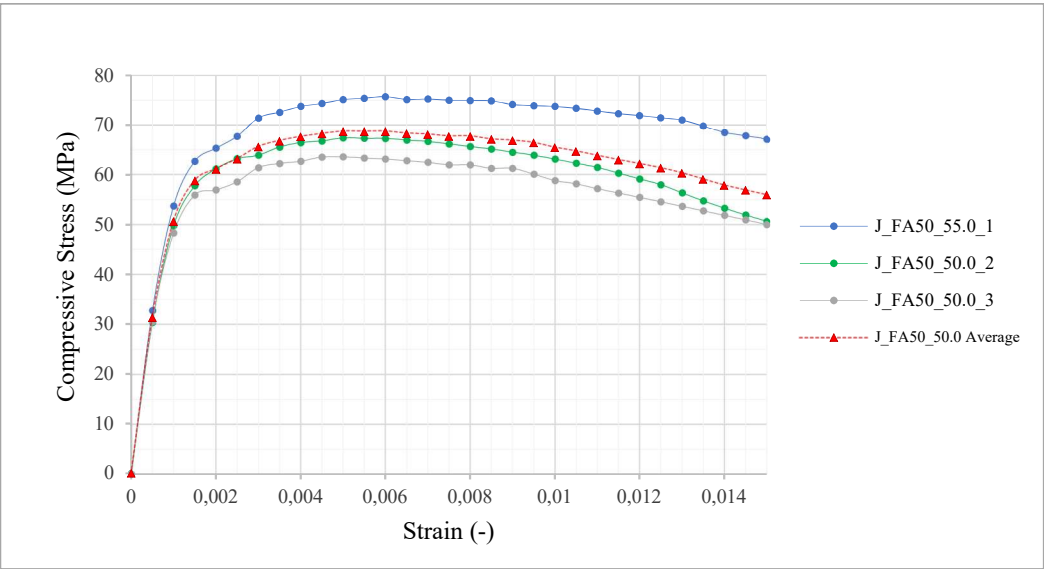


Figure 4.1 - Example of average curve tracing

All stress-strain graphs referred to each specimen are fully reported in Annex 6, Annex 7, Annex 8 and Annex 9.

4.1.1 Compressive Stress

The results of the compression test are shown following the sequence this series: FA0, FA20, FA50, FA70.

- **UHP-FRCC FA0 series**

In Figure 4.2 the average stress-strain diagrams of concrete cores confined with different UHP-FRCC jacket without substitution of cement with fly ash are displayed.

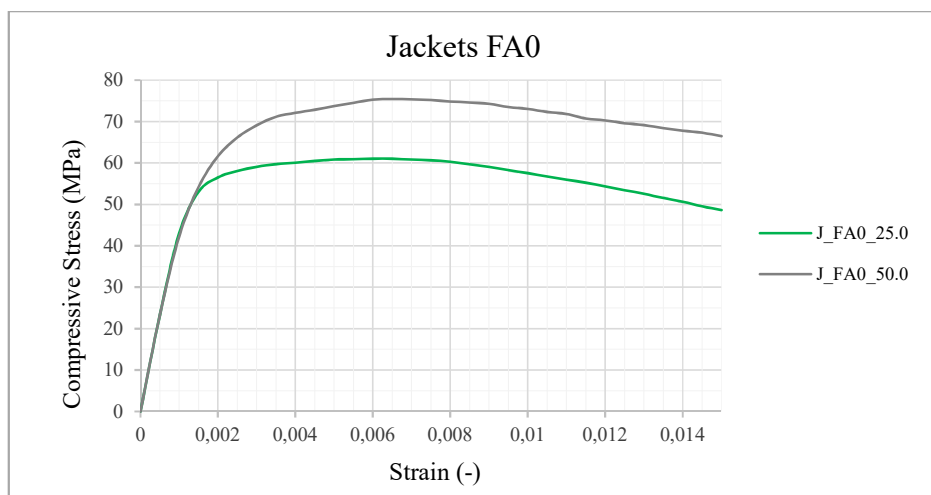


Figure 4.2 - Maximum compressive stress: UHP-FRCC FA0 jackets

Regardless of the thickness of the jacket, the trend of the stress-strain curve is basically the same for all the specimens: after an initial elastic behaviour, however exceeding the 70-80% threshold of the compression-resistant capacity, a loss of linearity can be noticed before reaching the maximum compression stress, and then a descending post-peak branch determined by the high volume of steel fibers.

For values of strain lower than 0.015, the compressive stress doesn't go below 70% of the maximum effort.

It may be useful to analyse these curves by referring to the compressive stress of an unreinforced cylinder, made of normal concrete.

The compressive strength of the normal concrete (NC) was obtained by testing four non-reinforced cylinders at 28 days. The test results are shown in Table 4.2.

Table 4.2 - Compression test results of normal concrete cores

Specimen	P_{max} (kN)	f_{c_CORE} (MPa)	ϵ_{v_max} (-)
NC_FA0_1	365,40	46,52	0,0022
NC_FA20_1	360,30	45,87	0,0021
NC_FA50_1	369,60	47,06	0,0024
NC_FA70_1	366,10	46,61	0,0021
Average	365,35	46,52	0,0022

In Figure 4.3 the curves are normalised dividing the compressive strength by the maximum stress reached for cores without reinforcements (f_{c_CORE}). The value of compressive stress of normal concrete cylinder is depicted as well.

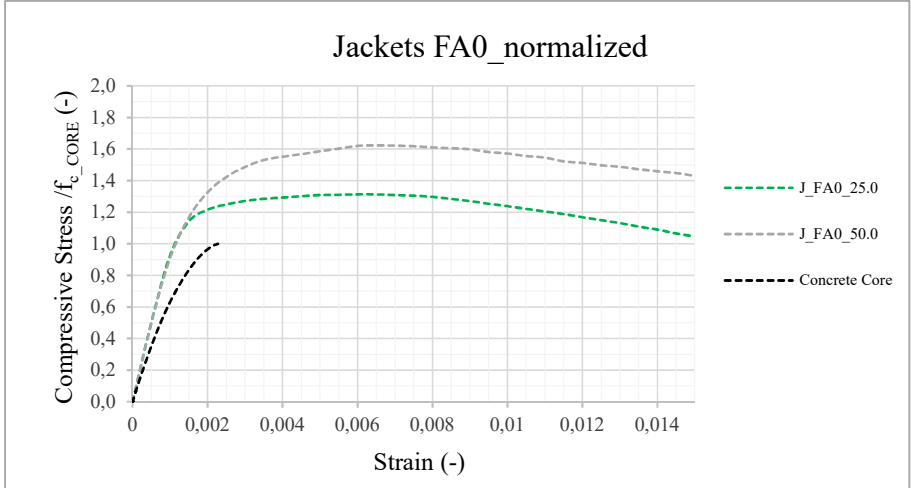


Figure 4.3 - Stress-strain curves: FA0 jackets (Values normalized with f_{c_CORE})

Overall, a progressive increase in compression stress is noticed as the size of the jacket increases, considering also the maximum load carrying capacity of the normal concrete cylinder (Figure 4.4Figure 4.6).

In this case, it has been obtained a percentage increase of 32% and 63% of the maximum compressive stress of unconfined concrete with jacket of 25 mm and 50 mm, respectively.

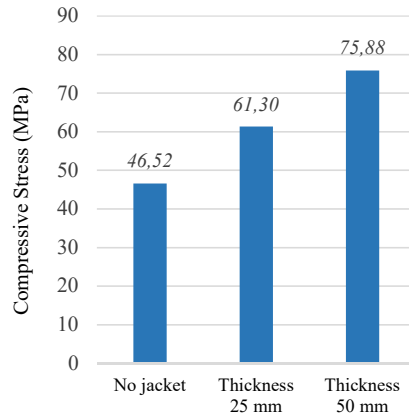


Figure 4.4 - Maximum compressive stress: UHP-FRCC FA50 jackets

- **UHP-FRCC FA20 series**

The following Figure 4.5 and Figure 4.6 provide the results of the compression test of normal concrete cylinder confined by UHP-FRCC jacket with 20% of cement replaced by fly ash.

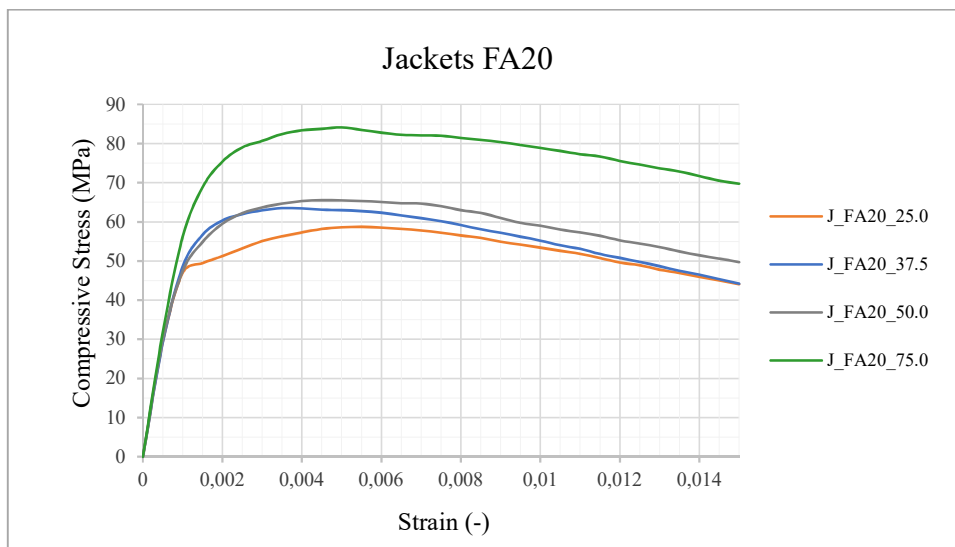


Figure 4.5 - Stress-strain curves: FA20 jackets

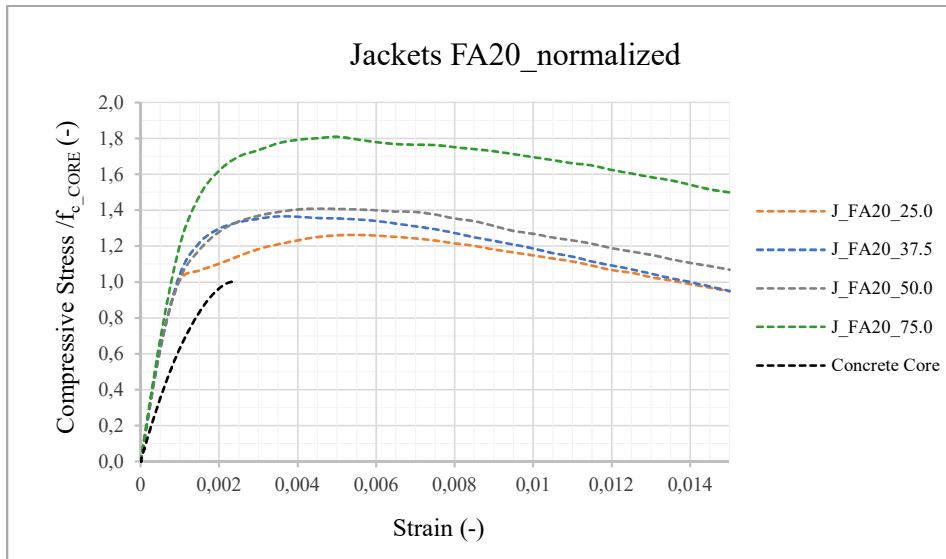


Figure 4.6 - Stress-strain curves: FA20 jackets (Values normalized with f_{c_CORE})

Similar to what happened in the previous results, the increase in size of the jacket significantly contributes to the growth of maximum compression capacity (Figure 4.7).

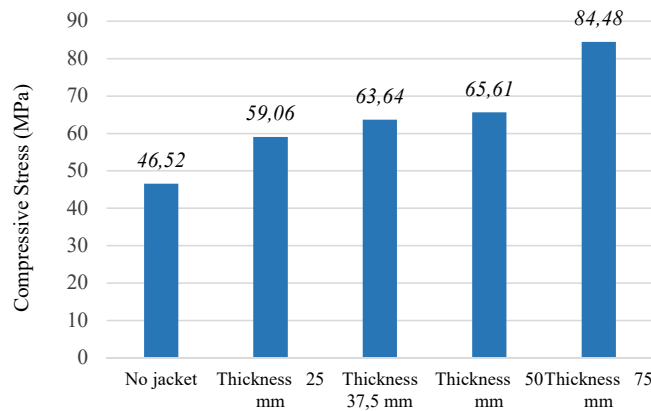


Figure 4.7 - Maximum compressive stress: UHP-FRCC FA20 jackets

The relationship between the maximum compressive stress and the thickness of the jacket is likely to be linear: only the results referred to the jackets of 50 mm are slightly lower than the main trend. Anyway, it is widely recognised that a margin of error may be generally expected in an experimental investigation. In case of the FA20 jackets, the resistance of normal concrete cylinder is increased by around 27%, 37%, 41% and 82%, with UHP-FRCC jackets of, respectively, 25 mm, 37.5 mm, 50 mm and 75 mm.

- **UHP-FRCC FA50 series**

Figure 4.8 shows the stress-strain curves of concrete cylinder reinforced by UHP-FRCC FA70 jackets; normalized values are reported in Figure 4.9.

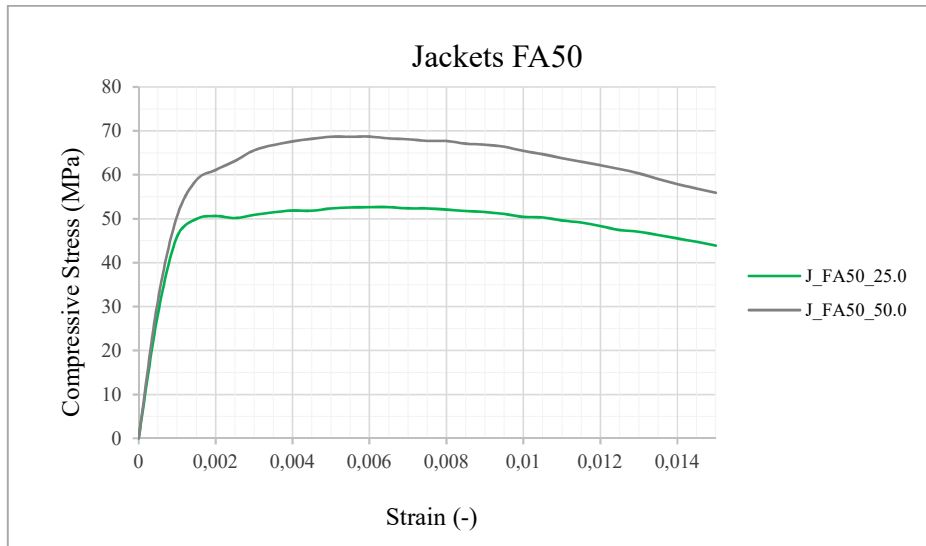


Figure 4.8 - Stress-strain curves: FA50 jacket

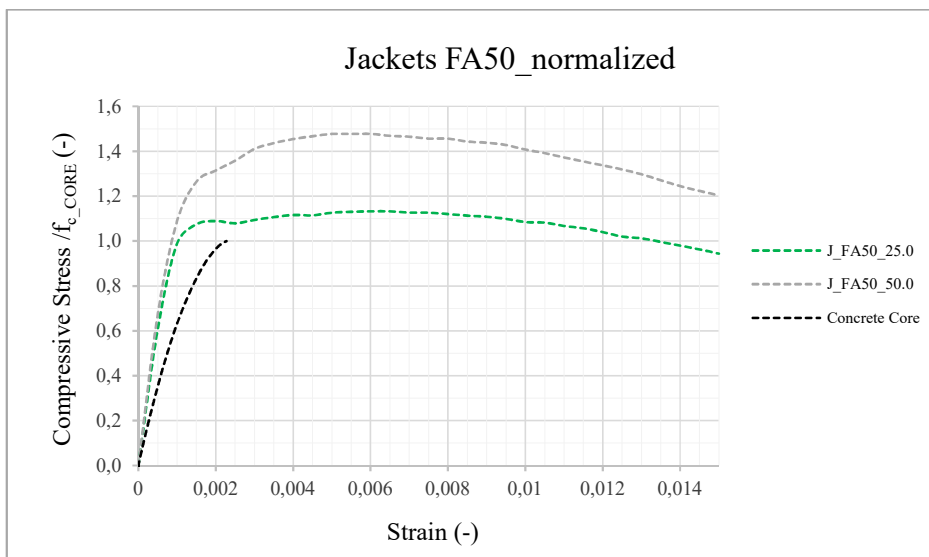


Figure 4.9 - Stress-strain curves: FA50 jackets (Values normalized with f_{c_CORE})

Here again, the resistance of the samples with the UHP-FRCC jackets is considerably greater than the carrying load capacity of non-reinforced concrete (Figure 4.10): from an increase of the maximum effort of 14% with a jacket of a thickness of 25 mm, it goes even to a 41% increase with a thickness of 50 mm.

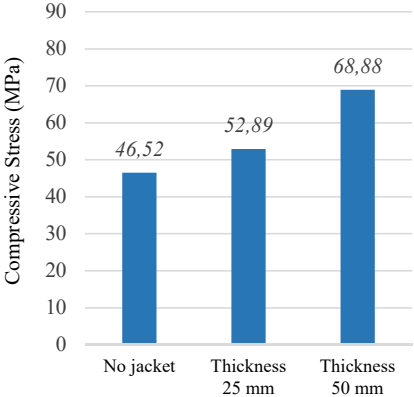


Figure 4.10 - Maximum compressive stress: UHP-FRCC FA50 jackets

- **UHP-FRCC FA70 series**

Figure 4.11 displays the average stress-strain diagrams of concrete cores confined with different UHP-FRCC FA70. As for the previous series, the curves have been normalized with respect to the maximum capacity of normal concrete cylinders (Figure 4.12).

With the progressive increase in the size of the jacket, the maximum load capacity grows in a linear way (Figure 4.13): normal concrete cylinder confined with jackets of 25 mm and 37.5 mm experiences a raise of the maximum load, respectively, 8% and 15%, representative percentages of a linear trend. Lastly, the effect of confinement of jackets with a thickness of 50 mm is the most effective, with a 41% increase in resistance compared to ordinary concrete samples.

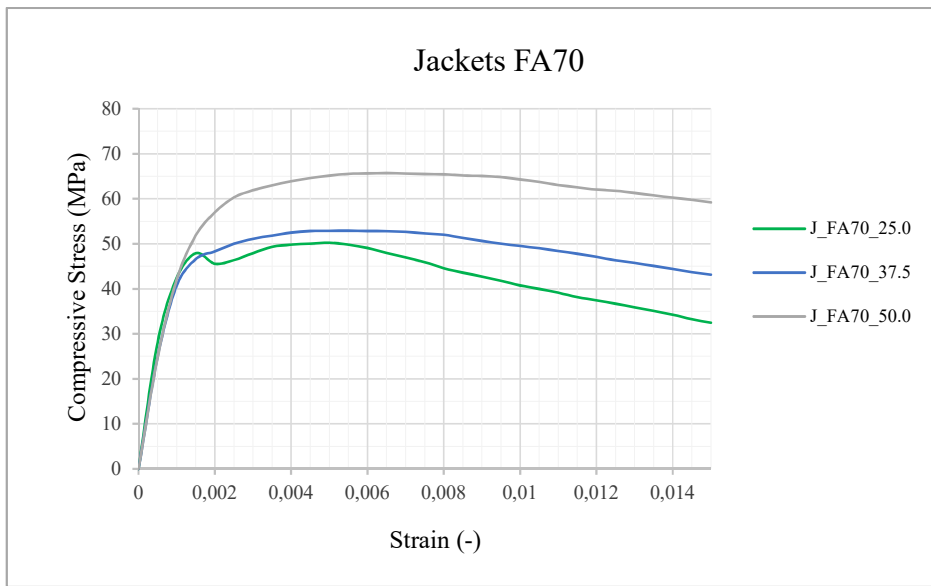


Figure 4.11 - Stress-strain curves: FA70 jackets

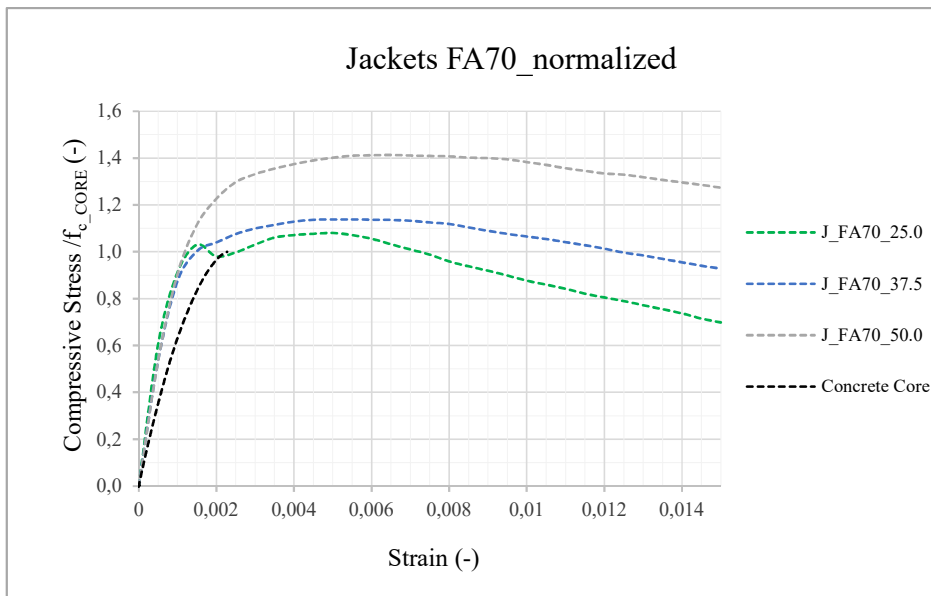


Figure 4.12 - Stress-strain curves: FA70 jackets (Values normalized with f_{c_CORE})

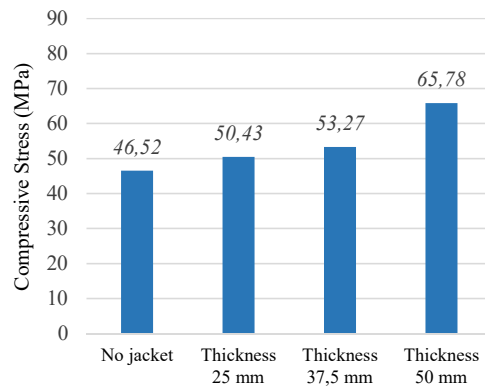


Figure 4.13 - Maximum compressive stress: UHP-FRCC FA70 jackets

A summary of all the values obtained with the compression test is reported in Table 4.3: the mechanical parameters that have been considered are the maximum load (P_{max}), the maximum compressive stress (σ_{max}), and the maximum compressive stress normalized with the capacity of not confined concrete cylinders

Table 4.3 - Summary table of test results

Mixture	Jacket Thickness (mm)	P_{max} (kN)	σ_{max} (MPa)	σ/f_{c_CORE} (-)
FA0	25	481,47	61,30	1,32
	50	595,93	75,88	1,63
FA20	25	463,86	59,06	1,27
	37,5	499,80	63,64	1,37
	50	515,27	65,61	1,41
	75	663,53	84,48	1,82
FA50	25	415,40	52,89	1,14
	50	541,00	68,88	1,48
FA70	25	396,07	50,43	1,08
	37,5	418,40	53,27	1,15
	50	516,60	65,78	1,41

After having individually analysed the results obtained for each single type of jacket containing different percentages in volume of fly ash, the effect of the substitution strategy, in terms of mechanical properties, has been evaluated.

Figure 4.14 and Figure 4.15 compare the results of compression test on concrete cylinder confined with jackets of the same thickness of 25 mm but having, respectively, 0%, 20%, 50%, 70% of cement replaced with fly.

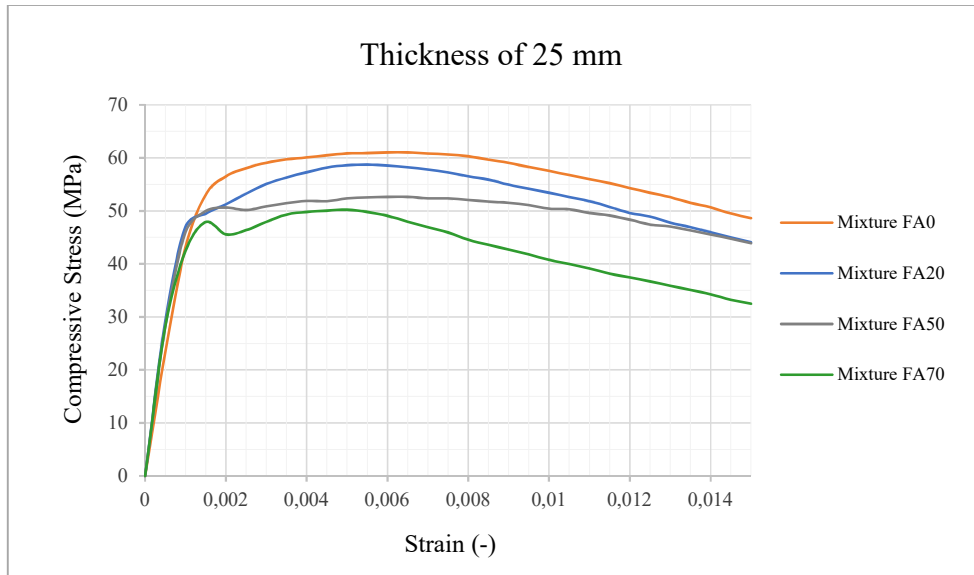


Figure 4.14 - Maximum compressive stress: jackets with a thickness of 25 mm

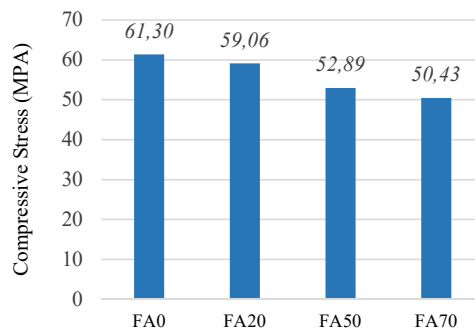


Figure 4.15 - Comparison of jackets with thickness of 25 mm

As it can be seen from the graphs, the composition of the UHP-FRCC binder considerably influence the mechanical compression response. Although the results obtained in the case of the FA20 mixture ($\sigma_{\max} = 59,06$ MPa) are close to those achieved from the FA0 mixture ($\sigma_{\max} = 61,30$ MPa), the replacement of 20% in weight of cement content is paid with a

loss of 4% of the maximum compression strength. Moreover, considering as a reference the cylinder confined with UHP-FRCC FA0 of 25 mm, with high volumes of fly ash, the decrease in compressive strength is about 14% and 18% with, respectively, 50% and 70% of cement replaced with industry by-products. A similar relationship is achieved by jackets with a thickness of 50 mm: also in this case, an almost linear decrease in the maximum compression capacity is detected, with the increase of the amount of fly ash used in the mix (Figure 4.16 and Figure 4.17).

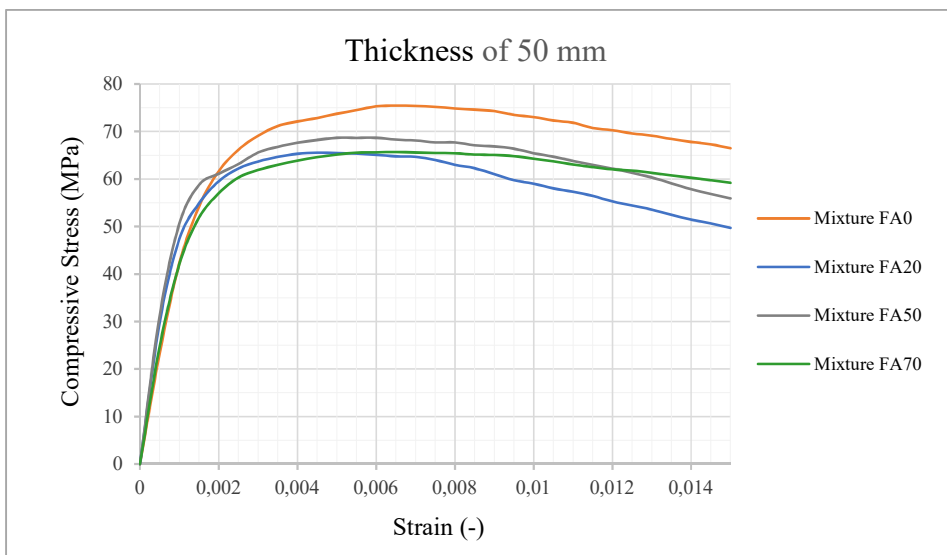


Figure 4.16 - Maximum compressive stress: jackets with a thickness of 50 mm

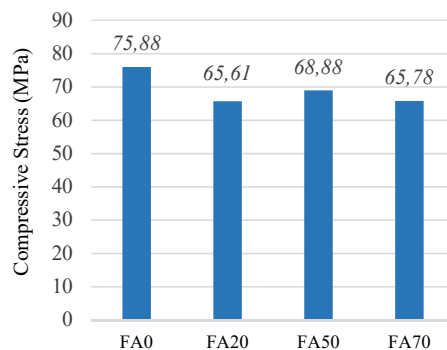


Figure 4.17 - Comparison of jackets with thickness of 50 mm

The fact that the jacket FA20 of 50 mm shows a slightly lower resistance is not significant and can be considered an acceptable error in the field of variations obtained in an experimental research. This value may be correctly estimated by means of data interpolation.

Accordingly, a linear interpolation has been carried out in order to find a more precise relationship between, at first, the thickness of the jacket and the compression strain and, secondly, between the percentage of cement replaced with fly ash and the maximum compression capacity of the cylinders.

The following graph (Figure 4.18) relates in a clear way the values of maximum compressive stress with the thickness of the jacket for each of the four mixtures.

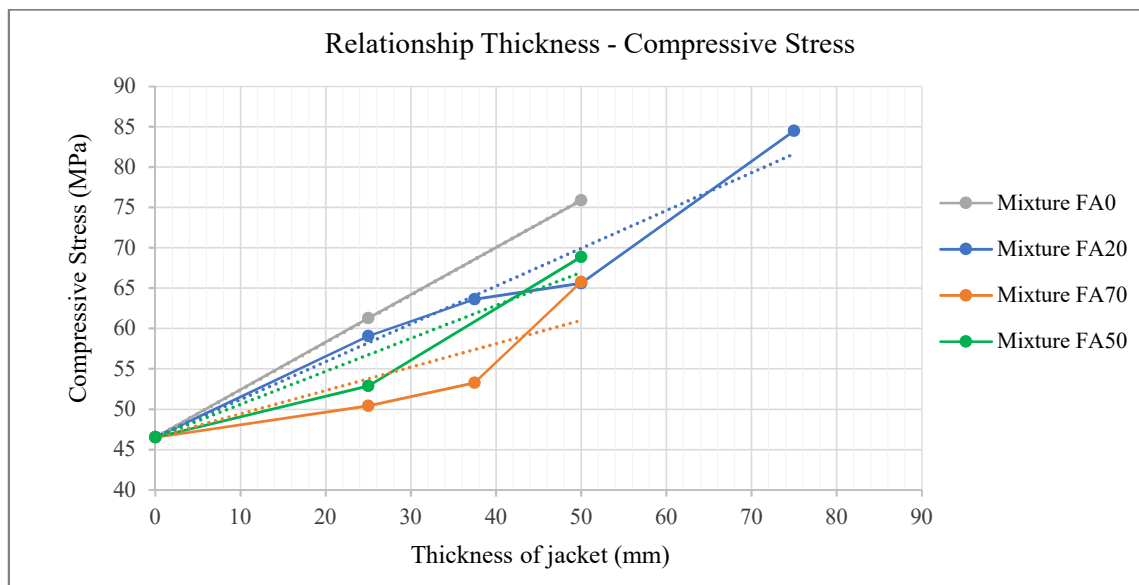


Figure 4.18 - Relationship between the Thickness of Jacket and Compressive Stress

To analyse the governing law which holds behind this experiment, a linear interpolation of the values has been considered. The dotted lines in the previous graph represent the linear interpolation that has been highlighted in Figure 4.19.

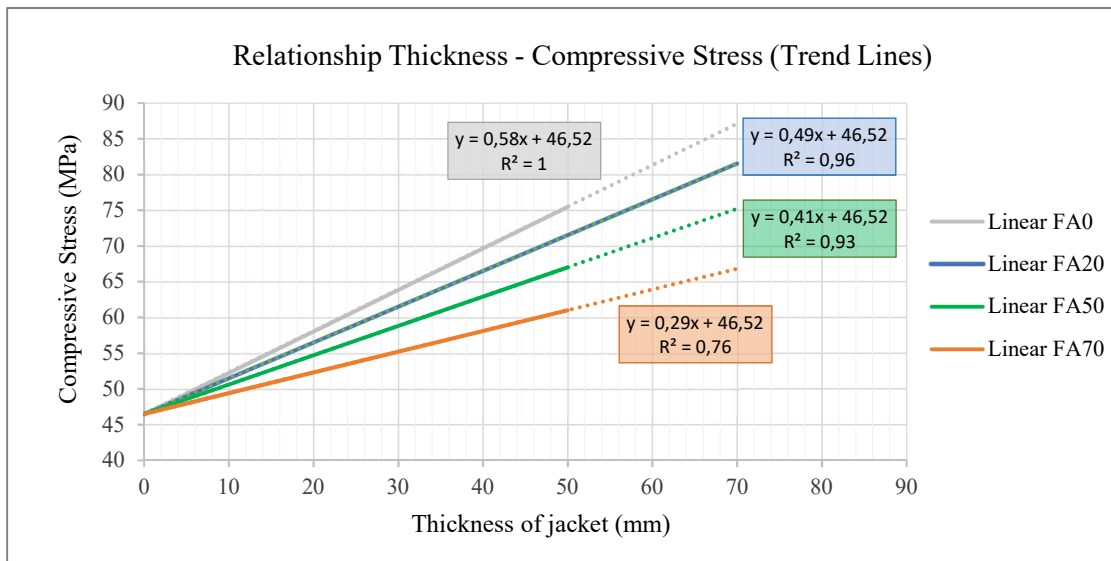


Figure 4.19 - Trend Lines (Relationship Thickness - Compressive Stress)

The coefficients of determination (R^2) that characterise the trend lines obtained from the experimental data are close to the unit. Because of an R^2 of 1 means the dependent variable (in this investigation, the compressive stress) can be predicted without statistically significant errors from the independent variable (thickness of the jacket), the regression analysis is an effective way to describe such relations.

Table 4.4 shows the values of the slope of the lines that correlate the thickness of the jacket to the maximum compressive stress and the values of the coefficients of determination.

Table 4.4 - Parameters of trends lines

Mixture	Slope	R^2
FA0	0,58	1
FA20	0,49	0,96
FA50	0,41	0,93
FA70	0,29	0,76

As a direct proportionality has been found, the amount of UHP-FRCC can be then computed, and the thickness of the jacket may be adjusted to achieve the desired mechanical performances.

In fact, using the graph in Figure 4.19, it is possible to identify the thickness of the jacket necessary to obtain a precise value maximum compressive stress: setting a value on the y-axis, the four lines of the graph provide us with four values of the jacket, one for each type of mixture, which are necessary to obtain the desired performance.

In Section 4.4, a methodology was analysed to identify which is the best choice among these four values, not only related to the mechanical properties, but also to the ecological ones.

More concerning the “material substitution strategy”, as it can be seen in Figure 4.19, with the increase of the amount of fly ash in the mixture, the slope of the trend lines gradually decreases. From the previous comments relating the experimental values of specimens having the same sizes of jacket but different binder composition, an almost linear descending relationship emerged.

A more accurate analysis has been carried out, linking the slope of the trend lines previously considered with the percentage of cement replaced with fly ash (Figure 4.20).

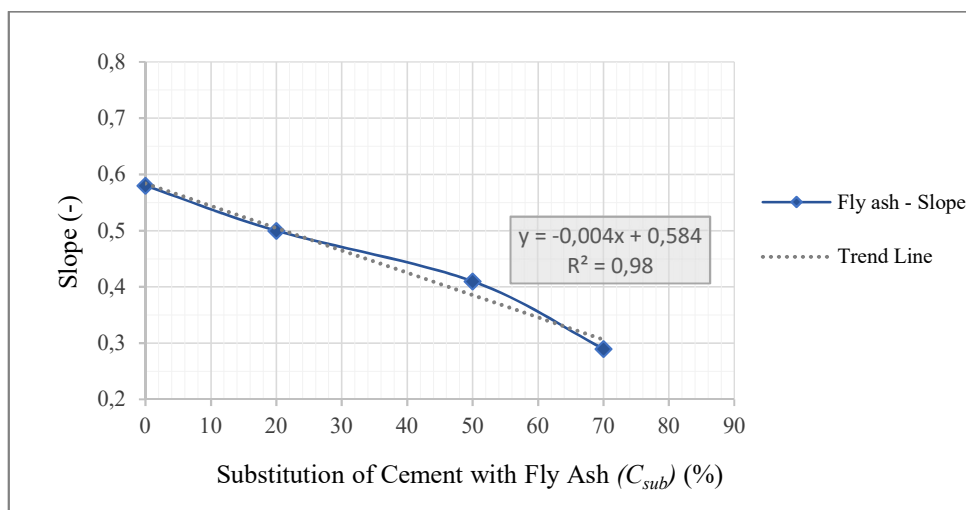


Figure 4.20 - Relationship between the Percentage of Fly Ash and the Slope⁶

⁶ “Slope” means the slope of the line that correlates the compression stress and the thickness of the jacket.

As it can be seen, the slope experiences a gradually reduction as the substitution of cement increases and a linear correlation has been found:

$$SLOPE = -0.004 * C_{sub} + 0,584$$

As in this analysis the slope is a parameter that well represents and describes the mechanical properties, a reliable relationship with the fly ash content in UHP-FRCC jackets has been determined.

A previous investigation has provided a relationship between the amount of fly ash and mechanical performances: also in that case, the maximum decrease progressively with the increase of the cement substitution. However, when the replacement of fly ash does not exceed 20%, such decrements are irrelevant when 20% of cement is replaced by fly ashes (Figure 4.21b) [36].

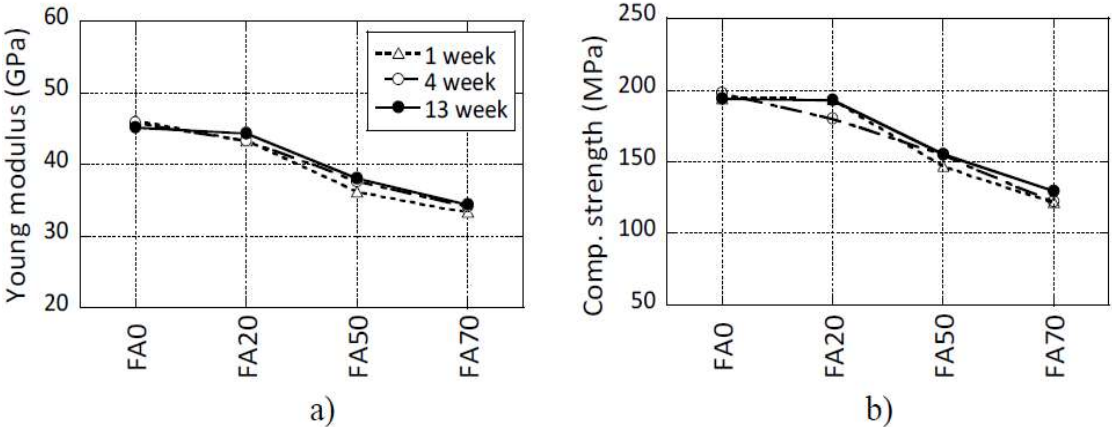


Figure 4.21 - Test results: (a) Young modulus in compression; (b) Compressive strength [36]

In that case, the experimental research did not concern the jacketing, but cylindrical specimens (diameter of 50 mm and height of 100) made only of UHP-FRCC were prepared and tested. Further research should be carried out to evaluate mechanical performance in the presence of small cement substitutions with fly ash.

4.1.2 Mechanical parameters

Two significant mechanical parameters for the behavioural characterisation of the cement composites are the Young's modulus and the Poisson's ratio. These has been calculated in order to find possible correlations with the thickness of the jackets and with the material composition of the mixtures.

- **Young's Modulus (E_{cm})**

The Young's Modulus of UHP-FRCC, as for ordinary concretes, presents increasing values with the compressive strength, as assumed by the different formulations present in the literature.

Whereas, however, in the ordinary concretes the compression modulus Young is essentially dependent on the mechanical properties of the cement matrix and is not influenced by the properties of the aggregates, in ultra high performance-fiber reinforced cementitious composites, due to the high strength of the matrix, it is also significantly dependent on the mechanical properties of the aggregates.

Eurocode 2 suggests an empirical equation that permits to predict the Young's Modulus (E_{cm}) from the maximum compressive strength (f'_c), expressed in MPa:

$$E_{cm} = 22000 \left(\frac{f'_c}{10} \right)^{0,3} \quad [50]$$

- **Poisson ration (ν)**

Poisson's ratio is defined as the ratio of transverse contraction strain to longitudinal extension strain in the direction of the applied load:⁷

$$\nu = - \frac{\varepsilon_t}{\varepsilon_l}$$

⁷ Tensile deformation is considered positive and compressive deformation is considered negative.

where

μ = Poisson's ratio

ε_t = transverse strain (m/m)

ε_l = longitudinal or axial strain (m/m).

In this experimental investigation, transverse strain is recorded by two horizontal strain gauges and the longitudinal strain is obtained with the embedded strain gauge. Both values have been calculated referring to a load equal to one third of the maximum effort ($P_{max}/3$), as required by Japanese Standards.

In Table 4.5 are shown the values of the Young's Modulus and Poisson's ratio obtained from the compression test.

Table 4.5 - Mechanical Parameters

Mixture	Thickness (mm)	E_{cm} (MPa)	ν (-)
FA0	25	37,90	0,120
	50	40,40	0,104
FA20	25	37,48	0,179
	37,5	38,30	0,157
	50	38,67	0,125
FA50	75	41,70	0,121
	25	36,25	0,195
	50	39,23	0,162
FA70	25	35,74	0,216
	37,5	36,33	0,168
	50	38,70	0,123

Young's modulus is directly connected to the maximum compression strain, and, although there isn't a linear proportionality, as the maximum effort increases, there is an increase in Young's modulus. Therefore, the same considerations stated in the previous paragraph apply: the modulus increases with the thickness of the jacket and, considering same sizes, there will be greater values with low percentages of cement replaced with fly ash.

In Figure 4.22, Poisson's ratio values for each mixture have been linked to the thickness of the jacket.

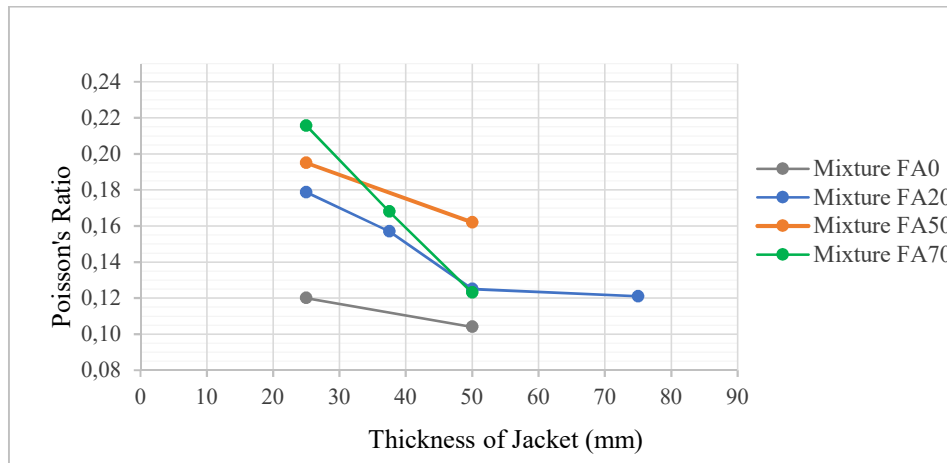


Figure 4.22 - Poisson's ratio

As it can be seen, with the progressive increase in the thickness of the jacket, there is a reduction of the Poisson's ratio. This behaviour can be easily explained using the definition: the Poisson's ratio is represented by the ratio between the transverse strain and longitudinal one. The transverse deformation is computed by the horizontal strain gauges applied to the surface of the jacket: so, it is fully consistent that there are minor deformations at a greater distance from the center of application of the load.

Moreover, a general trend may be found in the graph: the increase in the percentage of fly ash in the mixture corresponds to a parallel increase in the Poisson's ratio. This implies that jackets with high volumes of fly ash have a more ductile response than those where cement is the main element of the binder. A more detailed analysis of ductility will be presented in the next section.

However, there is no precise evidence on the truthfulness of this relationship because the Poisson's ratio of concrete cores confined by FA70 jackets with thicknesses of 37.5 mm and 50 mm do not follow this trend.

The values of deformations couldn't exactly represent a real behaviour in case they do not adhere perfectly to the surface of the jacket. Moreover, in case the break occurs

exactly in proximity to the sensors (Figure 4.23) the recorded Poisson's ratio may be not fully reliable.



Figure 4.23 - Strain gauges breakage

4.1.3 Ductility

The ductility of a material is a physical property that indicates its ability to deform under load by exhibiting plastic deformations before breaking: the greater is the plastic deformation reached before the break, the more ductile is therefore the material.

Moreover, the possibility of the structure to bear stresses deriving from a telluric event, without collapsing, depends on its ability to dissipate the energy produced.

From these considerations springs a fundamental principle of the design strategy of constructions in seismic areas: to resist without totally or partially collapsing to high-intensity earthquakes, the structures must have high deformation resources beyond their own elastic limits.

As previously anticipated, one of the main properties of UHP-FRCC is the ability to withstand loads for a long time before reaching the break, above all due to the role played by steel fibers. The main advantage offered by the fibers is the improvement of the ductility of the conglomerate in the phase following the first cracking phenomenon.

In fact, since the elongation at break of all the fibers is about 2-3 orders of magnitude greater than the breaking deformation of the cement matrix, the conglomerate crisis takes place long before the breakage of the fibers can occur. Therefore, the fibers relevantly reduce the fragile behaviour of the cement matrix.

Once the first cracks have been deformed, the fiber-reinforced concrete has an elastic-plastic behaviour (ductile behaviour) in the post-cracked phase, so it is able to bear loads even after the first cracks would appeared. In Figure 4.24, the main steps featuring the ductile behaviour of UHP-FRCC are highlighted: after a first section in which the response is almost linear and the deformations are still relatively low, then the deformations start to increase suddenly, with in response of a load that is more or less constant. The last part of the curve shows a smaller capacity to bear the load, until the moment when the break is reached. Different failure modes of the samples have been achieved; some patterns are shown in Annex 11.

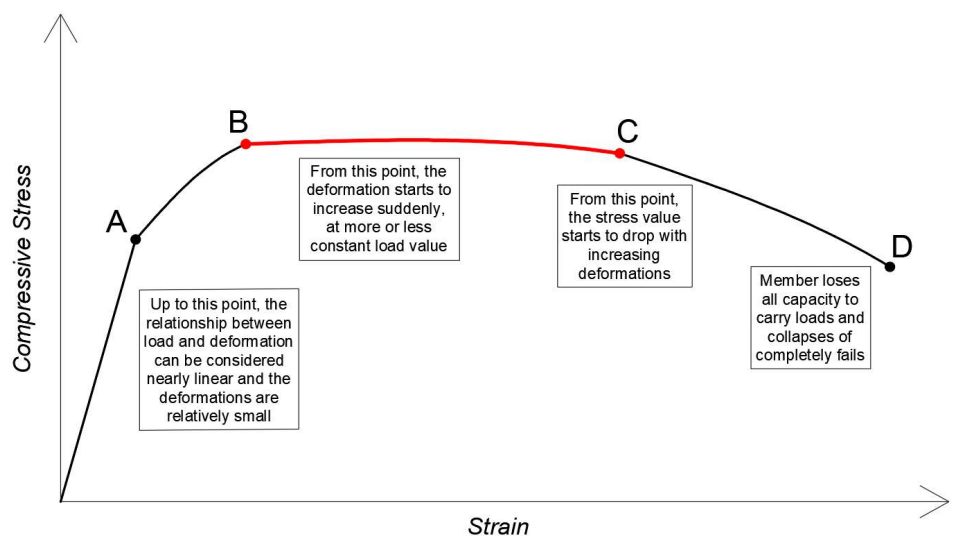


Figure 4.24 - Ductile behaviour of UHP-FRCC

In this analysis, attention has been paid on the red stretch in Figure 4.24, where the maximum compressive stress remains almost constant for higher and higher values of the deformation. In particular, it has been decided to compute the energy dissipated in the lapse between the achievement of the maximum stress (σ_{\max}) up to a loss of the carrying capacity of 10% ($0,9 \sigma_{\max}$), as shown in Figure 4.25.

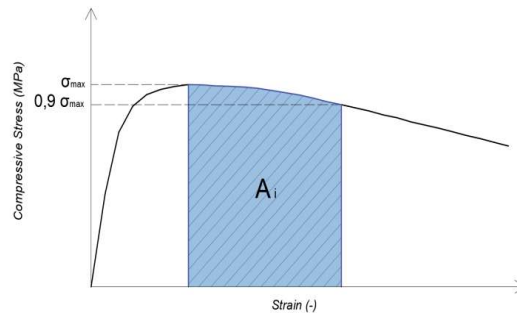


Figure 4.25 - Energy absorption between σ_{\max} and $0,9 \sigma_{\max}$

The area that has been computed refers to the average curve, whose tracing has been described in Figure 4.1. It was also verified that the area - calculated as the average of the values of the areas of the 3 samples - is almost equal to the value of the area obtained considering directly the average curve. Table 4.6 displays the areas related to the various samples (A_i) with reference to the area of the specimen having a jacket of 25 mm and without replacement of cement with fly ash (A_{FA0_25}).

Table 4.6 - Ductility evaluation: normalized areas

Mixture	Thickness (mm)	A_i/A_{FA0_25} (-)
FA0	25	1
	50	1,636
FA20	25	0,836
	37,5	1,181
	50	1,114
FA50	75	1,737
	25	0,915
FA70	50	1,492
	25	0,413
	37,5	0,989
	50	1,702

As it can be seen from the table, jackets with a thickness of 50 mm containing fly ash, experienced an increase in ductility with the increasing of the fly ash content, that even exceeds that of the FA0 mix, which generally shows better mechanical performance, with a 70% replacement. The values A_i/A_{FA0_25} of Table 4.6 have been especially used in the eco-mechanical analysis carried out in Section 4.3.2.

4.2 Ecological analysis

As discussed in the Sections 2.4 and 2.5, cement composites are a significant cause of the environmental pollution and considerable reduction of this ecologic impact may lie in a partial substitution of cement with fly ash, that is environmentally friendlier.

The parameter considered to evaluate the ecological performances is the amount of CO₂ emitted during the activities related the production of 1 m³ of UHP-FRCC.

The Japan Concrete Institute (JCI) has drawn up a list of the main materials used in cementitious composites with their relative CO₂ emissions. Table 4.1 shows the kilograms of CO₂ per ton released by the materials used in this experimental investigation.

Table 4.1 - Carbon footprint of some building materials

Materials	kg CO ₂ /t
Low Heat Cement	769
Fly ash	29
Silica sand	4,9
Water	34,8
Superplasticizer	150
Steel fibers	1320

From these values, the amount of CO₂ emitted per unit volume of each mixture has been calculated. In Table 4.2, the CO₂ reduction of mixtures containing fly ash compared to that in which the substitution strategy was not implemented has been reported as well.

Table 4.2 - CO₂ emissions of UHP-FRCCs

Mixture	kg of CO ₂ /m ³	Reduction of CO ₂
FA0	1209,63	-
FA20	1003,69	17%
FA50	719,02	41%
FA70	544,46	55%

When the amount of cement replaced with fly ash is quite high (>50%), the environmental impact is considerably reduced, up to being more than halved for FA70 mixture. Figure

4.26 shows the materials, with the percentage values, that are responsible for the main CO₂ emissions: for the mixtures FA0, FA20 and FA50, cement is the first source of pollution, with decreasing values as the fly ash content increases. Regarding the mixture FA70, instead, the steel fibers become the main source of CO₂ emissions, due to the high amount of cement substitution.

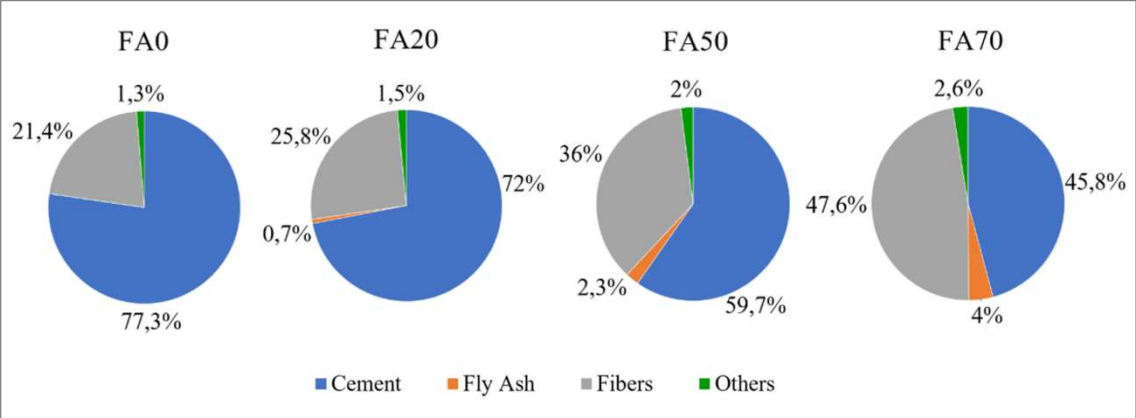


Figure 4.26 - Main materials responsible for environmental impact

After having featured the various mixtures from the point of view of the environmental impact, the CO₂ emissions of the individual specimens has been calculated. Results are provided in Table 4.7.

Table 4.7 – CO₂ emissions: UHP-FRCC jackets

Mixture	Thickness (mm)	Volume (m ³)	CO ₂ emission (kg)
FA0	25	0,0017	2,114
	50	0,0042	5,073
FA20	25	0,0017	1,754
	37,5	0,0029	2,894
	50	0,0042	4,209
	75	0,0073	7,367
FA50	25	0,0017	1,257
	50	0,0042	3,016
FA70	25	0,0017	0,951
	37,5	0,0029	1,570
	50	0,0042	2,283

In Figure 4.27, the environmental impact, in terms of CO₂ emissions, of the various UHP-FRCC jackets has been compared. For the sake of completeness, values of some specimens, that have not been tested, have been reported as well (dotted bars).

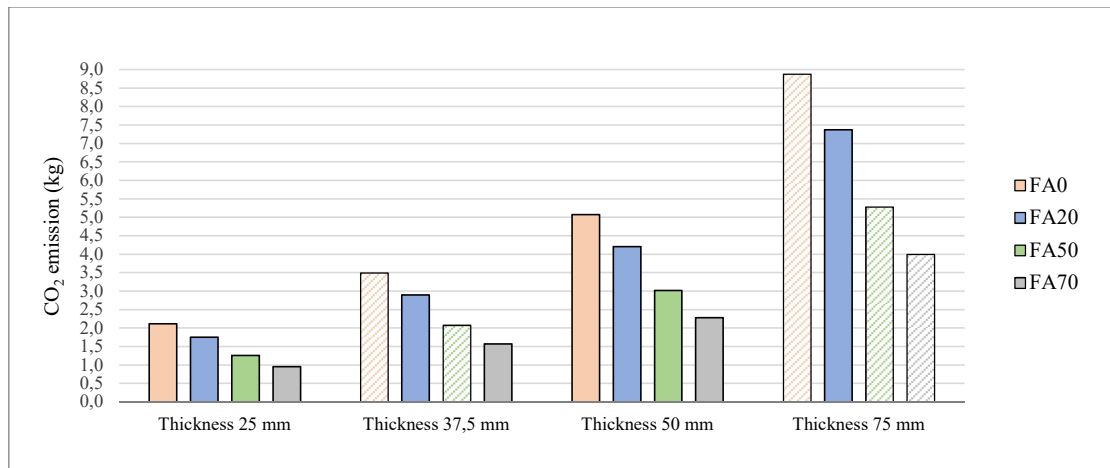


Figure 4.27 - Comparison of CO₂ emissions of UHP-FRCC jackets

From this graph, it may be easy to notice that a reduced environmental impact can be obtained by increasing the thickness of the jacket and, in parallel, by increasing the percentage of fly ash in the mixture.

These values have been used to carry out the eco-mechanical analysis, that will be described in the next section, in order to find a point of balance between mechanical and environmental performances.

4.3 Eco-mechanical performance

In this section, the mechanical and ecological performances of UHP-FRCC jackets, evaluated separately in Sections 4.1 and 4.2, has been analysed simultaneously, to assess which solutions may ensure a low environmental impact, without compromising the mechanical response. This eco-mechanical analysis is conducted with the chart proposed by Fantilli e Chiaia and already described in Section 2.6. Maximum compressive stress and ductility have been considered as mechanical parameters (MI), instead the ecological impact has been evaluated with CO₂ emissions (EI).

The reference values MI_{inf} and EI_{sup} refer to the concrete cylinder reinforced with UHP-FRCC jacket of 25 mm without substitution of cement with fly ash.

- **Compressive stress**

Figure 4.28 shows the results of the eco-mechanical analysis in which the mechanical index (MI/MI_{inf}) represents the maximum compressive stress.

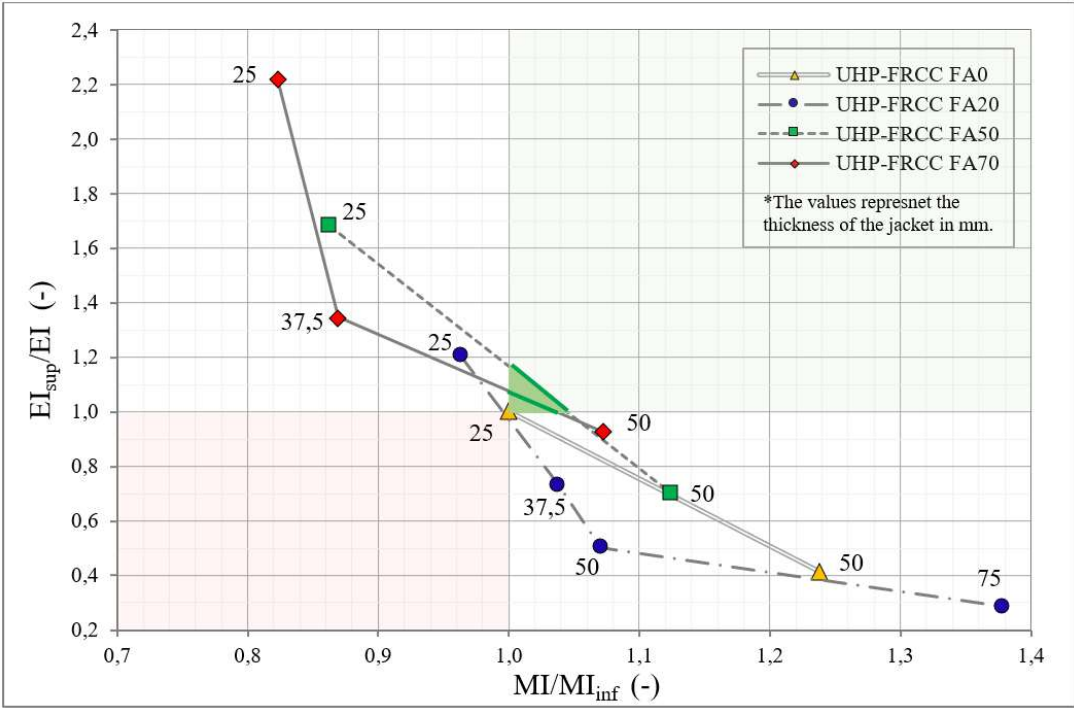


Figure 4.28 - Eco-Mechanical analysis: Compressive Stress

The central point of the coordinate graph (1;1) obviously represents the mechanical and ecological performances of the reinforced cylinder with a 25 mm jacket and without the application of the “material substitution strategy”; it has been drawn for the sake of completeness, since it helps to feature the FA0 curve.

The graph displays all the experimental values of the specimens that were tested. The segments connecting the experimental points have been traced assuming a linear trend: as the points are sufficiently close each others, this can allow to consider this assumption as reliable. As can be seen from the graph, most of the points fall in the Zone III, where the mechanical performances are increased at the expense of a higher environmental impact.

The other group of experimental values falls completely within the Zone I, showing ecological performances far greater than those shown by the reference specimen. However, the graph shows an area, coloured in green, in which the mechanical properties are improved without prejudging the ecological aspect. In particular, two precise segments, highlighted in darker green, can be identified in the graph: the first relating jackets with a thickness between 37.5 mm and 50 mm made of UHP-FRCC FA70; the second, concerning the FA50 mixture and a range of thickness between 25 and 50 mm. By linear interpolation, an estimation of the extreme values of the intervals can be provided: in the case of mixture FA70, the range of thicknesses falling in the Zone III is between 44.7 and 47.2 mm, instead, for the mixture FA50, values of thicknesses between 34.9 and 38.1 mm. For these values, it is possible to obtain up to a maximum decrease of CO₂ emission of about 20%, without compromising the load carrying, which is anyway higher than that shown by the reference specimen: putting it simply, the eco-mechanical analysis has identified solutions which may ensure a low environmental impact, without compromising the mechanical response.

Nevertheless, in the case of the mixture FA20, the increase in the jacket causes a growth of the compressive stress, but the low substitution of cement with fly is not enough to compensate the environmental impact.

- **Ductility**

Figure 4.29 shows the results of the eco-mechanical analysis in which the mechanical index (MI/MI_{inf}) refers to the ductility, evaluated as the energy dissipated in the lapse between the achievement of the maximum stress up to a loss of 10% of its value.

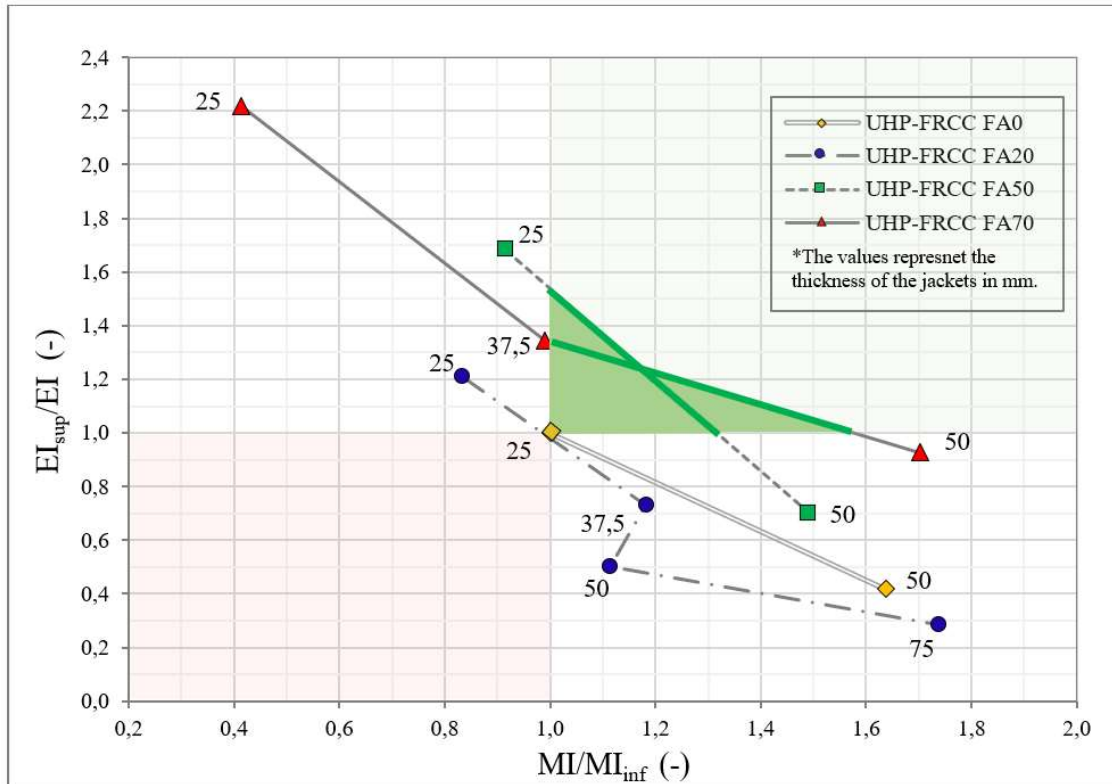


Figure 4.29 - Eco-Mechanical analysis: Ductility

As for the previous analysis, green coloured area in the graph represents the set of values for which both the mechanical and ecological performances have been increased compared to the reference specimen. In this case, the high percentage of cement replaced with fly ash, together with an increase of the thickness of the jacket, causes a consistent growth of the ductility of the confined cylinder, without entailing a high environmental impact. Particularly, almost all the thicknesses between 37.5 mm and 50 mm for UHP-FRCC jacket with the 70% of cement replaced by fly ash experience an increase in ductility and, in parallel, involve less CO₂ emissions. By linear interpolation, the range

between 37.6 and 47.2 mm has been estimated. Moreover, the mixture FA50 shows good ductility properties as well: the values of thicknesses falling in the Zone II are estimated between 26.9 and 38.1 mm.

As for the eco-mechanical analysis referring to the maximum compression stress, with the UHP-FRCC FA20 mixture it is possible to achieve greater mechanical performances than the specimen with a 25 mm jacket and without replacement of cement, at the expense, however, of a higher ecological impact.

4.4 Design procedure

As anticipated in Section 4.1.1, due to the linear relationships between the compressive stress and the thickness of the jacket, according to the type of mixture, it is possible to choose the exact size of the UHP-FRCC jacket necessary to obtain a precise value maximum compressive stress.

However, to limit the environmental impact as much as possible, it is necessary to consider, simultaneously, mechanical and ecological performances. Therefore, a design procedure, shown in Figure 4.30, has been developed, in order to optimise the UHP-FRCC jacketing system and to jointly reduce the CO₂ emissions.

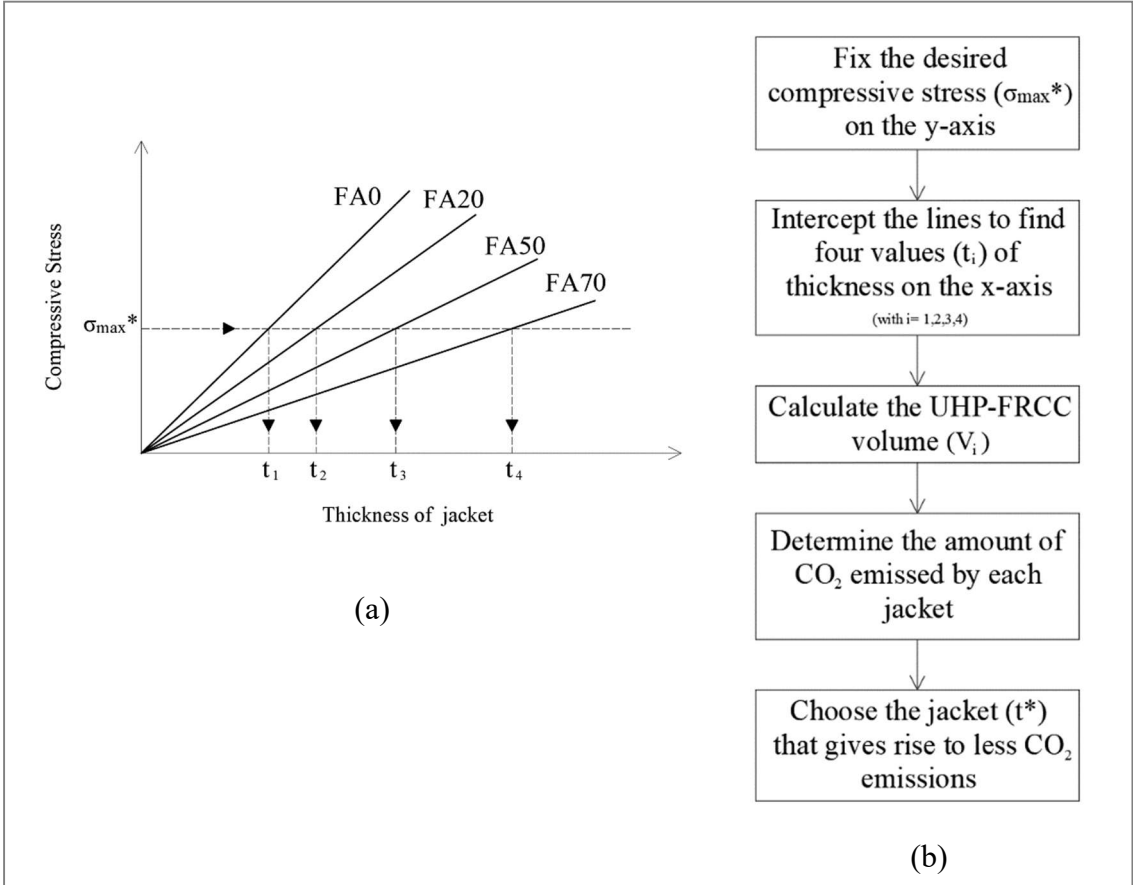


Figure 4.30 - (a) Reference scheme⁸; (b) Design process

⁸ A detailed scheme with the equations of the lines has been shown in Figure 4.19

Having fixed the desired maximum compressive stress to be achieved, using the reference scheme in Figure 4.30a, the trend lines provide 4 values of thicknesses of jacket on the x-axis (t_1, t_2, t_3, t_4), one for each type of mixture (FA0, FA20, FA50, FA70). Then, the volumes of UHP-FRCC are computed and, using the values provided in Table 4.2, the CO₂ emissions have been calculated. In this way, the UHP-FRCC jacket that, with the same mechanical performances, has a lower environmental impact, is determined.

Following this conceptual model, the graph Figure 4.31 has been drawn to show the relationship between the CO₂ emissions and the percentage of cement replaced with fly ash.

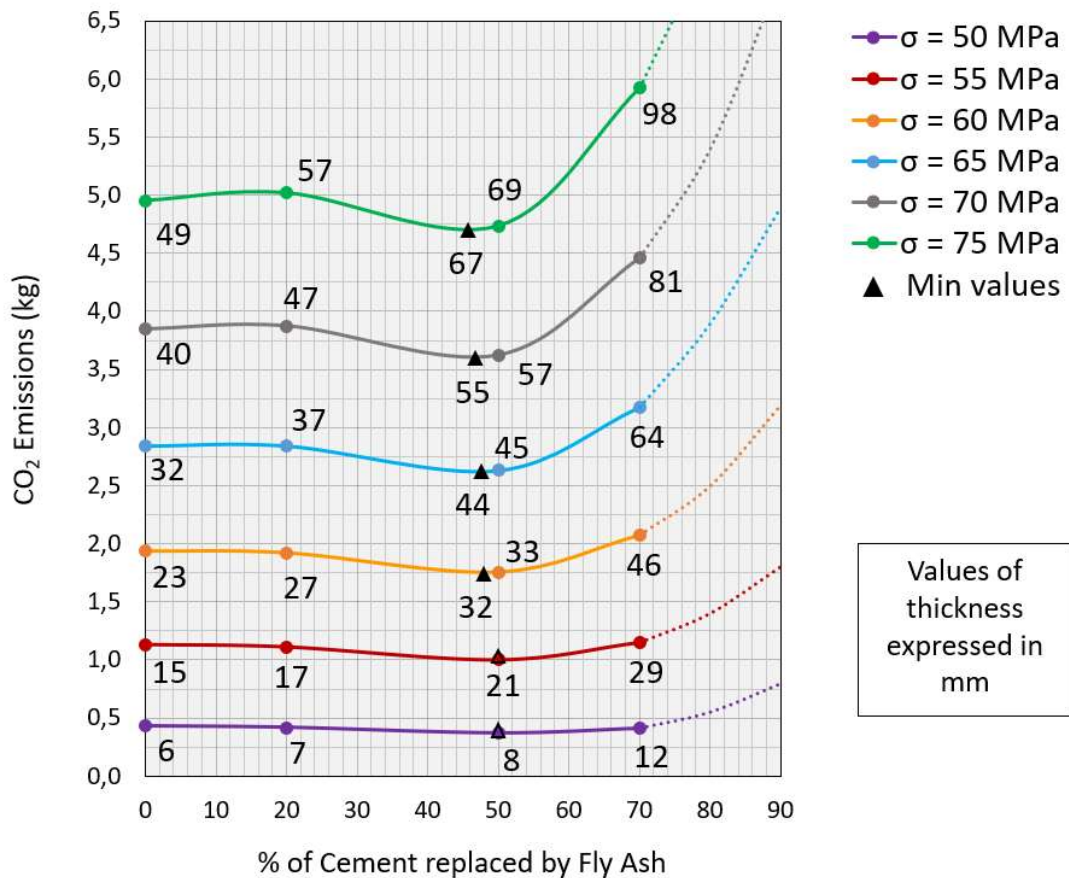


Figure 4.31 - The ecological impact of UHP-FRCC jackets made with different mixtures (having different σ_{max})

Maximum compressive stress from 50 MPa to 75 MPa, with an interval of 5 MPa, have been set and, for each load carrying capacity, four thicknesses of the jackets has been

obtained referring to the mixtures FA0, FA20, FA50, and FA70 (the values inside the graph in Figure 4.31 represent the thicknesses of the jackets, expressed in millimetres). In this case, other than reporting only the four values relating to the mixes that have been experimentally prepared, the curves that connect the four points have been drawn and a theoretical future trend has been shown (dashed segments).

In this way, not uniquely the best combination of thickness and mixture between four possibilities can be established, but it is also possible to refine the research. Using the graph in Figure 3.31, it can be noticed, for instance, that the optimal replacement of cement with fly ash to achieve a compressive stress of 75 MPa is 46%.

Therefore, it is possible to find a common trend that characterises the minimum ecological impact of UHP-FRCC jackets (Figure 4.32).

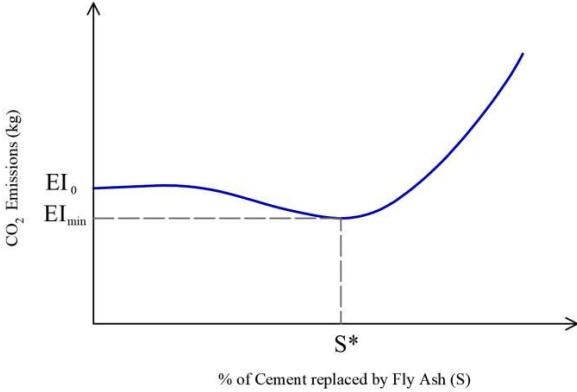


Figure 4.32 - The minimum ecological impact of a UHP-FRCC jackets (having a specific σ_{max})

For a given maximum compressive stress, the impact of UHP-FRCC jacket has a minimum ecological impact (EI_{min}) in correspondence of the substitution rate S* (where 0 < S* < 100%). For low substitutions of cement, CO₂ emissions are still high, with a gradual decrease until the minimum value S* is reached. Indeed, when the substitution strategy is forced to higher percentages, the same mechanical performances can be obtained only through solutions with a high environmental impact.

An equivalent trend was obtained by Fantilli *et al.*, in an investigation on reinforced concrete beam: also in that case, an optimal value for the replacement of cement with fly ash was found, in order to obtain the lowest environmental impact [38].

CHAPTER 5

CONCLUSION AND FUTURE RESEARCH

The aim of this experimental research was to evaluate the effect of confinement of normal concrete cylinders with UHP-FRCC jackets, in order to investigate the applications on retrofitting of existent structures.

In fact, UHP-FRCC is often recently used for the repair, strengthening and seismic retrofitting of old constructions, due to the high mechanical properties, as high compressive strength, high ductility, durability and energy absorption capacity compared with normal concrete.

Particularly, a widely application is to 'harden' those parts of the structure that are exposed to high environmental and mechanical loading, such as columns and beams, especially in the most highly stressed sections and in the critical structural points.

However, although these cementitious composites improve the mechanical responses, their ecological impact are very high, due to both the copious amount of cement used in the UHP-FRCC's mixtures and the steel fibers. In fact, a large quantity of CO₂ is released during the cement production, especially for the calcination of limestone and the for the manufacturing.

To overcome the high environmental impact, in this investigation industrial by-product, as fly ash, are used in the binder in substitution of different percentages of cement.

Thus, replacing part of the cement content with fly ash could be an effective way to improve also the ecological properties of UHP-FRCC composites.

The main goal of this experimental research is to examine the behaviour, under compressive load, of normal concrete cylinder, having radius of 50 mm and height of 200 mm, are reinforced with UHP-FRCC jackets, with different thicknesses, respectively of 25 mm, 37.5 mm, 50 mm and 75 mm.

Moreover, four mixtures were prepared, modifying only the percentage of cement and fly ash, being unchanged the portions of other materials: FA0, FA20, FA50, FA70, respectively with 0%, 20%, 50%, 70% of cement replaced by fly ash.

The specimens were tested under uniaxial compression and the deformation is the controlled parameter.

A linear relationship between the thickness of the jackets and the compressive stress has been found: with the progressive increase in the size of the jacket, the maximum load capacity grows in a linear way.

Therefore, the amount of UHP-FRCC can be then computed, and the thickness of the jacket may be adjusted to achieve the desired performances.

Another considerable finding that emerged from this research is that the mechanical properties of the specimens decrease linearly with the increase of cement substitution with fly ash, and the linear relationship has been found.

With an eco-mechanical analysis, it has been possible to identify solutions which may ensure a low environmental impact, without compromising the mechanical response.

The eco-mechanical analysis was performed according to the non-dimensional chart proposed by Fantilli and Chiaia [43], in which ecological and mechanical performances has been combined respectively through the Ecological Index (EI) and the Mechanical Index (MI).

The mechanical properties that have been considered are the maximum compressive stress and the ductility, estimated through the absorption energy. Instead, in place of ecological parameter, the emission of CO₂ released by the production of 1 m³ of UHP-FRCC mixture has been considered.

As reference sample, it has been chosen that with no cement replacement and with a jacket of 25 mm.

The eco-mechanical analysis showed that the partial replacement of cement with fly ash, combined with an increase in the thickness of the jacket, simultaneously guarantees better mechanical and ecological performance: various thicknesses of jackets made of UHP-FRCC FA50 and FA70 may ensure higher eco-mechanical response.

On the contrary, UHP-FRCC jackets made with the 20% of cement replaced by fly ash exhibited a remarkable carrying load capacity, that, however, can't compensate the high CO₂ emissions.

Finally, in this research, a design procedure has been developed to optimise the UHP-FRCC jacketing system and to jointly reduce the environmental impact.

Particularly, it has been found that, for a given maximum compressive stress, the impact of UHP-FRCC jacket has a minimum ecological impact in correspondence of the substitution rate: the percentage of cement replaced by fly ash that guarantees both mechanical and ecological properties ranges between 40% and 50%.

This implies that UHP-FRCC jackets with low fly ash concentrations show mechanical responses that don't compensate the high environmental; in the same way, for high amounts of cement substitution, the jacketing system is so thick to cause an even higher environmental impact.

For this reason, in the future, new UHP-FRCC mixtures should be prepared by focusing on intervals around 40% and 50%.

On the basis of this thesis, some research topics are suggested for further investigations:

1. Specific study of UHP-FRCC mix design is recommended. Especially, changes in the volume of steel fibers and the use of other industry by-product can be assessed, in order to optimize the performance of the mixture.
2. New specimens with greater height may be designed and tested to get closer to the real case of jacketing. In fact, in real case, the ratio between the height of the column and the thickness of the jacket is much higher than that used in laboratory specimens. Therefore, it is necessary to investigate how the height of the cylinders is linked to the maximum load carrying capacity and the ductility of the jacketing system.
3. Linked to point 2, new casting methods for larger scale specimens should be searched and evaluated. In fact, the excellent workability obtained for the mixtures prepared during this experimental research, may no longer be suitable to cast specimens with greater height.

ANNEXES

ANNEX 1: GEOMETRICAL PROPERTIES

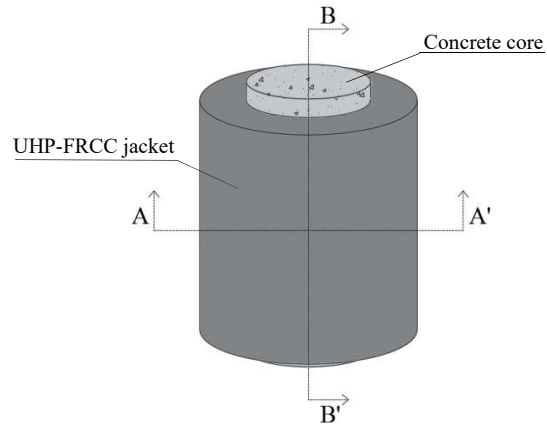
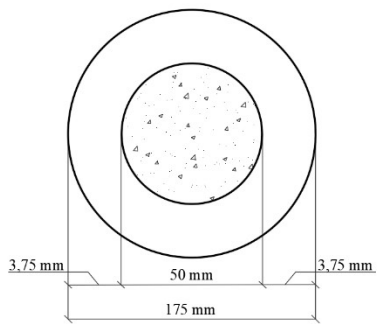
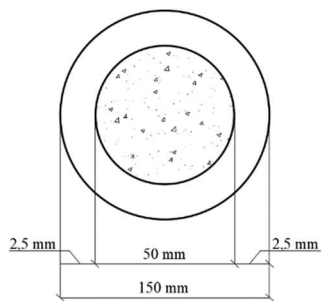
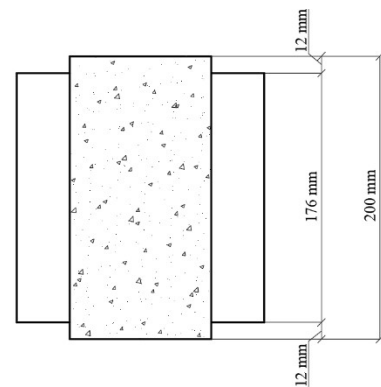
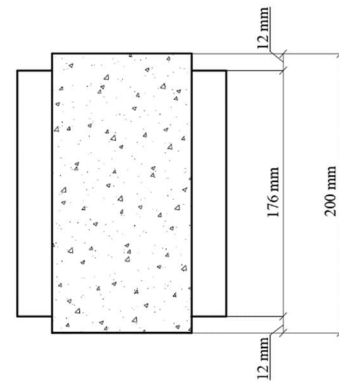


Figure 6.1 - Scheme of concrete cylinder reinforced with UHP-FRCC jacket

Sections A-A'



Sections B-B'



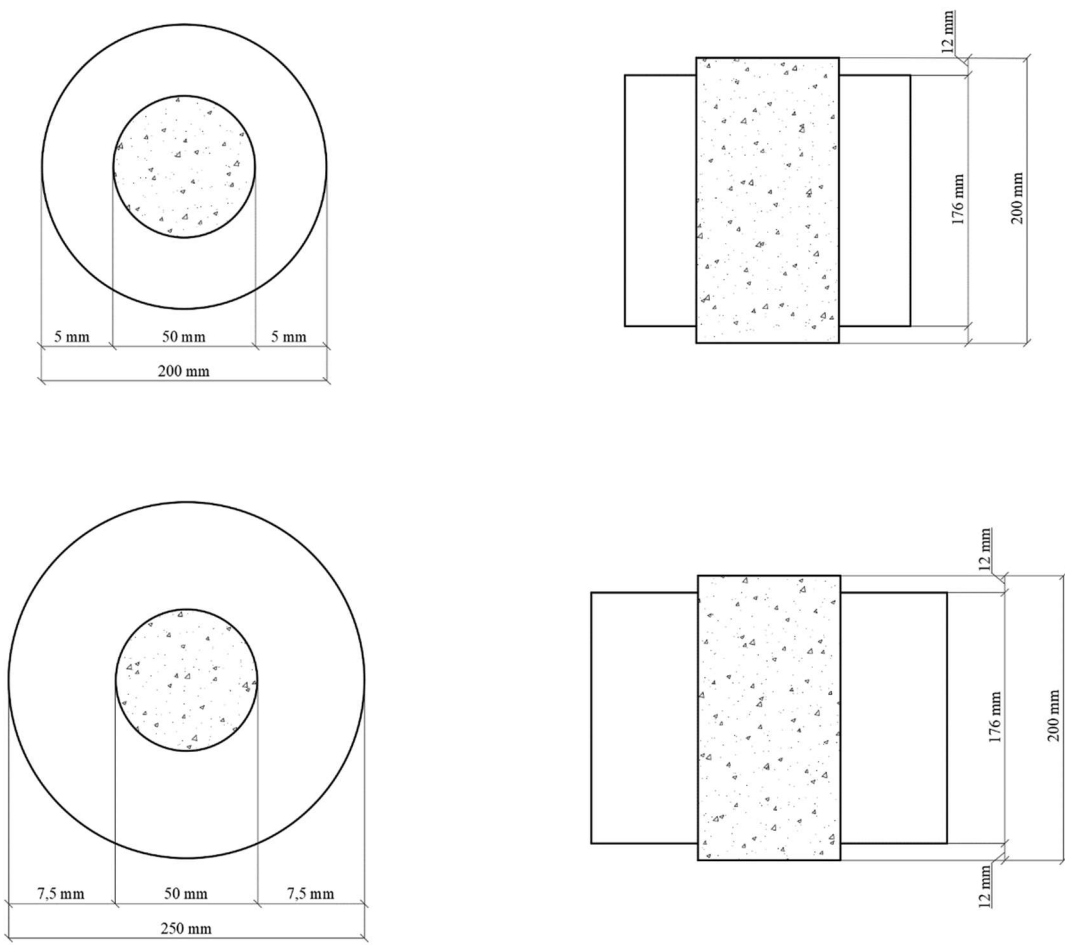


Figure 6.2- Crossing Sections

ANNEX 2: CODIFICATION OF SPECIMENS

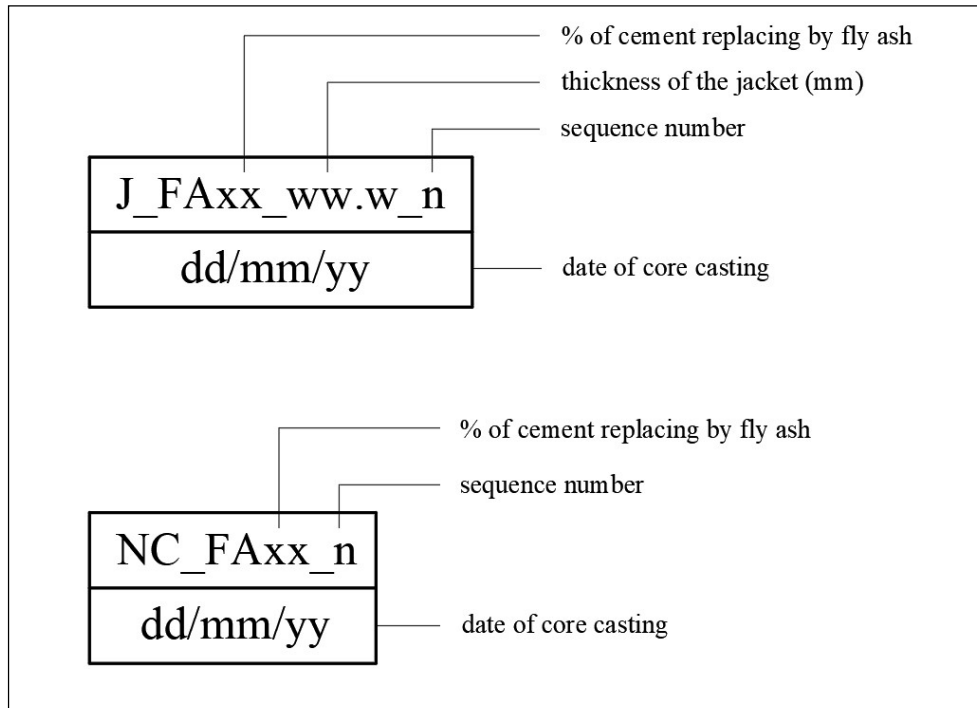


Figure 6.3 - Codification⁹

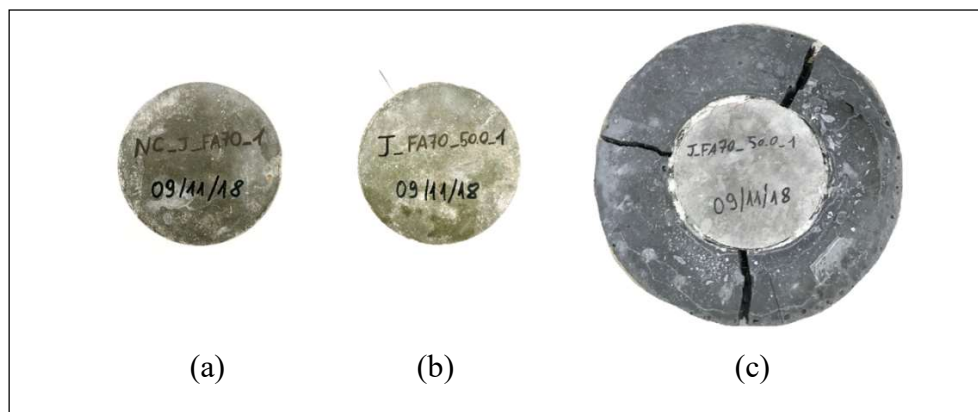


Figure 6.4 - Codification of normal concrete cylinder (a), confined cylinder before (b) and after (c) casting

⁹ J = Jacket NC = Normal Concrete; FA = Fly Ash

ANNEX 3: SLUMP TEST

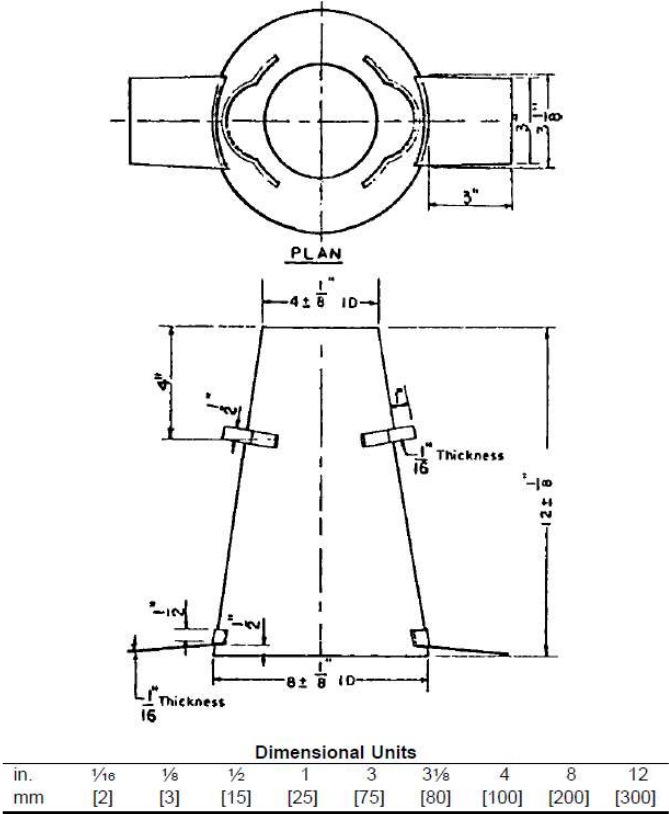


Figure 6.5 - Mold for Slump Test [50]

Table 6.1 - Slump Test: results

Date	Concrete Temperature (°C)	Slump (cm)	Notes
15/10/2018	19	8,7	Trial
25/10/2018	20	8,0	-
09/11/2018	17	8,1	-
20/11/2018	14	8,2	-
21/12/2019	12	8,2	-

ANNEX 4: AIR CONTENT TEST

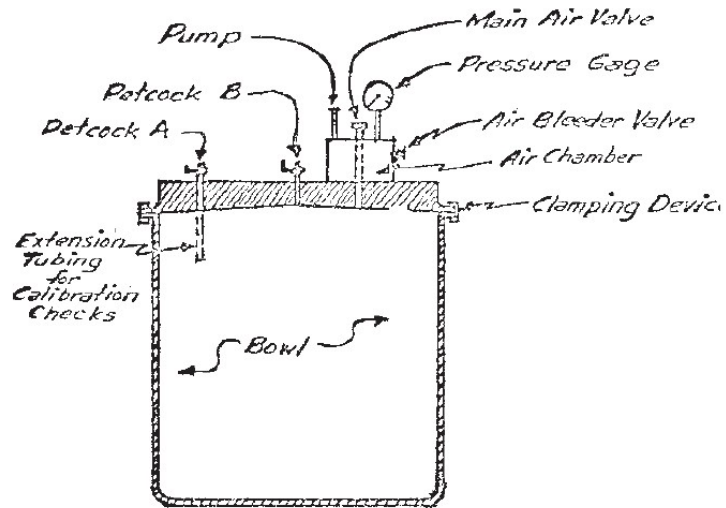


Figure 6.6 - Schematic Diagram – Type-B Meter [51]

Table 6.2 - Air Content Test: results

Date	Concrete Temperature (°C)	Air Content (%)
15/10/2018	19	2,6
25/10/2018	20	1,5
09/11/2018	17	1,9
20/11/2018	14	-
21/12/2019	12	2,4

ANNEX 5: FLOW TABLE TEST

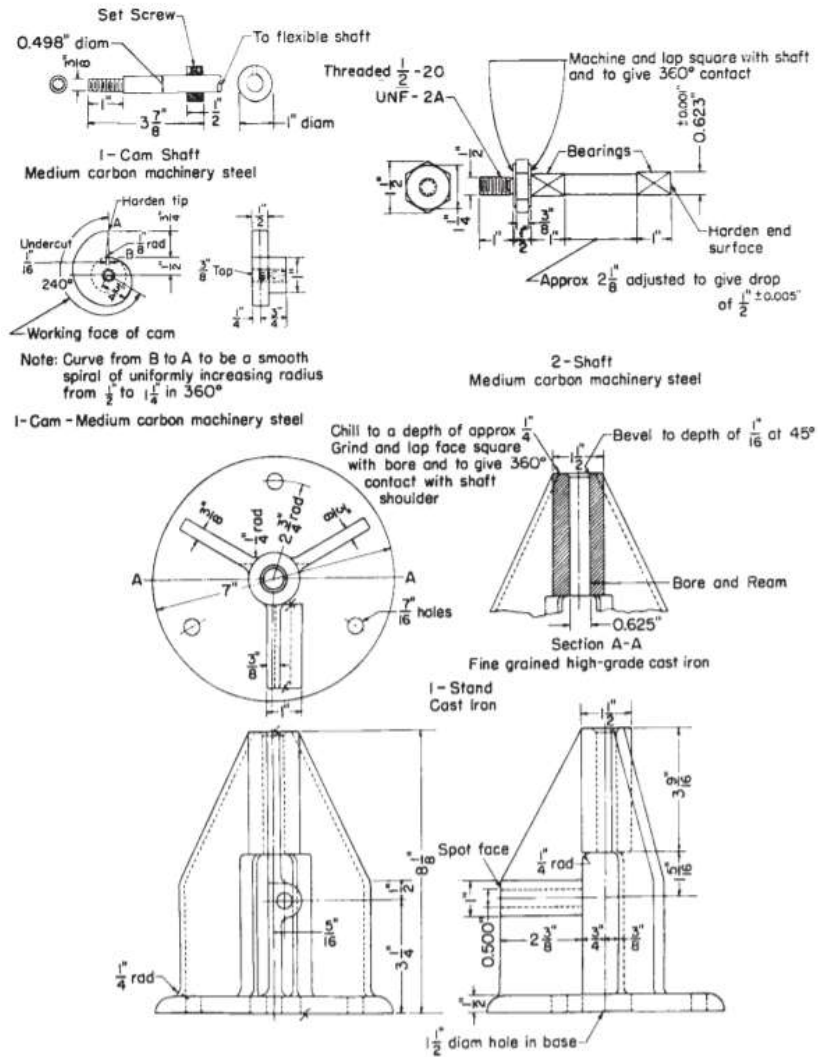


Figure 6.7 - Flow Table and Accessory Apparatus [52]

Table 6.3 - Flow Table Test: results

Date	Mixture	Mixture Temperature (°C)	Flow ($f_1 - f_2$) (mm)
05/11/2018	FA20	23	264 - 256
19/11/2018	FA70	23	245 - 250
03/12/2018	FA50	20	290 - 285
07/01/2019	FA0	18	190 - 192

ANNEX 6: RESULTS MIXTURE FA0

Table 6.4 - Mixture FA0: jackets of 25 mm

Specimen	P_{max} (kN)	σ_{max} (MPa)	σ/f_c CORE (MPa)
J FA0 25.0 1	482,40	61,42	1,32
J FA0 25.0 2	475,00	60,48	1,30
J FA0 25.0 3	487,00	62,01	1,33
Average	481,47	61,30	1,32

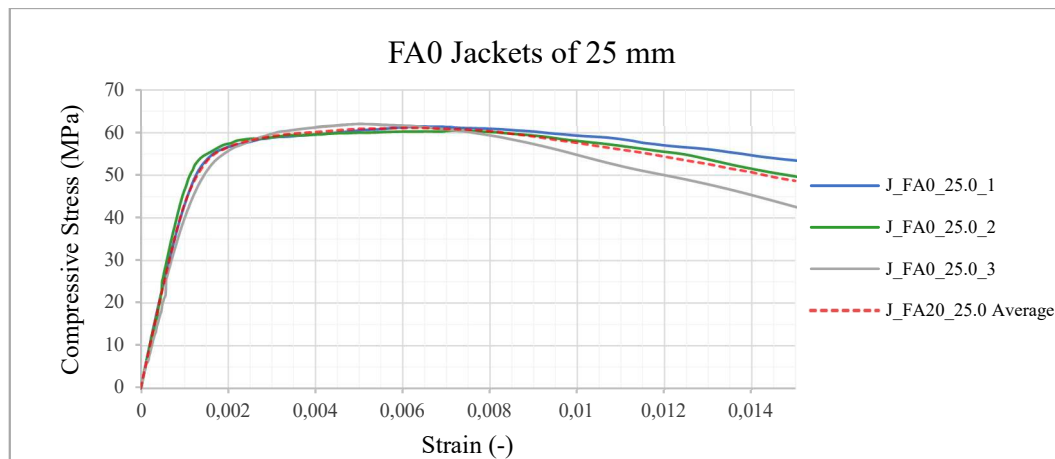


Figure 6.8 - Stress-strain curves: FA0 Jackets of 25 mm

Table 6.5 - Mixture FA0: jackets of 50 mm

Specimen	P_{max} (kN)	σ_{max} (MPa)	σ/f_c CORE (MPa)
J FA0 50.0 1	595,60	75,83	1,63
J FA0 50.0 2	580,60	73,92	1,59
J FA0 50.0 3	611,60	77,87	1,67
Average	595,93	75,88	1,63

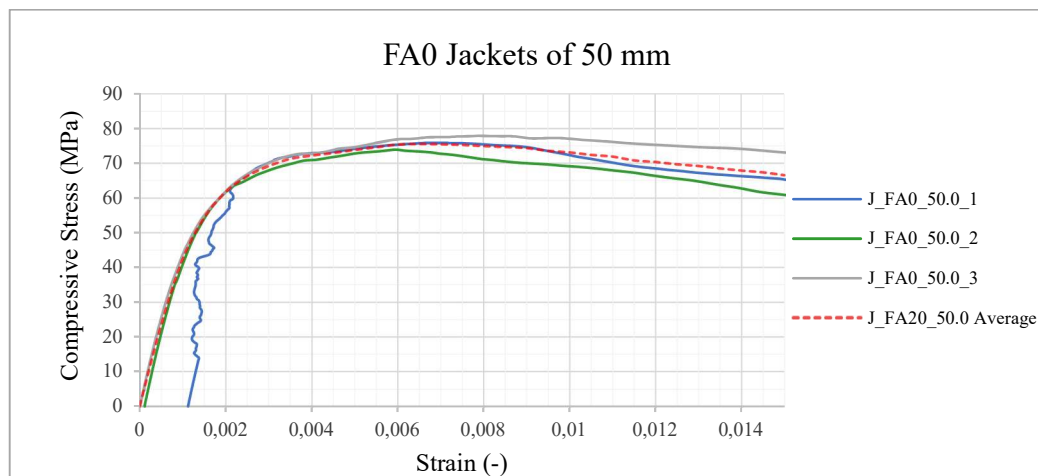


Figure 6.9 - Stress-strain curves: FA0 Jackets of 50 mm

ANNEX 7: RESULTS MIXTURE FA20

Table 6.6 - Mixture FA20: jackets of 25 mm

Specimen	P_{max} (kN)	σ_{max} (MPa)	σ/f_c CORE (MPa)
J FA20 25.0 1	468,40	59,64	1,28
J FA20 25.0 2	461,60	58,77	1,26
J FA20 25.0 3	461,60	58,77	1,26
Average	463,87	59,06	1,27

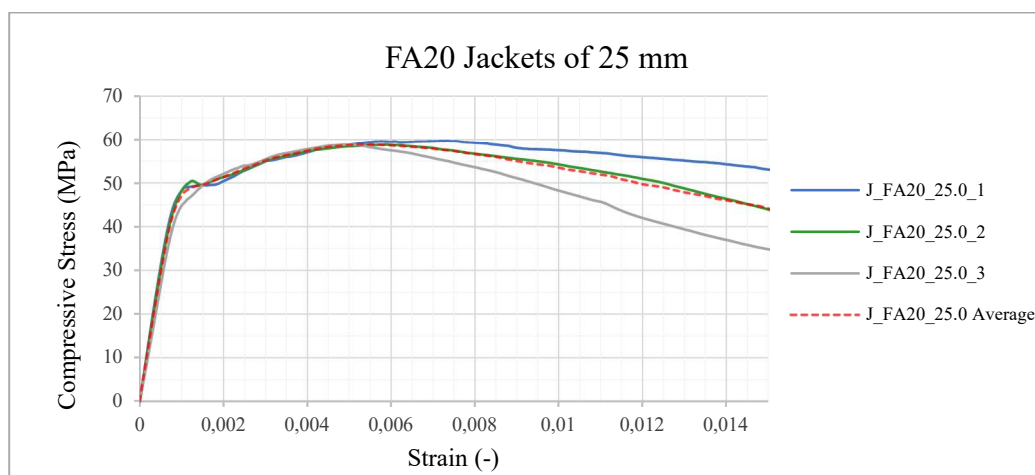


Figure 6.10 - Stress-strain curves: FA20 Jackets of 25 mm

Table 6.7 - Mixture FA20: jackets of 37,5 mm

Specimen	P_{max} (kN)	σ_{max} (MPa)	σ/f_c CORE (MPa)
J FA20 37.5 1	490,00	62,39	1,34
J FA20 37.5 2	552,60	70,36	1,51
J FA20 37.5 3	456,80	58,16	1,25
Average	499,80	63,64	1,37

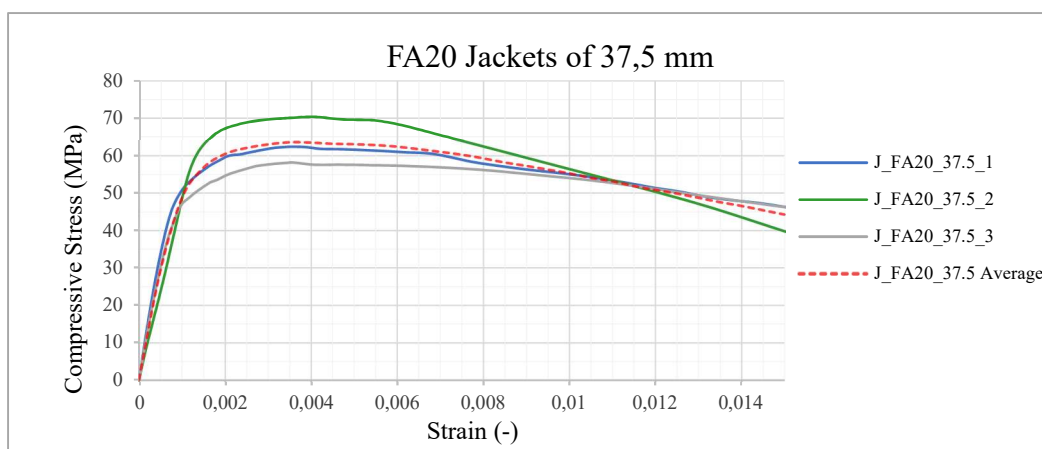


Figure 6.11 - Stress-strain curves: FA20 Jackets of 37,5 mm

Table 6.8 - Mixture FA20: jackets of 50 mm

Specimen	P_{max} (kN)	σ_{max} (MPa)	σ/f_c CORE (MPa)
J FA20 50.0 1	488,40	62,19	1,34
J FA20 50.0 2	517,00	65,83	1,42
J FA20 50.0 3	540,40	68,81	1,48
Average	515,27	65,61	1,41

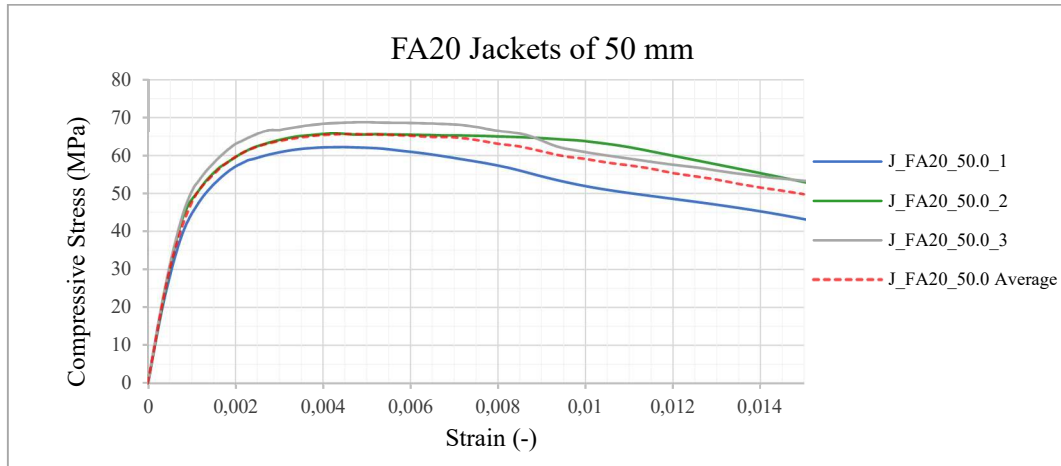


Figure 6.12 - Stress-strain curves: FA20 Jackets of 50 mm

Table 6.9 - Mixture FA20: jackets of 25 mm

Specimen	P_{max} (kN)	σ_{max} (MPa)	σ/f_c CORE (MPa)
J FA20 75.0 1	588,80	74,97	1,61
J FA20 75.0 2	675,60	86,02	1,85
J FA20 75.0 3	726,20	92,46	1,99
Average	663,53	84,48	1,82

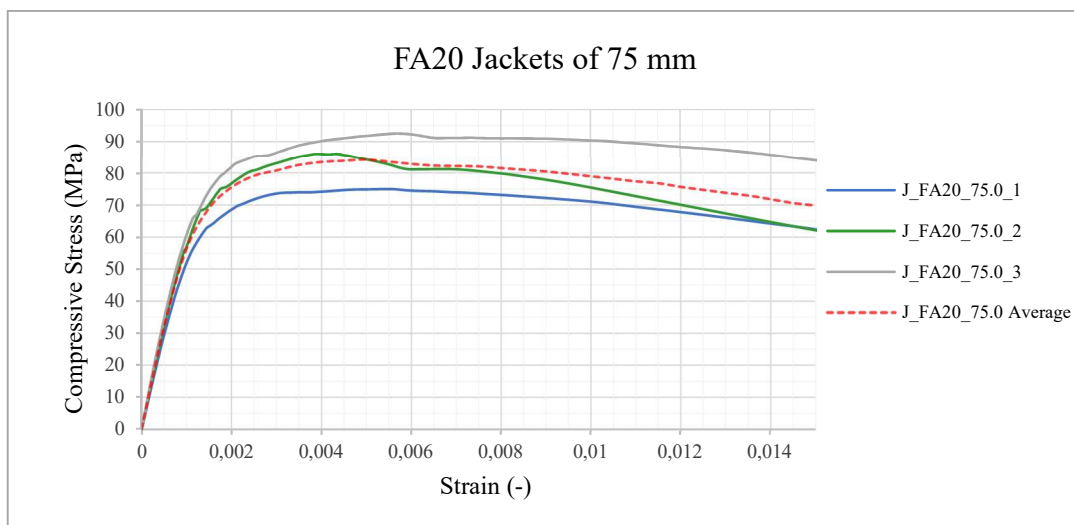


Figure 6.13 - Stress-strain curves: FA20 Jackets of 75 mm

ANNEX 8: RESULTS MIXTURE FA50

Table 6.10 - Mixture FA50: jackets of 25 mm

Specimen	P_{max} (kN)	σ_{max} (MPa)	σ/f_c CORE (MPa)
J FA50 25.0 1	394,20	50,19	1,08
J FA50 25.0 2	439,40	55,95	1,20
J FA50 25.0 3	412,60	52,53	1,13
Average	415,40	52,89	1,14

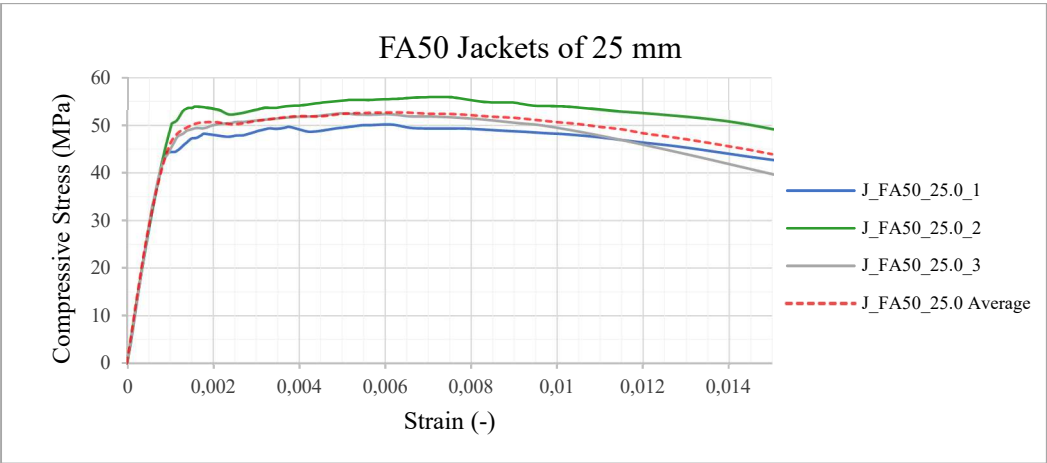


Figure 6.14 - Stress-strain curves: FA50 Jackets of 25 mm

Table 6.11 - Mixture FA50: jackets of 50 mm

Specimen	P_{max} (kN)	σ_{max} (MPa)	σ/f_c CORE (MPa)
J FA50 50.0 1	594,80	75,73	1,63
J FA50 50.0 2	529,00	67,35	1,45
J FA50 50.0 3	499,20	63,56	1,37
Average	541,00	68,88	1,48

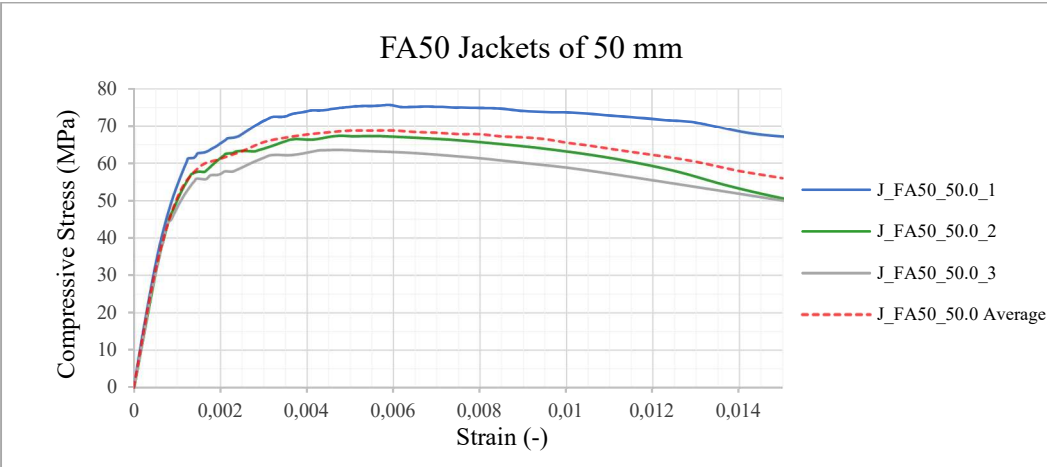


Figure 6.15 - Stress-strain curves: FA50 Jackets of 50 mm

ANNEX 9: RESULTS MIXTURE FA70

Table 6.12 - Mixture FA70: jackets of 25 mm

Specimen	P_{max} (kN)	σ_{max} (MPa)	σ/f_c CORE (MPa)
J FA70 25.0 1	393,80	50,14	1,08
J FA70 25.0 2	405,60	51,64	1,11
J FA70 25.0 3	388,80	49,50	1,06
Average	396,07	50,43	1,08

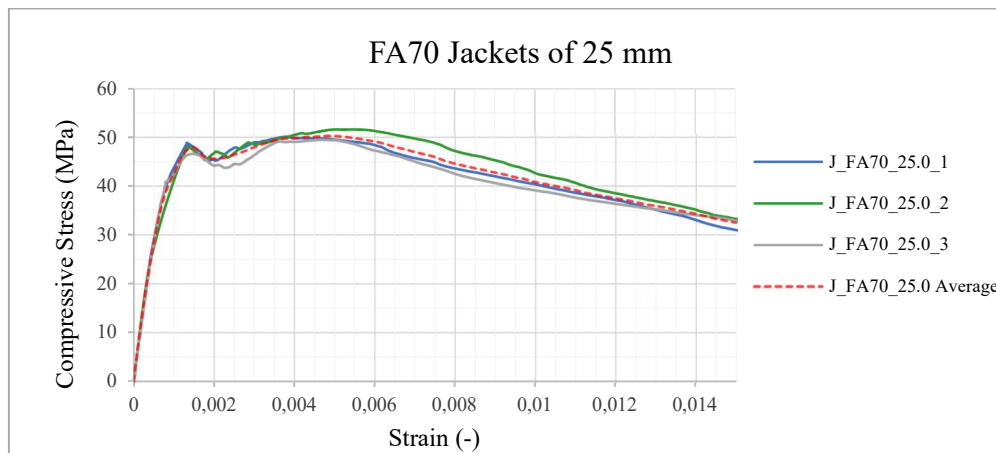


Figure 6.16 - Stress-strain curves: FA70 Jackets of 25 mm

Table 6.13 - Mixture FA70: jackets of 37,5 mm

Specimen	P_{max} (kN)	σ_{max} (MPa)	σ/f_c CORE (MPa)
J FA70 37.5 1	399,60	50,88	1,09
J FA70 37.5 2	450,00	57,30	1,23
J FA70 37.5 3	405,60	51,64	1,11
Average	418,40	53,27	1,15

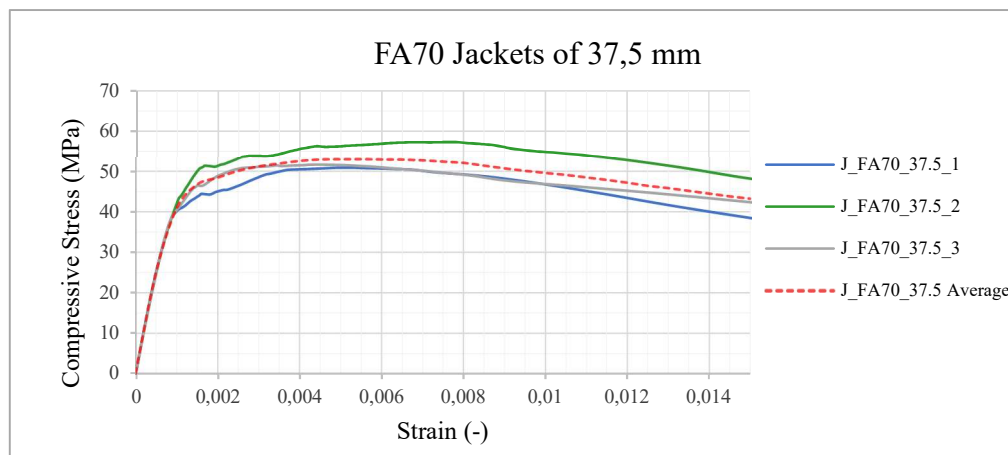


Figure 6.17 - Stress-strain curves: FA70 Jackets of 37,5 mm

Table 6.14 - Mixture FA70: jackets of 50 mm

Specimen	P_{max} (kN)	σ_{max} (MPa)	σ/f_c CORE (MPa)
J FA70 50.0 1	516,80	65,80	1,41
J FA70 50.0 2	483,00	61,50	1,32
J FA70 50.0 3	550,00	70,03	1,51
Average	516,60	65,78	1,41

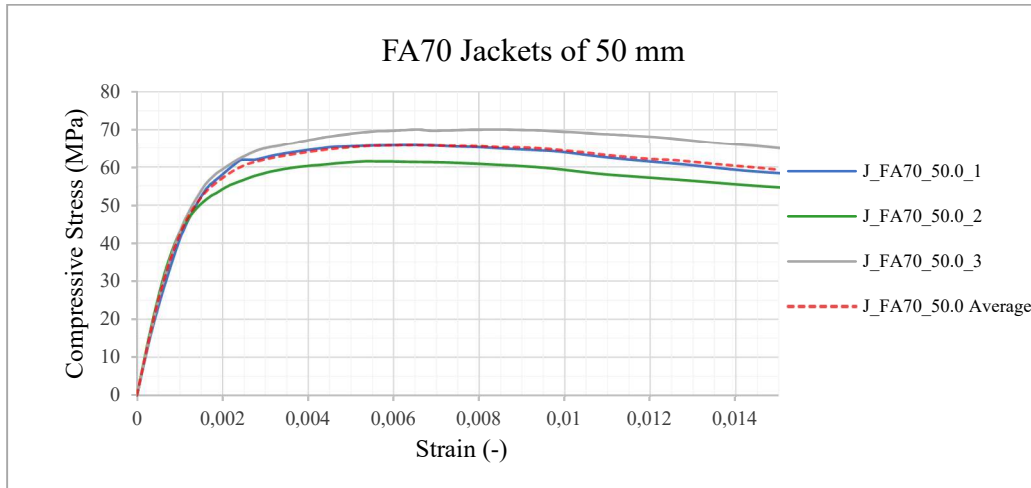


Figure 6.18 - Stress-strain curves: FA70 Jackets of 50 m

ANNEX 10: EVALUATION OF DUCTILITY

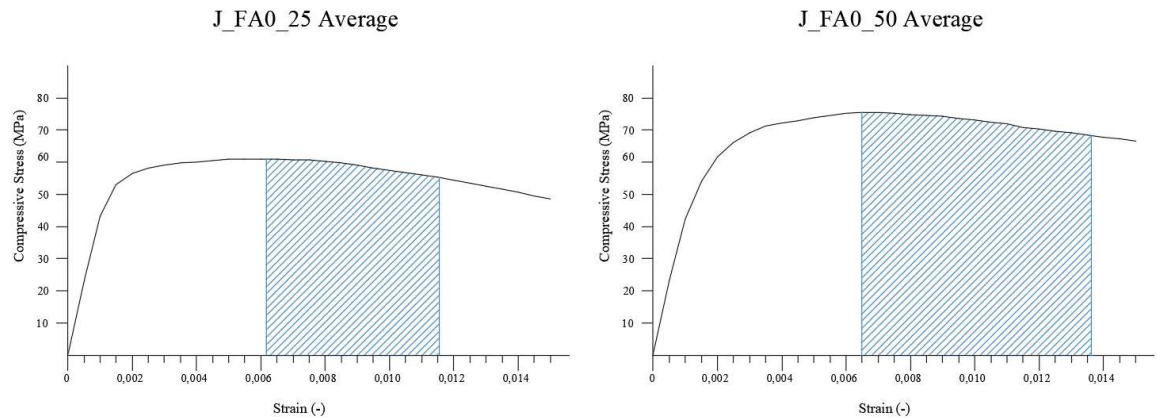


Figure 6.19 - Evaluation of ductility: FA0 mixture

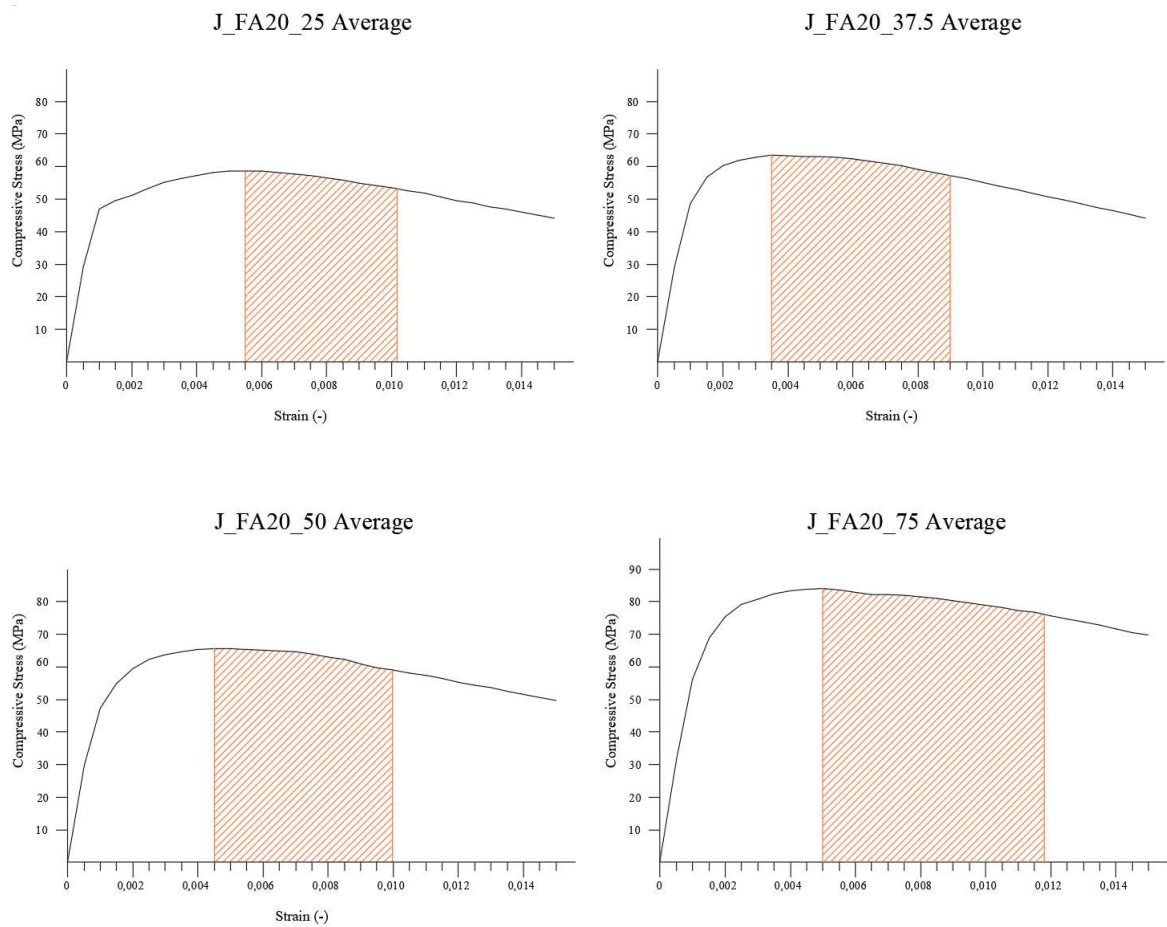


Figure 6.20 - Evaluation of ductility: FA20 mixture

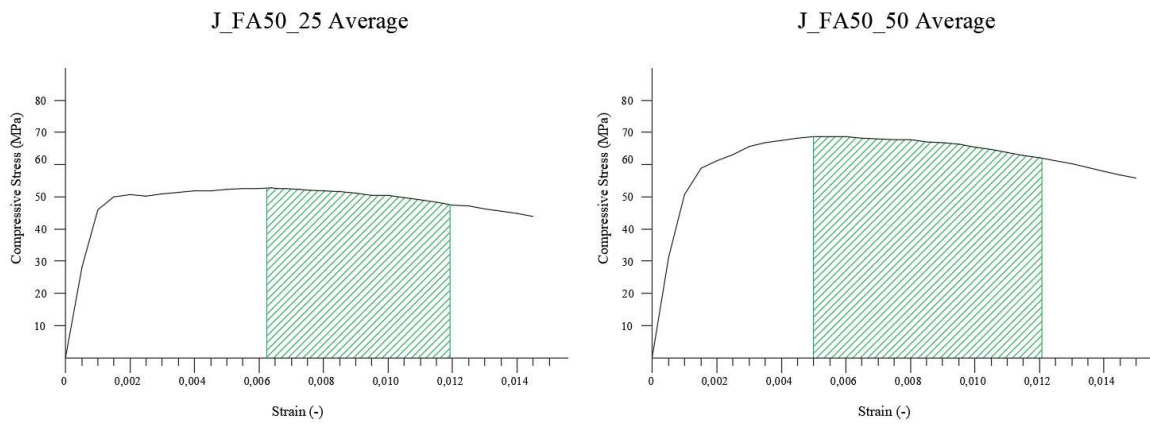


Figure 6.21 - Evaluation of ductility: FA50 mixture

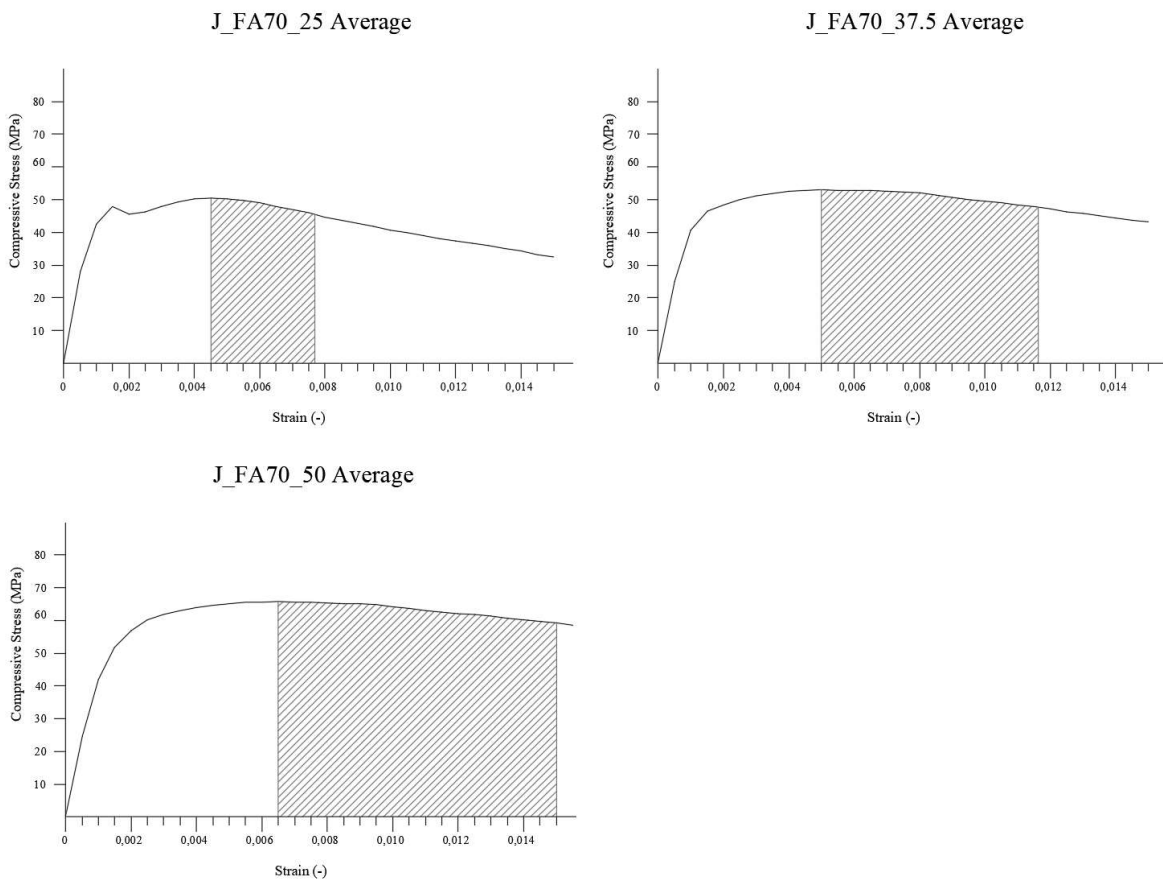


Figure 6.22 - Evaluation of ductility: FA70 mixture

ANNEX 11: FAILURE MODES



Figure 6.23 - Failure patterns: top view

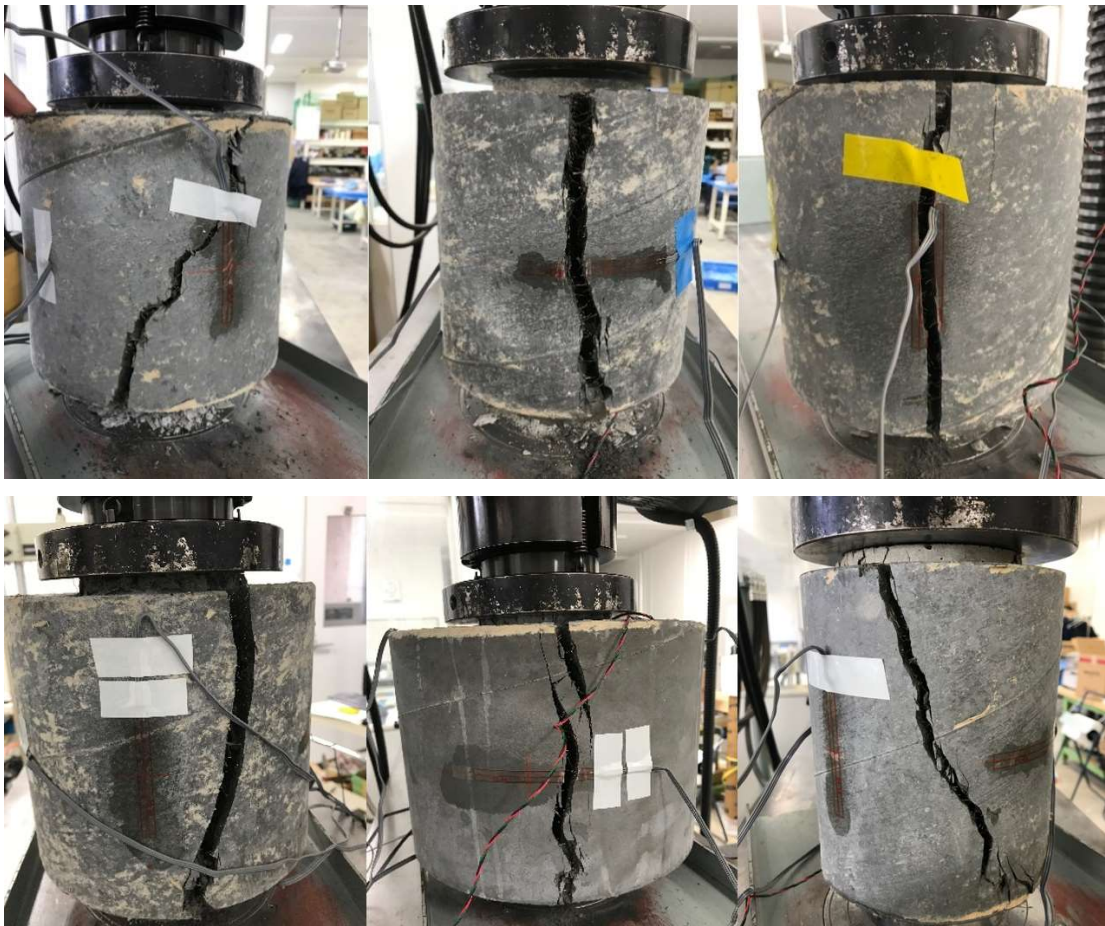


Figure 6.24- Failure patterns: lateral view

REFERENCES

- [1] B. Bresler e A. C. Scordelis, «Shear Strength of Reinforced Concrete Beams,» *ACI Materials Journal*, vol. 60, n. 1, pp. 51-74, 1963.
- [2] P. Casanova, P. Rossi e I. Schaller, «Can Steel Fibers Replace Transverse Reinforcements in Reinforced Concrete Beams,» *ACI Materials Journal*, vol. 94, n. 5, pp. 341-351, 1997.
- [3] A. E. Naaman e H. W. Reinhardt, «Proposed classification of HPFRC composites based on their tensile response,» *Maer. Struct.*, vol. 39, pp. 547-555.
- [4] K. Habel, «Structural behaviour of composite UHPFRC-concrete elements,» in *Doctoral thesis n°3036*, Swiss Federal Institute of Tecnology, Lausanne, Switzerland, 2004.
- [5] N. M. Azmee e N. Shafiq, «Ultra-high performace concrete: From fundamental to applications,» *Case Studies in Construction Materials*, 2018.
- [6] A. Naaman e K. Wille, «The Path to Ultra-High Performance Fiber Reinforced Concrete (UHP-FRC): Five Decades of Progress,» in *Proceedings of Hipermat 2012 - 3rd International Symposium on UHPC and Nanotechnology for Construction Materials*, Kassek University, Germany, 2012.
- [7] R. Deeb, A. Ghambari e B. L. Karihaloo, «Development of self-compacting high and ultra high performance concretes with and without steel fibers,» in *Cement and Coconcrete Composites*, 2012, pp. 185-190.
- [8] C. Vogt, *Ultrafine particles in concrete*, KTH: Stockholm: School of Architecture and the Built Environment, Division of Concrete Structures, 2010.
- [9] J. Resplendino, *Designing and building with UHPFRC - State of the Art and Development*, London: Toutlemonde and J. Resplendino Editors, 2011, pp. 3-12.
- [10] P. K. Mahta e P. J. M. Monteiro, *Concrete, Microstructure, Properties and Materials*, Mc Graw Hill, 2005, p. 650.
- [11] *Fib. Bulletin, Structural Concrete - Textbook on behaviour, design and performance*, vol. 1, Lausanne: fédération internationale du béton (fib), pp. 95-149.

- [12] A. Hermann, E. A. Langaro, S. H. Lopes Da Silva e N. S. Klein, «Particle packing of cement and silica fume in pastes using an analytical model,» *IBRACON de Estruturas e Materiais*, vol. 9, n. 1, 2016.
- [13] K. Habel, «Structural behaviour of elements combining Ultra-High Performance Fibre Reinforced Concretes (UHPFRC) and reinforced concrete,» in *Faculté Environnement naturel, architectural et construit - Institut de structures - Section de Génie Civil*, École Polytechnique Fédérale de Lausanne: Lausanne, 2004.
- [14] R. Mathur, A. K. Misra e P. Goel, «Marble slurry dust and wollastonite-inert mineral admixtures for cement concrete,» *Indian Highways*, 2007.
- [15] R. Deep, A. Ghanbari e B. L. Karihaloo, «Development of self-compacting high and ultra high performance concretes with and without steel fibers.,» *Cement and Concrete Composites*, vol. 34, n. 2, pp. 185-190, February 2012.
- [16] B. P. Hughes e N. I. Fattuhi, «The workability of steel-fibre reinforced concrete,» *Magazine of Concrete Research*, vol. 28, n. 96, pp. 157-161, 1976.
- [17] «ACI 544.3R-93: Guide for specifying, proportioning, mixing, placing and finishing steel fibre reinforced concrete,» 1998.
- [18] T. Kanstad, «Forslag til retningslinjer for dimensjonering, utførelse og kontroll av fiberarmerte betongkonstruksjoner,» in *COIN Project report*, SINTEF Building and Infrastructure, 2011.
- [19] P. Rossi, «Ultra-High Performance Fibre Reinforced Concretes (UHPFRC): An overview,» *Proceedings of the 5th International RILEM Symposium*, 2000.
- [20] G. Herold e H. S. Müller, «Measurement of porosity of Ultra High Strength Fibre Reinforced Concrete,» *Proceedings of the International Symposium on Ultra High Performance Concrete*, pp. 685-694, 2014.
- [21] E. Fehling, «Design relevant properties of hardened Ultra High Performance,» *Proceedings of the international symposium on Ultra-High Performance Concrete*, pp. 327-338, 2011.
- [22] B. A. Graybeal, «Characterization of the behaviour of Ultra-High Performance Concrete,» MD, USA.
- [23] A. E. Naaman, «High performance fiber reinforced cement composites: classification and applications,» in *International Workshop "Cement Based Materials and Civil Infrastructure (CBMCI)"*, Karachi, Pakistan, 2007.

- [24] A. E. Naaman, «High performance fiber reinforced cement composites,» in *High-Performance Construction Materials: science and application*, Singapore, 2008, pp. 91-153.
- [25] S. Kwon, «Development of ultra high-performance fiber-reinforced cementitious composites using multi-scale fiber-reinforced system,» Sendai, 2015.
- [26] B. A. Graybeal, «Material Property Characterization of Ultra-High Performance,» 2006.
- [27] R. Toledo Filho, E. Koenders, S. Formagini e E. Fairbairn, «Performance assessment of Ultra High Performance Fiber Reinforced Cementitious Composites in view of sustainability,» *Materials & Design*, 2012.
- [28] S. Miller, A. Harvath, P. Monteiro e C. Ostertag, «Greenhouse gas emissions from concrete can be reduced by using mix proportions, geometric aspects, and age as design factors,» *Environ. Res. Lett.*, vol. 10, n. 11, p. 114017, 2015.
- [29] N. Randl, T. Steiner, S. Ofner, E. Baumgartner e Mészöly, «Development of UHPC mixtures from an ecological point of view,» *Construction Building Materials*, vol. 67, n. PART C, pp. 373-378, 2014.
- [30] M. Schmidt e E. Fehling, «Ultra-Hochfester Beton - Planung und Bau der ersten Brücke mit UHPC in Europa,» Kassel University Press..
- [31] J. Olivier e H. Peter, «Trends in global CO2 emissions: 2015 report,» 2015.
- [32] R. Thorstensen e P. Fidjestol, Inconsistencies in the pozzolanic strength activity index (SAI) for silica fume according to EN and ASTM, *Mater. Struct.*, 2014, pp. 3979-3990.
- [33] «Use of LCI for the decision-making of a Belgian cement producer: a common methodology for accounting CO2 emissions related to the cement life cycle,» in *Eighth LCA case studies symposium SETAC-Europe*, 2000.
- [34] G. Habert e N. Roussel, «Study of two concrete mix-design strategies to reach carbon mitigation objectives,» *Cement & Concrete Composites*, vol. 31, pp. 397-402, 2009.
- [35] L. Turner e F. Collins, «Carbon dioxide equivalent (CO2-e) emissions: A comparison between geopolymers and OPC cement concrete,» *Construction and Building Materials*, vol. 43, pp. 125-130, 2013.

- [36] T. Nishiwaki, K. Suzuki, A. Fantilli, G. Igarashi e S. Kwon, «Ecological and Mechanical Properties of Ultra High Performance – Fiber Reinforced Cementitious Composites containing High Volume of Fly Ash,» 2017.
- [37] A. Fantilli, F. Tondolo, B. Chiaia e G. Habert, «A sustainable approach to the design of reinforced concrete beams».
- [38] J. Dragas, S. Marinković, I. Ignjatovic e N. Tosic, «Properties of high-volume fly ash concrete and its role in sustainable development,» *Journal of Faculty of Civil Engineering Conference*, pp. 849-858, 2014.
- [39] P. Mehta e P. Monteiro, *Concrete - microstructure, properties, and materials*, vol. 4, New York: McGraw-Hill, 2014.
- [40] «High-Volume Fly Ash System: concrete solution for sustainable Development,» *ACI Materials Journal*, vol. 97, n. 1, pp. 41-48, 2000.
- [41] K. Holman, J. Volz e J. Myers, «Comparative Study on the Mechanical and Durability Behaviour of High-Volume Fly Ash Concrete versus Conventional Concrete,» in *First International Conference on Concrete Sustainability (ICCS 2013)*, 2013.
- [42] A. Fantilli e B. Chiaia, «The work of fracture in the eco-mechanical performances of structural concrete,» *Journal of Advanced Concrete Technology*, vol. 11, pp. 282-290, 2013.
- [43] M. Longo, «The behavior of concrete confined by Ultra High Performance - Fiber Reinforced Cementitious Composite,» Tohoku University, Sendai, 2017.
- [44] A. E. Naaman, «High Performance Fiber Reinforced Cement Composites,» in *High Performance Construction Materials - Science and Applications*, World Scientific Publishing Co. Pte. Ltd, 2007, p. 68.
- [45] A. E. Naaman e H. Reinhardt, *High Performance Fiber Reinforced Cement Composites*, London: E & FN Spon, 1996, p. 505.
- [46] A. E. Naaman, «Properties and applications in repair and rehabilitation,» in *High Performance Fiber-Reinforced Concrete in Infrastructural Repair and Retrofit*, Detroit: ACI, 2000.
- [47] R. Bergamante, P. De Donato, P. Manetta e S. Maringoni, «Intervento di miglioramento sismico di un edificio in c.a. a Coppito (AQ) classificato con esito E a seguito del sisma del 06.04.2009,» *Progettazione Sismica*, n. 02-2013, pp. 125-130, 2013.

- [48] E. Denarié e E. Brühwiler, «Cast-on site UHPFRC for improvement of existing structures - Achievements over the last 10 years in practice and research,» in *HPFRCC7: 7th workshop on High Performance Fiber Reinforced Cement Composites*, Stuttgart, Germany, 2015.
- [49] V. Lisi, «Ecological and mechanical properties of Ultra High Performance-Fiber Reinforced Cementitious Composites containing fly ash,» 2018.
- [50] E. 1992-1-1, *Eurocode 2: Design of concrete structures - Part 1-1: General rules and rules for building*, Brussels: E. for Standardization, 2005.
- [51] *ASTM C 143/C 143M-00: "Standard Test Method for Slump of Hydraulic-Cement Concrete"*.
- [52] *ASTM C231-03: "Standard Test Method for Air Content Of Freshly Mixed Concrete by the Pressure Method"*.
- [53] *ASTM C 1437-01: "Standard Test Method for Flow of Hydraulic Cement Mortar"*.
- [54] H. El-Enein, H. Azimi, K. Sennah e F. Ghrib, «Flexural strengthening of reinforced concrete slab-column connection using CFRP sheets,» *Construction and Building Materials*, vol. 57, pp. 126-137, 2014.
- [55] J. A. 1149:2017, *Method of test for static modulus of elasticity of concrete*, Japanese Industrial Standard/Japanes Standards Association, 2017.
- [56] T. Nishiwaki, K. Suzuki, S. Kwon, G. Igarashi e A. Fantilli, *Ecologica and Mechanical Properties of Ultra High Performance - Fiber Reinforced Cementitious Composites containing High Volume Fly Ash*, 2017.